



universität  
wien

# DIPLOMARBEIT

Titel der Diplomarbeit

Pair Production of Stop Quarks in  $e^+e^-$  Annihilation close  
to Threshold

Verfasser

Peter Poier

angestrebter akademischer Grad

Magister der Naturwissenschaften (Mag. rer. nat.)

Wien, 2012

Studienkennzahl lt. Studienblatt:

A 411

Studienrichtung lt. Studienblatt:

Diplomstudium Physik

Betreuerin / Betreuer:

Univ.-Prof. Dr. André Hoang



## Danksagung

Als erstes möchte ich mich bei meiner Familie für die langjährige Unterstützung bedanken, ohne die es mir gar nicht erst möglich gewesen wäre Physik zu studieren.

Prof. André Hoang bin ich sehr dankbar für die Betreuung meiner Diplomarbeit und dabei besonders für die vielen Einsichten in Physik und Mathematik, welche er mir durch das geduldige Beantworten meiner Fragen, sowie durch viele hervorragende Vorlesungen und Vorträge ermöglicht hat.

Sehr dankbar bin ich André Hoang auch dafür, dass er mir Pedro Ruiz Femenía zur Seite gestellt hat, der mir gerade in der Anfangszeit eine große Hilfe war und sich sehr bemüht hat meine Fragen zu verstehen und zu beantworten. Pedro wird mir auch auf Grund seiner menschlichen Qualitäten immer in bester Erinnerung bleiben.

Ein großer Dank gebührt auch Maximilian Stahlhofen, der sich ebenfalls oft mit meinen Fragen und Verständnisproblemen auseinandergesetzt hat. Seine Antworten haben mir ebenfalls oft die Augen geöffnet und ich konnte in Diskussionen mit ihm viel über Physik lernen.

Bei der ganzen Teilchenphysik Gruppe möchte ich mich für die freundliche Arbeitsatmosphäre bedanken.

Ich hatte während meines Studiums das große Glück, dass ich viele Mitstudenten getroffen habe, die gute Freunde von mir geworden sind. In zahlreichen Diskussionen konnte ich von ihnen eine Menge lernen und dabei vor allem auch viel Spaß an der Physik haben. Dafür ein großes Dankeschön an meine Kollegen!

Nicht zuletzt danke ich meiner Freundin Sabine dafür, dass sie mich während meiner gesamten Studienzeit unterstützt hat. Durch sie fühle ich mich in Wien auch zuhause.



# Contents

1.	Introduction . . . . .	1
<b>I.</b>	<b>Full theory calculation at 1-loop order</b>	<b>5</b>
2.	Tree order . . . . .	7
3.	Virtual Corrections . . . . .	11
3.1.	Wave-function and mass renormalization . . . . .	11
3.2.	1-loop correction to the vertex . . . . .	13
3.3.	Virtual corrections to the cross section . . . . .	15
4.	Real radiation . . . . .	16
5.	Result for the cross section at 1-loop order . . . . .	18
<b>II.</b>	<b>Effective theory calculation</b>	<b>19</b>
6.	Motivation . . . . .	21
7.	Effective Field Theories . . . . .	24
7.1.	A short introduction to Effective Field Theories . . . . .	24
7.2.	Matching and the threshold expansion . . . . .	25
8.	Optical Theorem and Cutkosky rules . . . . .	29
9.	Operators and fields in vNRQCD . . . . .	31
9.1.	The label formalism of vNRQCD . . . . .	31
9.2.	$e^+e^-$ fields in the EFT . . . . .	32
9.3.	Operators in vNRQCD . . . . .	32
9.4.	Factorization formula . . . . .	34
10.	Greenfunction . . . . .	36
10.1.	Definition of the Greenfunction and its Fourier transform . . . . .	36
10.2.	Connection between the Greenfunction and <i>ladder diagrams</i> . . . . .	37
10.3.	Solution for the Coulomb Greenfunction . . . . .	40
10.4.	Calculating $\mathcal{A}^{lk}$ at leading order . . . . .	41
10.5.	Calculating the P-wave Coulomb vertex function . . . . .	42
11.	Concept of Phase Space Matching . . . . .	45
11.1.	Restricting the PS integrals to the domain of vNRQCD . . . . .	45
11.2.	Power Counting . . . . .	46
11.3.	Analysis of the cut propagator . . . . .	46
11.4.	Phase Space Matching formalism . . . . .	48
12.	Additional Operators for the Phase Space Matching . . . . .	50
12.1.	Additional Operators . . . . .	50
12.2.	Factorization formula . . . . .	51

13.	Phase space matching . . . . .	52
13.1.	Calculation of cut diagrams in vNRQCD . . . . .	52
13.2.	Matching to the EFT . . . . .	57
14.	RG evolution due to PS divergences . . . . .	63
15.	Numerical comparison to a Madgraph simulation . . . . .	65
15.1.	Madgraph simulation for $e^+e^- \rightarrow \tilde{t}_1\tilde{t}_1 \rightarrow b\tilde{\chi}_1^+\bar{b}\tilde{\chi}_1^-$ . . . . .	65
15.2.	Madgraph simulation for $e^+e^- \rightarrow b\tilde{\chi}_1^+\bar{b}\tilde{\chi}_1^-$ . . . . .	68
16.	Preliminary result . . . . .	72
17.	Conclusion . . . . .	74
<b>III. Appendix</b>		<b>75</b>
18.	Scalar n-point Integrals . . . . .	77
18.1.	Prerequisites . . . . .	77
18.2.	1-point integral . . . . .	77
18.3.	2-point integral . . . . .	78
18.4.	3-point integral . . . . .	79
19.	Tensor-Reduction . . . . .	81
19.1.	Introduction . . . . .	81
19.2.	2-point integral . . . . .	81
19.3.	3-point integral . . . . .	82
20.	Phase space integrals . . . . .	83
20.1.	2 particle phase space integrals . . . . .	83
20.2.	3 particle phase space integrals . . . . .	84

# 1. Introduction

The aim of physics is to answer deep questions about how the universe behaves and how it started. By addressing these questions research in physics made great technological advances possible and transformed the way we perceive the world around us. Everyday phenomena such as the stability of matter, the distinctive qualities of working materials, the anomaly of water, electricity, etc. that have important implications on our life are connected to physical laws at scales and energies that are beyond our everyday experience. The idea of particle physics is that by understanding the behaviour of elementary particles which constitute the basic building blocks of nature, we can understand all these phenomena.

A major challenge in this field is to produce elementary particles and to acquire their properties in experiments. To achieve this large particle accelerators were constructed throughout the last century. Einstein's famous equation  $E = mc^2$  makes it possible to produce new particles by accelerating well-known ones like electrons or protons and colliding them at high energies. In the framework of Quantum Field Theories (QFTs) one can describe which particles will be produced in these experiments and how they will behave. By comparing the predictions of these theories to the experimental results remarkable progress has been achieved. In the 20th century the Standard model (SM) of particle physics was developed and triumphantly confirmed in many experiments.

Despite the successes of the SM and although there is no experiment in direct violation with its predictions, physicists are already sure that it cannot be the end of the story. One of the reasons is connected to the Higgs Boson, which is the only particle of the SM which has not yet been discovered. The search for the Higgs is a major aim of the LHC experiment at CERN. At the end of 2011 the ATLAS and CMS experiment announced new results that indicate a Higgs boson with a mass of around 125GeV [1, 2]. But the experimental data was not yet strong enough for the physical community to announce the *discovery of the Higgs*. The importance of the Higgs Boson is on the one hand founded on its central position in the Standard Model but also due to the fact that it constitutes a window to *new physics*.

There is for instance the so-called *hierarchy problem*: Large quantum corrections to the Higgs mass in the SM make an unnatural fine-tuning, such that independent contributions cancel, necessary. If it was not for this fine-tuning, these contributions would render the Higgs mass so large that the SM would be internally inconsistent. One of the possible solutions to the *hierarchy problem* is to introduce Supersymmetry (SUSY) as it assures that the large Quantum corrections to the Higgs mass cancel without the necessity of extreme fine-tuning [36]. This is one of the reasons why supersymmetric theories became very popular.

The Minimal Supersymmetric Standard Model (MSSM) was originally proposed in 1981 by Howard Georgi and Savas Dimopoulos [16] to solve the hierarchy problem. In the MSSM every particle of the SM has a superpartner that is connected to the original SM particle via SUSY. Therefore the spectrum of a supersymmetric theory that includes the SM contains at least two times as many particles as the SM. This means that if Supersymmetry is realized in nature there is a lot of discovery potential. There is also a very interesting connection to the dark matter problem in astronomy, as the spectrum of the MSSM contains neutralinos which are weakly interacting massive particles (WIMPs) that are considered as possible dark matter candidates [18].

In this work we concentrate on the superpartners of the top quark  $t$  which are called stop squarks  $\tilde{t}_1, \tilde{t}_2$ . Unlike the top, which has spin  $\frac{1}{2}$ , they are scalars. One needs to introduce two stops as a spin  $\frac{1}{2}$  particle carries two times the degrees of freedom of a scalar particle. The top quark has an exceptional position in the SM because of its large mass of  $172.9 \pm 1.5\text{GeV}$  [38], which is more than

40 times the mass of the b-quark. Due to this fact also the stop squarks are special. On the one hand, the mass gap that separates the two stop squarks can be very large because of the high mass of the top [19, 23, 39]. Therefore the mass of the lighter stop  $\tilde{t}_1$  is expected to be the squark with the lowest mass that will first be accessible to experiments. In addition there are arguments that in order to avoid the hierarchy problem through the introduction of SUSY while reproducing recent results at CERN both stops in the MSSM have to be light [30]. This is due to the fact that because of the large top mass (which implies a stronger coupling between the Higgs and the top) the largest contribution to the radiative correction to the Higgs mass comes from the top quark loop and the stop squarks have to be light enough to cancel most of the top loop contribution [15]. Searching for the stops is therefore an important test of whether SUSY can provide a natural solution to the hierarchy problem.

There is an extensive search for stops and one hopes to find the first signals of SUSY at the LHC. At the future International Linear Collider (ILC) [3] it might then be possible to perform a scan of the total cross section  $\sigma(e^+e^- \rightarrow \tilde{t}_1\tilde{t}_1)$  in the threshold region. This means that one studies  $e^+e^-$  collisions for  $\sqrt{s} \approx 2m$ , where  $m$  is the  $\tilde{t}_1$  mass and  $\sqrt{s}$  the energy of the  $e^+e^-$  pair in the center of mass system (CMS). By fitting the theoretical predictions on the experimental results one can thus determine parameters of the MSSM like the stop mass  $m$  and its decay width  $\Gamma_{\tilde{t}_1}$ .

With respect to  $\sigma(e^+e^- \rightarrow t\bar{t})$  the cross section to stops is suppressed by a factor  $v^2$ , where  $v$  is the velocity of the produced stops. This is due to the fact that stops are scalars and therefore the squarks production vertex involves an additional factor of  $p_{\tilde{t}_1}$ , where  $p_{\tilde{t}_1}$  is the momentum of the produced stops. For the theoretical prediction of  $\sigma(e^+e^- \rightarrow t\bar{t})$  a relative precision of around 3% is desired in view of the expected experimental precision at the ILC [37, 25]. For  $\sigma(e^+e^- \rightarrow \tilde{t}_1\tilde{t}_1)$  the experimental precision depends on unknown parameters like  $m$ , but as the statistics will decrease by at least a factor of  $v^2 \approx \frac{1}{100}$  we expect that a theoretical precision of about 20–30% will be sufficient. A result at leading-logarithmic order (LL) might achieve this theoretical precision, however a next-to-leading-logarithmic order (NLL) calculation is desirable if only to check the convergence of the perturbation series.

For calculating the cross section close to threshold an expansion in powers of the strong coupling  $\alpha_S$  alone will not be sufficient, as there are contributions at arbitrarily high orders in  $\alpha_S$  that are of leading order (LO). A suitable framework to carry out the calculation is non relativistic QCD (NRQCD), which is an effective description of QCD in the non-relativistic regime. In this theory we carry out a double expansion in  $\alpha_S$  and  $v$ . In our problem we encounter three different scales, namely the hard scale  $\sim m$ , the soft scale  $\sim p_{\tilde{t}_1}$  and the ultrasoft scale  $\sim E$ , where  $E$  is the combined kinetic energy of the produced stops. To sum up the logarithms between these scales we will apply vNRQCD [34] which is an extension of NRQCD.

Singularities related to the instability of the stop are of particular importance in the calculation of  $\sigma(e^+e^- \rightarrow \tilde{t}_1\tilde{t}_1)$ . To handle these effects we will introduce cuts on the decay products of the stops and apply the phase space (PS) matching formalism that was also used in [28] to handle analogous effects for the calculation of  $\sigma(e^+e^- \rightarrow \tilde{t}_1\tilde{t}_1)$ . However, unlike in top production for stop production these effects appear already at LO. This is related to the fact that for  $e^+e^- \rightarrow \tilde{t}_1\tilde{t}_1$  the  $\tilde{t}_1\tilde{t}_1$  angular momentum state is a P-wave, while for  $e^+e^- \rightarrow t\bar{t}$  one has a S-wave state. This work is the first, where the PS matching formalism is applied for calculating the cross section to a P-wave angular momentum state, which is an additional motivation for carrying out this analysis.

The outline is as follows: In the first part of this work we will do the calculation in the full theory at one-loop order. The result that we obtain in this part is valid off threshold and we will see explicitly that the perturbation series in orders of  $\alpha_S$  does not converge close to threshold. In the second part



we start by giving a motivation for applying vNRQCD to our problem. In chapter 7 we then give a short introduction to the principles of effective field theories (EFTs). In chapter 8 we introduce the optical theorem and the Cutkosky rules which are essential in our calculation. In chapter 9 we present the operators and fields of vNRQCD. Chapter 10 treats the resummation of ladder diagrams via the Coulomb Greenfunction. In chapter 11 we introduce the idea of the PS matching formalism to treat the singularities related to finite lifetime effects. In chapter 12 we present the operators that we need in addition to the operators of vNRQCD in our EFT with PS matching. In chapter 13 we calculate the Wilson coefficients of these operators. In chapter 14 we solve the renormalization group equation (RGE) related to the anomalous dimension due to the PS divergences. To estimate the effect of background diagrams that are neglected in our treatment we carried out a Monte Carlo simulation in Madgraph [6] which we present in chapter 15. Finally we present the preliminary result of our calculation in chapter 16 and conclude.



## **Part I.**

### **Full theory calculation at 1-loop order**



In this part we calculate the cross section for the production process

$$e^+ e^- \rightarrow \tilde{t}_1 \tilde{t}_1^*$$

to 1-loop order.  $\tilde{t}_1$  is the lighter of the two supersymmetric partners of the standard-model's top quark.  $\tilde{t}_1$  and  $\tilde{t}_2$  are mixtures of the left and right handed squarks, where the L/R mixing angle is given by  $\theta_t$ [44]. The Feynman diagrams contributing to the process at 1-loop order are given in figure 1. Electroweak corrections are neglected.

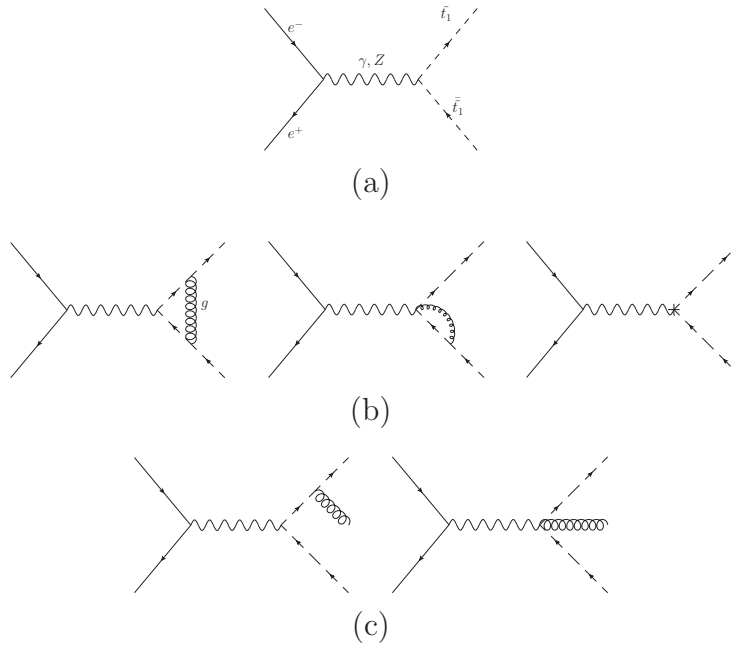


**Figure 1.:** This figure shows the various diagrams that contribute to the total cross section at 1-loop order, if one neglects electroweak corrections. (a) tree level; (b) virtual radiation and counter term; (c) real radiation. (symmetric diagrams not shown)[8]

## 2. Tree order

The vertices of a  $\tilde{t}_1 \tilde{t}_1^*$  pair with a photon and Z boson are both of the form:

$$\begin{array}{c} \tilde{t}_1 \\ \swarrow \\ \mu \text{ wavy } \gamma, Z \\ \searrow \\ \tilde{t}_1^* \end{array} = -ie_0 \tilde{Q}_{\gamma/Z} (p_{\tilde{t}_1} - p_{\tilde{t}_1^*})^\mu, \quad (2.1)$$

where  $e_0 = \sqrt{4\pi\alpha}$  is the electromagnetic coupling and  $p_{\tilde{t}_1}, p_{\tilde{t}_1^*}$  the momenta of the stop and antistop particles.  $\tilde{Q}_{\gamma/Z}$  are given as:

$$\begin{aligned} \tilde{Q}_\gamma &= Q_t, \\ \tilde{Q}_Z &= (\cos^2 \theta_t - 2Q_t \sin^2 \theta_W) / \sin 2\theta_W, \end{aligned} \quad (2.2)$$

where  $\theta_W$  is the electroweak mixing angle and  $Q_t e_0 = 2/3 e_0$  the charge of the stop quark.

The vertex of an  $e^+ e^-$  pair with the Z boson is:

$$\begin{array}{c} e^- \\ \diagdown \\ \text{---} \text{---} \text{---} \text{---} \text{---} \\ \diagup \\ e^+ \end{array} = -i \frac{2e_0}{\sin 2\theta_W} \gamma^\mu (v_e + a_e \gamma^5), \quad (2.3)$$

where  $v_e = -1/4 + \sin^2 \theta_W$  and  $a_e = 1/4$ .

The propagator of the Z boson close to threshold and in the on-shell scheme is given by:

$$\begin{array}{c} p \rightarrow \\ \text{---} \text{---} \text{---} \text{---} \text{---} \\ z \end{array} = \frac{-i g_{\mu\nu}}{p^2 - M_Z^2 + i\Gamma_Z M_Z}, \quad (2.4)$$

where  $M_Z$  is the mass and  $\Gamma_Z$  the total decay width of the Z boson [8]. Using this, the matrix element of the tree level diagrams is given as:

$$M = M^{(\gamma)} + M^{(Z)}, \quad (2.5)$$

with:

$$\begin{aligned} M^{(\gamma)} &= \bar{v}(p_{\bar{e}}) (-i Q_e e_0) \gamma^\mu u(p_e) \frac{-i g_{\mu\nu}}{s + i\epsilon} (-i \tilde{Q}_\gamma e_0) (p_{\tilde{t}_1} - p_{\tilde{t}_1^-})^\nu, \\ M^{(Z)} &= \bar{v}(p_{\bar{e}}) \left( -i \frac{2e_0}{\sin 2\theta_W} \right) \gamma^\mu (v_e + a_e \gamma^5) u(p_e) \frac{-i g_{\mu\nu}}{s - M_Z^2 + i\Gamma_Z M_Z} (-i \tilde{Q}_Z e_0) (p_{\tilde{t}_1} - p_{\tilde{t}_1^-})^\nu. \end{aligned} \quad (2.6)$$

$Q_e e_0 = -e_0$  is the charge of the electron,  $p_e, p_{\bar{e}}$  the momenta of  $e^-, e^+$  respectively,  $q = p_e + p_{\bar{e}}$  the total momentum and  $s = q^2$  the squared energy in the center of mass system (CMS).  $M^{(\gamma)}$  and  $M^{(Z)}$  correspond to the diagram with the photon and Z boson respectively. One can write the matrix element as follows:

$$M = L_\nu (p_{\tilde{t}_1} - p_{\tilde{t}_1^-})^\nu, \quad (2.7)$$

with

$$\begin{aligned} L_\nu &= L_\nu^{(\gamma)} + L_\nu^{(Z)}, \\ L_\nu^{(\gamma)} &= \bar{v}(p_{\bar{e}}) (-i Q_e e_0) \gamma^\mu u(p_e) \frac{-i g_{\mu\nu}}{s + i\epsilon} (-i \tilde{Q}_\gamma e_0), \\ L_\nu^{(Z)} &= \bar{v}(p_{\bar{e}}) \left( -i \frac{2e_0}{\sin 2\theta_W} \right) \gamma^\mu (v_e + a_e \gamma^5) u(p_e) \frac{-i g_{\mu\nu}}{s - M_Z^2 + i\Gamma_Z M_Z} (-i \tilde{Q}_Z e_0). \end{aligned} \quad (2.8)$$

We will call  $L_\nu$  the lepton tensor. To compute  $\sigma_{\text{tot}}$  we have to square the matrix element, integrate over the phase space and sum over colours and spins.  $L_\nu$  does not depend on the outgoing momenta and can thus be factored out of the phase space integration.

$$\begin{aligned} \sigma^{(t)} &= \frac{1}{4 |p_e|_{\text{CMS}} \sqrt{s}} \int \sum_{\text{colours}} \frac{1}{4} \sum_{\text{spins}} |M|^2 \text{dLIPS}_2(q) \\ &= \frac{N_C}{8s} \left( \sum_{\text{spins}} L_\mu L_\nu^* \right) \underbrace{\int (p_{\tilde{t}_1} - p_{\tilde{t}_1^-})^\mu (p_{\tilde{t}_1} - p_{\tilde{t}_1^-})^\nu \text{dLIPS}_2(q)}_{\equiv I^{(t)\mu\nu}} \end{aligned} \quad (2.9)$$

$\sigma^{(t)}$  is the total cross section at tree order,  $N_C = 3$  the number of colours and  $|p_e|_{\text{CMS}}$  the momentum of the ingoing electron in the CMS. In the following, we neglect the electron mass and thus set  $|p_e|_{\text{CMS}} = \frac{\sqrt{s}}{2}$ .  $d\text{LIPS}_n(q)$  is the invariant, n-particle phase space measure (20.2). For doing the phase space integration we make an Ansatz:

$$I^{(t)\mu\nu} = I^{(t)}(q^\mu q^\nu - g^{\mu\nu} q^2). \quad (2.10)$$

$I^{(t)\mu\nu}$  can only be a linear combination of  $q^\mu q^\nu$  and  $g^{\mu\nu}$ , because of Lorentz invariance. In addition, one can use that  $I^{\mu\nu} q_\nu = 0$ , as  $(p_{\tilde{t}_1} - p_{\tilde{t}_1}^*)^\mu q_\mu = (p_{\tilde{t}_1} - p_{\tilde{t}_1}^*)(p_{\tilde{t}_1} + p_{\tilde{t}_1}^*)_\mu = (m^2 - m^2) = 0$ . Here  $m$  is the mass of  $\tilde{t}_1$  and  $\tilde{t}_1^*$ . This restricts  $I^{\mu\nu}$  to the Ansatz above. One can now compute the scalar  $I^{(t)}$  as

$$I^{(t)} = \frac{I^{(t)\mu}{}_\mu}{(1-d)q^2}, \quad (2.11)$$

where  $g^\mu{}_\mu = d$  is the dimension of space-time.

$$\begin{aligned} I^{(t)\mu}{}_\mu &= \int (p_{\tilde{t}_1} - p_{\tilde{t}_1}^*)^\mu (p_{\tilde{t}_1} - p_{\tilde{t}_1}^*)_\mu d\text{LIPS}_2(q) \\ &= \int (2m^2 - 2p_{\tilde{t}_1} \cdot p_{\tilde{t}_1}^*) d\text{LIPS}_2(q) \\ &= (4m^2 - q^2) \int d\text{LIPS}_2(q) \end{aligned} \quad (2.12)$$

It was used that  $-2p_{\tilde{t}_1} \cdot p_{\tilde{t}_1}^* = 2m^2 - q^2$  due to energy-momentum conservation. The two-particle phase space integral in  $d = 4 - 2\epsilon$  dimensions is calculated in the appendix (20.6)

$$\int d\text{LIPS}_2(q) = \text{PS}_2(q^2, \epsilon) = \frac{\beta}{8\pi} + O(\epsilon), \quad (2.13)$$

where  $\beta = \sqrt{1 - \frac{4m^2}{s}}$ . In the non-relativistic approximation\*  $\beta$  is approximately the velocity  $v$  of one of the two outgoing particles in the CMS. One thus gets:

$$I^{(t)\mu}{}_\mu = \frac{-s\beta^3}{8\pi} \quad (2.14)$$

Finally we need to calculate

$$\sum_{\text{spins}} L_\mu L_\nu^* = \sum_{\text{spins}} L_\mu^{(\gamma)} L_\nu^{(\gamma)*} + L_\mu^{(Z)} L_\nu^{(Z)*} + (L_\mu^{(\gamma)} L_\nu^{(Z)*} + L_\mu^{(Z)} L_\nu^{(\gamma)*}) \quad (2.15)$$

$(L_\mu^{(\gamma)} L_\nu^{(Z)*} + L_\mu^{(Z)} L_\nu^{(\gamma)*}) I^{\mu\nu} = 2\text{Re} (L_\mu^{(\gamma)} L_\nu^{(Z)*}) I^{\mu\nu}$  as  $I^{\mu\nu}$  is symmetric. Therefore we can use  $2\text{Re} (L_\mu^{(\gamma)} L_\nu^{(Z)*})$  instead of  $(L_\mu^{(\gamma)} L_\nu^{(Z)*} + L_\mu^{(Z)} L_\nu^{(\gamma)*})$ . In the following we will neglect the electron mass  $m_e$ .

$$\sum_{\text{spins}} L_\mu^{(\gamma)} L_\nu^{(\gamma)*} = \frac{e_0^4 \tilde{Q}^2}{s^2} \text{Tr} [\not{p}_e \gamma_\mu \not{p}'_e \gamma_\nu] \quad (2.16)$$

---

\* $v \ll 1$ ,  $c \equiv 1$

$$\sum_{spins} L_\mu^{(Z)} L_\nu^{(Z)*} = \frac{2e_0^4 \tilde{Q}_Z^2}{\sin 2\theta_W} \frac{1}{(s - M_Z)^2 + (\Gamma_Z M_Z)^2} \text{Tr} [\not{p}_{\bar{e}} \gamma_\mu (v_e + a_e \gamma^5) \not{p}_e \gamma_\nu (v_e + a_e \gamma^5)] \quad (2.17)$$

We know that

$$\text{Tr} [\gamma_\mu \gamma_\nu \gamma_\rho \gamma_\sigma \gamma^5] \sim \epsilon_{\mu\nu\rho\sigma}. \quad (2.18)$$

The contraction of this structure with  $I^{(t)\mu\nu}$ , which is symmetric, vanishes. Therefore the traces with only one  $\gamma^5$  matrix give no contribution and we can thus neglect them:

$$\sum_{spins} L_\mu^{(Z)} L_\nu^{(Z)*} \cong \frac{4e_0^4 \tilde{Q}_Z^2}{\sin^2 2\theta_W} \frac{1}{(s - M_Z)^2 + (\Gamma_Z M_Z)^2} (v_e^2 + a_e^2) \text{Tr} [\not{p}_{\bar{e}} \gamma_\mu \not{p}_e \gamma_\nu]. \quad (2.19)$$

$$\sum_{spins} L_\mu^{(\gamma)} L_\nu^{(Z)*} = -\frac{2e_0^4 \tilde{Q}_\gamma \tilde{Q}_Z}{\sin 2\theta_W} \frac{1}{s(s - M_Z - i\Gamma_Z M_Z)} \text{Tr} [\not{p}_{\bar{e}} \gamma_\mu \not{p}_e \gamma_\nu (v_e + a_e \gamma^5)] \quad (2.20)$$

Neglecting again the trace with one  $\gamma^5$  matrix, which vanishes when we do the contraction with  $I^{(t)\mu\nu}$ , we get:

$$2\text{Re} \left( \sum_{spins} L_\mu^{(\gamma)} L_\nu^{(Z)*} \right) \cong -\frac{4e_0^4 \tilde{Q}_\gamma \tilde{Q}_Z}{\sin 2\theta_W} \frac{2(s - M_Z^2)}{s(s - M_Z)^2 + (\Gamma_Z M_Z)^2} v_e \text{Tr} [\not{p}_{\bar{e}} \gamma_\mu \not{p}_e \gamma_\nu]. \quad (2.21)$$

There is only a single trace of  $\gamma$  matrices left to calculate. One easily obtains the result by using the anti-commutation relations for the  $\gamma$  matrices:

$$\text{Tr} [\not{p}_{\bar{e}} \gamma_\mu \not{p}_e \gamma_\nu] = 4(p_{e\mu} p_{\bar{e}\nu} + p_{\bar{e}\mu} p_{e\nu} - (p_e \cdot p_{\bar{e}}) g_{\mu\nu}). \quad (2.22)$$

By using (2.14), (2.16), (2.19), (2.21) and (2.22) to compute (2.9) one obtains

$$\begin{aligned} \sigma^{(t)} &= (\delta_{\gamma\gamma} + \delta_{ZZ} + \delta_{\gamma Z}) \frac{8N_C \pi^2 \alpha^2}{s^2(1-d)} I^{(t)\mu}{}_\mu \\ \delta_{\gamma\gamma} &= \tilde{Q}_\gamma^2 \\ \delta_{ZZ} &= \frac{4\tilde{Q}_Z^2 (v_e^2 + a_e^2) s^2}{\sin^2 2\theta_W [(s - M_Z^2)^2 + (\Gamma_Z M_Z)^2]} \\ \delta_{\gamma Z} &= -\frac{4v_e \tilde{Q}_\gamma \tilde{Q}_Z s (s - M_Z^2)}{\sin 2\theta_W [(s - M_Z^2)^2 + (\Gamma_Z M_Z)^2]}, \end{aligned} \quad (2.23)$$

where  $\alpha = \frac{e_0^2}{4\pi}$ .



### 3. Virtual Corrections

For taking into account QCD corrections of  $O(\alpha_S)$  we will have to compute 1-loop corrections to the vertices coupling the squarks to the photon and the Z boson. We will not have to compute loop corrections to the squark propagator, as there are no squark propagators in the tree diagrams. However, we will have to compute the squarks wave-function renormalization as it appears in the counter-term of the vertex:

$$\begin{array}{c} \text{---} \mu \text{---} \\ \text{---} \mu \text{---} \end{array} \begin{array}{c} \text{---} \tilde{t}_1 \\ \text{---} \tilde{t}_1 \end{array} = -ie_0 \tilde{Q}_{\gamma/Z} (p_{\tilde{t}_1} - p_{\tilde{t}_1}^{\bar{}})^{\mu} \underbrace{(\delta Z_{\phi} + 1/2\delta Z_A + \delta Z_{\tilde{Q}})}_0, \quad (3.1)$$

where  $\delta Z_A$  and  $\delta Z_{\phi}$  are the wave-function renormalizations of the photon, Z and squark field respectively. Due to gauge invariance we know that  $1/2\delta Z_A + \delta Z_{\tilde{Q}} = 0$ .

The vertex up to  $O(\alpha_S)$  corresponds to the following sum of diagrams and can be expressed as the original vertex times a form factor  $F(q^2) = 1 + \delta F(q^2)$ , where  $\delta F(q^2) = O(\alpha_S)$ :

$$\begin{aligned} \Gamma^{\mu} &\equiv -ie_0 \tilde{Q}_{\gamma/Z} (p_{\tilde{t}_1} - p_{\tilde{t}_1}^{\bar{}})^{\mu} F(q^2) = \begin{array}{c} \text{---} \mu \text{---} \\ \text{---} \mu \text{---} \end{array} \begin{array}{c} \text{---} \tilde{t}_1 \\ \text{---} \tilde{t}_1 \end{array} \\ &= \begin{array}{c} \text{---} \mu \text{---} \\ \text{---} \mu \text{---} \end{array} \begin{array}{c} \text{---} \tilde{t}_1 \\ \text{---} \tilde{t}_1 \end{array} + \begin{array}{c} \text{---} \mu \text{---} \\ \text{---} \mu \text{---} \end{array} \begin{array}{c} \text{---} \tilde{t}_1 \\ \text{---} \tilde{t}_1 \end{array} + \begin{array}{c} \text{---} \mu \text{---} \\ \text{---} \mu \text{---} \end{array} \begin{array}{c} \text{---} \tilde{t}_1 \\ \text{---} \tilde{t}_1 \end{array} + \begin{array}{c} \text{---} \mu \text{---} \\ \text{---} \mu \text{---} \end{array} \begin{array}{c} \text{---} \tilde{t}_1 \\ \text{---} \tilde{t}_1 \end{array} + \begin{array}{c} \text{---} \mu \text{---} \\ \text{---} \mu \text{---} \end{array} \begin{array}{c} \text{---} \tilde{t}_1 \\ \text{---} \tilde{t}_1 \end{array}. \quad (3.2)
 \end{aligned}$$

The reason why  $\Gamma^{\mu}$  will always be proportional to  $(p_{\tilde{t}_1} - p_{\tilde{t}_1}^{\bar{}})^{\mu}$  is that it can only be a linear combination of  $p_{\tilde{t}_1}^{\mu}$  and  $p_{\tilde{t}_1}^{\bar{\mu}}$  and has to fulfil the Ward identity[51]  $\Gamma^{\mu} q_{\mu} = 0$ , where  $q = p_{\tilde{t}_1} + p_{\tilde{t}_1}^{\bar{}}$  is the momentum of the incoming photon or Z boson.

#### 3.1. Wave-function and mass renormalization

It can be proven that the exact propagator for scalar particles can always be written in the Lehmann-Källén form [46, p. 93]:

$$\begin{aligned} i\Delta(k^2) &= \int d^d x \exp(ikx) \langle 0|T\phi(x)\phi(0)|0\rangle \\ &= \frac{Zi}{k^2 - m^2 + i\epsilon} + \int_{4m^2}^{\infty} ds \rho(s) \frac{i}{k^2 - s + i\epsilon}. \quad (3.3)
 \end{aligned}$$

Z is the residuum of the isolated pole\* and its position is the definition of the pole mass  $m$ . We will use the pole-mass scheme for our calculation. One can further show that  $Z = |\langle 0|\phi(0)|p\rangle|^2$ , where  $|p\rangle$  is the one-particle state of the  $\phi$  field with 4-momentum  $p$ .

The LSZ formalism [32] states that one has to divide the amputated n-point function in momentum space by  $\sqrt{Z}$  for every external scalar particle to get the corresponding transition amplitude. We will use the on-shell scheme where the wave-function renormalization is chosen such that  $Z = 1$  and

---

\*The pole is only isolated in the massive case.

the LSZ formalism becomes particularly simple. The on-shell scheme roughly means that we require [46]:

$$\begin{array}{c} p \rightarrow \\ \text{---} \\ \text{---} + \text{---} * \text{---} + \text{---} \text{---} \text{---} \text{---} \text{---} \\ p^2 \rightarrow m^2 \end{array} \equiv \begin{array}{c} p \rightarrow \\ \text{---} \\ \text{---} \end{array} \quad (3.4)$$

We define  $\Pi(p^2)$  as the following correction to the squarks self-energy:

$$i\Pi(p^2) \equiv \begin{array}{c} p \rightarrow \\ \text{---} \\ \text{---} \end{array} \quad (3.5)$$

With this we can write a more precise version of (3.4):

$$\begin{aligned} & \frac{i}{p^2 - m^2 + i\epsilon} + \frac{i}{p^2 - m^2 + i\epsilon} [i\delta Z_\phi(p^2 - m^2) - i\delta Z_m m^2 + i\Pi(p^2)] \frac{i}{p^2 - m^2 + i\epsilon} \\ & = \frac{i}{p^2 - m^2 + i\epsilon} + O((p^2 - m^2)^0). \end{aligned} \quad (3.6)$$

If this equation is fulfilled the isolated pole lies at  $p^2 = m^2$  and its residuum  $Z$  is equal to one. (3.6) is equivalent to two equations for  $\delta Z_\phi$  and  $\delta Z_m$ :

$$\begin{aligned} \Pi(m^2) - \delta Z_m m^2 &= 0, \\ \frac{\partial}{\partial p^2} \Pi \Big|_{p^2=m^2} + \delta Z_\phi &= 0. \end{aligned} \quad (3.7)$$

For determining  $\delta Z_m$  we therefore need to calculate  $\Pi(m^2)$  and for  $\delta Z_\phi$ ,  $\Pi'(m^2)$ . In scalar QCD the vertex between a squarks pair and a gluon is:

$$\begin{array}{c} \tilde{t}_1 \\ \swarrow \\ \text{---} \\ \mu \\ \text{---} \\ \searrow \\ \tilde{t}_1' \end{array} \quad g = (-ig_S)T^A(p_{\tilde{t}_1} + p'_{\tilde{t}_1})^\mu, \quad (3.8)$$

where  $g_S$  is the strong-coupling,  $T^A$  the Gellman Matrices and  $p_{\tilde{t}_1}, p'_{\tilde{t}_1}$  the incoming and outgoing momenta of the squarks.

$$i\Pi(p^2) = \int \tilde{d}^d k (-ig_S \tilde{\mu}^\epsilon) (2p - k)^\mu T^A \frac{i}{(p - k)^2 - m^2 + i\epsilon} \frac{-i\delta_{AB}}{k^2 + i\epsilon} (-ig_S \tilde{\mu}^\epsilon) (2p - k)_\mu T^B, \quad (3.9)$$

where  $\tilde{d}^d k$  stands for  $\frac{d^d k}{(2\pi)^d}$ . We will find I.R. and U.V. divergences and therefore work in dimensional regularization in  $d = 4 - 2\epsilon$  dimensions [48].  $\tilde{\mu}$  is the renormalization scale in the MS-scheme. Using  $\sum_A T^A T^A = C_F \mathbf{1}_3$ , with  $C_F = \frac{4}{3}$  one obtains:

$$i\Pi(p^2) = -C_F g_S^2 \underbrace{\int \tilde{d}^d k \tilde{\mu}^{2\epsilon} \frac{(2p - k)^2}{[(p - k)^2 - m^2]_+ k_+^2}}_I, \quad (3.10)$$

where  $x_+$  is an abbreviation for  $x + i\epsilon$ .  $I$  can be reduced to two scalar integrals\*:

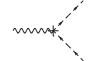
$$\begin{aligned} I &= 2(p^2 + m^2) \int \tilde{d}^d k \frac{\tilde{\mu}^{2\epsilon}}{[(p - k)^2 - m^2]_+ k_+^2} - \int \tilde{d}^d k \frac{\tilde{\mu}^{2\epsilon}}{[k^2 - m^2]_+} \\ &= 2(p^2 + m^2) \hat{B}_0(p^2) - A_0. \end{aligned} \quad (3.11)$$

---





\*Write  $(2p - k)^2$  as  $2[(p + k)^2 - m^2] - k^2 + 2(m^2 + p^2)$  and write a separate integral for each of these 3 terms. This reduction method is explained in section 19.

$A_0$ ,  $\hat{B}_0(p^2)$  and  $\left. \frac{\partial \hat{B}_0}{\partial p^2} \right|_{p^2=m^2}$  are calculated in the appendix\*. We thus get an expression for  $\Pi(m^2)$  and  $\left. \frac{\partial}{\partial p^2} \Pi \right|_{p^2=m^2}$ , which we can use in (3.7) to determine  $\delta Z_m$  and  $\delta Z_\phi$ :

$$\begin{aligned} \delta Z_m &= -\frac{C_F g_S^2}{16\pi^2} \left[ \frac{3}{\epsilon} + 3 \ln \left( \frac{\mu^2}{m^2} \right) + 7 \right], \\ \delta Z_\phi &= \frac{C_F g_S^2}{8\pi^2} \left[ \frac{1}{\epsilon} + \ln \left( \frac{\mu^2}{m^2} \right) - \frac{1}{\epsilon_{IR}} - \ln \left( \frac{\mu_{IR}^2}{m^2} \right) \right]. \end{aligned} \quad (3.12)$$

$\epsilon$ ,  $\mu$  refer to the U.V. and  $\epsilon_{IR}$ ,  $\mu_{IR}$  to the I.R. divergences. Without making this distinction,  $\delta Z_\phi$  would be 0. Inserting  $\delta Z_\phi$  into (3.1) gives .


### 3.2. 1-loop correction to the vertex

In order to calculate  via (3.2) we still have to compute ,  and . In the first two diagrams, there appears a vertex coupling a photon or Z boson with a gluon and two squarks [8]:

$$\begin{array}{c} \text{Diagram: } \mu \text{---} \gamma/Z \text{---} \nu \text{---} g \text{---} \nu \text{---} \mu \\ \text{with external lines } i_1, \bar{i}_1 \end{array} = 2ig_S \tilde{Q}_{\gamma/Z} T^A g^{\mu\nu}. \quad (3.13)$$

Using this we obtain:

$$\begin{aligned} & \text{Diagram: } \mu \text{---} \gamma/Z \text{---} \nu \text{---} g \text{---} \nu \text{---} \mu \\ &= \sum_A \int \bar{d}^d k (-ig_S \tilde{\mu}^\epsilon) T^A (2p_{\bar{t}_1} + k)^\mu \frac{i}{[(k + p_{\bar{t}_1})^2 - m^2]_+} 2ig_S \tilde{\mu}^\epsilon \tilde{Q}_{\gamma/Z} \tilde{\mu}^\epsilon T^A \frac{-i}{k_+^2} \\ &= 2C_F g_S^2 \tilde{Q}_{\gamma/Z} \tilde{\mu}^\epsilon \left\{ 2p_{\bar{t}_1}^\mu \int \bar{d}^d k \frac{\tilde{\mu}^{2\epsilon}}{[(k + p_{\bar{t}_1})^2 - m^2]_+ k_+^2} + \int \bar{d}^d k \frac{\tilde{\mu}^{2\epsilon} k^\mu}{[(k + p_{\bar{t}_1})^2 - m^2]_+ k_+^2} \right\} \\ &= 2C_F g_S^2 \tilde{Q}_{\gamma/Z} \tilde{\mu}^\epsilon \left\{ 2p_{\bar{t}_1}^\mu \hat{B}_0(m^2) + \hat{B}_1^\mu(p_{\bar{t}_1}) \right\}. \end{aligned} \quad (3.14)$$

In the appendix,  $\hat{B}_1^\mu(p_{\bar{t}_1})$  is expressed as a sum of scalar integrals times  $p_{\bar{t}_1}^\mu$  (19.5). The diagram  is completely equivalent, except that  $p_{\bar{t}_1} \rightarrow -p_{\bar{t}_1}$ . Thus we get:

$$\begin{aligned} \delta \Gamma^\mu &\equiv \text{Diagram: } \mu \text{---} \gamma/Z \text{---} \nu \text{---} g \text{---} \nu \text{---} \mu + \text{Diagram: } \mu \text{---} \gamma/Z \text{---} \nu \text{---} g \text{---} \nu \text{---} \mu \\ &= C_F g_S^2 \tilde{Q}_{\gamma/Z} \tilde{\mu}^\epsilon \left( 4\hat{B}_0(m^2) - \frac{A_0}{m^2} \right) (p_{\bar{t}_1} - p_{\bar{t}_1})^\mu. \end{aligned} \quad (3.15)$$

\*see (18.3), (18.7) and (18.9)

There is one more diagram to compute for the virtual corrections to the vertex:

$$\begin{aligned}
\delta\Gamma^\mu &\equiv \text{Diagram} \\
&= \sum_A \int d^d k (-ig_S \tilde{\mu}^\epsilon) (2p_{\bar{t}_1} + k)^\nu T^A \frac{i}{[(p_{\bar{t}_1} + k)^2 - m^2]_+} (-i\tilde{Q}_{\gamma/Z} \tilde{\mu}^\epsilon) \\
&\quad (p_{\bar{t}_1} - p_{\bar{t}_1} + 2k)^\mu \frac{i}{[(p_{\bar{t}_1} - k)^2 - m^2]_+} (-ig_S \tilde{\mu}^\epsilon) (-2p_{\bar{t}_1} + k)_\nu T^A \frac{-i}{k_+^2} \\
&= -\tilde{\mu}^\epsilon \tilde{Q}_{\gamma/Z} g_S^2 \int d^d k \tilde{\mu}^{2\epsilon} \frac{(2k + p_{\bar{t}_1} - p_{\bar{t}_1})^\mu (2(p_{\bar{t}_1} - p_{\bar{t}_1})k + k^2 - 4p_{\bar{t}_1} p_{\bar{t}_1})}{[(p_{\bar{t}_1} + k)^2 - m^2]_+ [(p_{\bar{t}_1} - k)^2 - m^2]_+ k_+^2}. \quad (3.16)
\end{aligned}$$

Next we expand the numerator and rewrite  $2p_{\bar{t}_1/\bar{t}_1} k$  as  $[(k + p_{\bar{t}_1/\bar{t}_1})^2 - m^2] - k^2$ . We write a separate integral for each distinct term in the numerator and can then reduce terms like  $[(k + p_{\bar{t}_1})^2 - m^2]$  with the denominator. We want to rewrite all the tensor integrals in terms of those, which we reduce in section 19. To achieve this, we have to make a shift of the integration variable  $k \rightarrow k + p_{\bar{t}_1}$  in some integrals. We arrive at the following expression:

$$\begin{aligned}
\delta\Gamma^\mu &= -\tilde{\mu}^\epsilon \tilde{Q}_{\gamma/Z} g_S^2 \left[ 2\hat{B}_0(m^2) (p_{\bar{t}_1} - p_{\bar{t}_1})^\mu - \tilde{B}_0(q^2) (p_{\bar{t}_1} + p_{\bar{t}_1})^\mu + \right. \\
&\quad 2 \left[ \hat{B}_1^\mu(p_{\bar{t}_1}) + \hat{B}_1^\mu(-p_{\bar{t}_1}) \right] - 2\tilde{B}_1^\mu(q) \\
&\quad \left. - 4(p_{\bar{t}_1} \cdot p_{\bar{t}_1}) \tilde{C}_0(q^2) (p_{\bar{t}_1} - p_{\bar{t}_1})^\mu - 8(p_{\bar{t}_1} \cdot p_{\bar{t}_1}) \tilde{C}_1^\mu(p_{\bar{t}_1}, p_{\bar{t}_1}) \right], \quad (3.17)
\end{aligned}$$

where  $q = p_{\bar{t}_1} + p_{\bar{t}_1}$  is the total momentum. In the appendix in section 19, the tensor integrals are rewritten in terms of scalar integrals. Using these results, we obtain a simplified expression:

$$\begin{aligned}
\delta\Gamma^\mu &= -\tilde{\mu}^\epsilon \tilde{Q}_{\gamma/Z} g_S^2 \left[ -4(p_{\bar{t}_1} \cdot p_{\bar{t}_1}) \tilde{C}_0(q^2) \right. \\
&\quad \left. - \frac{8(p_{\bar{t}_1} \cdot p_{\bar{t}_1})}{4m^2 - q^2} \left( \hat{B}_0(m^2) - \tilde{B}_0(q^2) \right) - \frac{A_0}{m^2} + 2\hat{B}_0(m^2) \right] (p_{\bar{t}_1} - p_{\bar{t}_1})^\mu. \quad (3.18)
\end{aligned}$$

The various scalar integrals are computed in the appendix. There are U.V. and I.R. divergences in this expression. The I.R. divergence is in  $\tilde{C}_0(q^2)$ . We can now compute the form factor  $F = 1 + \delta F$  using (3.2). Observable quantities like the total cross section only depend on  $|F|^2$ . As  $\delta F = O(\alpha_S)$ , one gets:

$$|F|^2 = |1 + \delta F|^2 = 1 + 2Re(\delta F) + O(\alpha_S^2). \quad (3.19)$$

This means that up to  $O(\alpha_S)$  only the real part of the form factor  $F$  contributes to observable quantities like the total cross section. We get:

$$2Re \delta F = 2Re \left( \delta Z_\phi + \delta F_{\text{Diagram}} + \delta F_{\text{Diagram}} \right). \quad (3.20)$$

$\delta Z_\phi$  is the contribution of the counter-term, while  $\delta F_{\text{tree}}$  and  $\delta F_{\text{loop}}$  come from the corresponding diagrams.  $\delta Z_\phi = \text{Re } \delta Z_\phi$  is given in (3.12).

$$2\text{Re } \delta F_{\text{tree}} = -C_F \frac{\alpha_S}{2\pi} \left[ \frac{3}{\epsilon} + 3 \log \left( \frac{\mu^2}{m^2} \right) + 7 \right], \quad (3.21)$$

$$\begin{aligned} 2\text{Re } \delta F_{\text{loop}} = & C_F \frac{\alpha_S}{\pi} \left[ \frac{(1+\beta^2)}{\beta} \left( -\frac{\log(w)}{2\epsilon_{IR}} - \frac{1}{2} \log(w) \log \left( \frac{\mu_{IR}^2}{m^2} \right) + \text{Li}_2(w) \right. \right. \\ & \left. \left. - \frac{1}{4} \log^2(w) + \log(1-w) \log(w) - \log(w) + \frac{\pi^2}{3} \right) \right. \\ & \left. + \frac{1}{2\epsilon} + \frac{1}{2} \log \left( \frac{\mu^2}{m^2} \right) + \frac{3}{2} \right]. \end{aligned} \quad (3.22)$$

Using these results we get:

$$\begin{aligned} 2\text{Re } \delta F = & C_F \frac{\alpha_S}{\pi} \left[ \frac{(1+\beta^2)}{\beta} \left( -\frac{\log(w)}{2\epsilon_{IR}} - \frac{1}{2} \log(w) \log \left( \frac{\mu_{IR}^2}{m^2} \right) + \text{Li}_2(w) \right. \right. \\ & \left. \left. - \frac{1}{4} \log^2(w) + \log(1-w) \log(w) - \log(w) + \frac{\pi^2}{3} \right) \right. \\ & \left. - \frac{1}{\epsilon_{IR}} - \log \left( \frac{\mu_{IR}^2}{m^2} \right) - 2 \right]. \end{aligned} \quad (3.23)$$

There are still I.R. divergences left. However, in the sum of the cross sections  $\sigma(e^+e^- \rightarrow \tilde{t}_1 \tilde{t}_1^-) + \sigma(e^+e^- \rightarrow \tilde{t}_1 \tilde{t}_1^- g_{soft})$ , where  $g_{soft}$  corresponds to a gluon with an infinitesimally small energy, the I.R. divergences will cancel in agreement with the Kinoshita-Lee-Nauenberg theorem [31].  $e^+e^- \rightarrow \tilde{t}_1 \tilde{t}_1^- g$  corresponds to the so-called real radiation and we will compute the total cross section to the real radiation in the next section.

### 3.3. Virtual corrections to the cross section

To determine the contribution of the virtual corrections to  $\sigma(e^+e^- \rightarrow \tilde{t}_1 \tilde{t}_1^-)$  we investigate how the formula for the cross section at tree level (2.9) changes due to  $\delta F$ . In this formula we simply get an additional factor  $1 + 2\text{Re}(\delta F)$ , which can be factored out of the phase space integration. However, as  $\delta F$  still includes a divergence, we have to be careful about the phase space integration, which we did in 4 dimensions, when doing the tree computation. Doing the phase space integration in  $d = 4 - 2\epsilon$  dimensions gives an additional contribution of  $O(\epsilon)$  and multiplying this with the  $\frac{1}{\epsilon}$  term, which corresponds to the divergence, gives a contribution of  $O(1)$ .

The only thing that changes with respect to the tree level computation is given by the following replacement prescription:

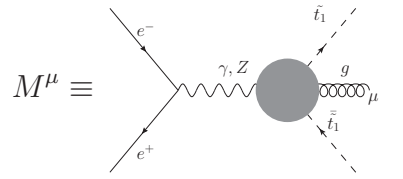
$$\begin{aligned} I^{(t)\mu}{}_\mu & \rightarrow I^{(t)\mu}{}_\mu + I^{(v)\mu}{}_\mu, \\ I^{(v)\mu}{}_\mu & = 2\text{Re}(\delta F) \int (p_{\tilde{t}_1} - p_{\tilde{t}_1^-})^\mu (p_{\tilde{t}_1} - p_{\tilde{t}_1^-})_\mu d\text{LIPS}_2(q) \\ & = -2\text{Re}(\delta F) s \beta^2 \text{PS}_2(q^2, \epsilon), \end{aligned} \quad (3.24)$$

where  $\text{PS}_2(q^2, \epsilon)$  is the two particle phase space volume in d-dimensions. It has to be computed up to  $O(\epsilon)$  because of the  $\frac{1}{\epsilon}$  divergence in  $\delta F$ . The result for  $\text{PS}_2(q^2, \epsilon)$  is given in (20.6).

## 4. Real radiation

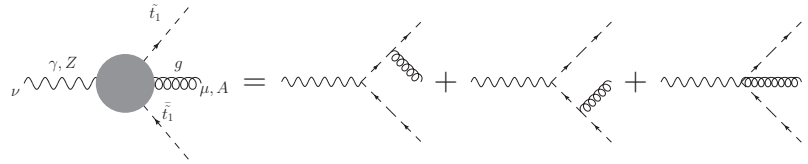
In the last section we found I.R. divergences in the virtual corrections to the cross section  $\sigma(e^+e^- \rightarrow \tilde{t}_1\tilde{t}_1^*)$ . Strictly speaking this cross section is not an observable, as one cannot differ between a  $\tilde{t}_1, \tilde{t}_1^*$  pair and a  $\tilde{t}_1, \tilde{t}_1^*$  pair of practically the same energy with an infinitesimally soft gluon. In the sum of the two cross sections  $\sigma(e^+e^- \rightarrow \tilde{t}_1\tilde{t}_1^*) + \sigma(e^+e^- \rightarrow \tilde{t}_1\tilde{t}_1^*g_{soft})$  the I.R. divergences cancel due to the Kinoshita-Lee-Nauenberg theorem [31]. In this section we will compute the cross section  $\sigma(e^+e^- \rightarrow \tilde{t}_1\tilde{t}_1^*g)$ , where we integrate over the entire phase space, including those parts where the gluon has a high energy. The I.R. divergences that we will encounter, when doing the phase space integration, will again be handled using dimensional regularization.

The amplitude of the real radiation is therefore given by the following diagram:



$$M^\mu \equiv \text{Diagram}, \quad (4.1)$$

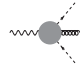
with



$$\text{Diagram} = \text{Diagram}_1 + \text{Diagram}_2 + \text{Diagram}_3. \quad (4.2)$$

Analogously to (2.7) we can write  $M^\mu$  as:

$$M^\mu = L_\sigma \hat{\Gamma}_A^{\sigma\mu}, \quad (4.3)$$

where  $L^\mu$  is the lepton tensor, defined in (2.8) and  $\hat{\Gamma}_A^{\mu\sigma}$  corresponds to  without  $-i(\tilde{Q}_{\gamma/Z})$ .  $\hat{\Gamma}_A^{\nu\mu}$  gives:

$$\begin{aligned} \hat{\Gamma}_A^{\nu\mu} &= (p_{\tilde{t}_1} - p_{\tilde{t}_1^*} + p_g)^\nu \frac{i}{[(p_{\tilde{t}_1} + p_g)^2 - m^2]_+} (-ig_S) (2p_{\tilde{t}_1} + p_g)^\mu T^A + \\ & (p_{\tilde{t}_1} - p_{\tilde{t}_1^*} - p_g)^\nu \frac{i}{[(p_{\tilde{t}_1^*} + p_g)^2 - m^2]_+} (-ig_S) (-2p_{\tilde{t}_1^*} - p_g)^\mu T^A \\ & - 2g_S T^A g^{\nu\mu}. \end{aligned} \quad (4.4)$$

$p_g$  is the momentum of the gluon. We define the following phase space integral:

$$I^{(r)\mu\nu}(q) \equiv - \sum_A \int \hat{\Gamma}_A^{\mu\sigma} \left( \hat{\Gamma}_{A\sigma}^\nu \right)^* dLIPS_3(q) \quad (4.5)$$

$I^{(r)\mu\nu}$  is related to  $\sigma(e^+e^- \rightarrow \tilde{t}_1\tilde{t}_1^*g)$  in exactly the same way as  $\sigma^{(t)}$  was related to the phase space

integral  $I^{(t)\mu\nu}$  (2.9):

$$\begin{aligned}\sigma\left(e^+e^- \rightarrow \tilde{t}_1\tilde{t}_1^*g\right) &= \frac{1}{4|p_e|_{\text{CMS}}\sqrt{s}} \sum_{\text{colours}} \frac{1}{4} \sum_{\text{spins}} L_\mu L_\nu^* I^{(r)\mu\nu} \\ &= \frac{N_C}{8s} \left( \sum_{\text{spins}} L_\mu L_\nu^* \right) I^{(r)\mu\nu}.\end{aligned}\quad (4.6)$$

As in the case of  $I^{(t)\mu\nu}$ ,  $I^{(r)\mu\nu}$  depends only on the total momentum  $q = p_e + p_{\bar{e}}$  and fulfils the Ward-identity  $I^{(r)\mu\nu}q_\nu$ . Therefore we can make the same Ansatz as we had for  $I^{(t)\mu\nu}$  (2.10):

$$I^{(r)\mu\nu} = I^{(r)}(q^\mu q^\nu - g^{\mu\nu} q^2). \quad (4.7)$$

$\sigma\left(e^+e^- \rightarrow \tilde{t}_1\tilde{t}_1^*g\right)$  can therefore be computed with the same formula as  $\sigma^{(t)}$  in (2.23), with the only difference that:

$$I^{(t)\mu}{}_\mu \rightarrow I^{(r)\mu}{}_\mu. \quad (4.8)$$

For computing  $I^{(r)\mu}{}_\mu$  we introduce the following variables for parametrizing the phase space dependency of the integrand:

$$x \equiv \frac{2(p_{\tilde{t}_1} \cdot q)}{q^2}, \quad y \equiv \frac{2(p_{\tilde{t}_1^*} \cdot q)}{q^2}, \quad z \equiv \frac{2(p_g \cdot q)}{q^2}. \quad (4.9)$$

$x$ ,  $y$  and  $z$  are twice the energy of the  $\tilde{t}_1$ ,  $\tilde{t}_1^*$  or gluon, divided by total energy in the CMS. The identity

$$x + y + z = 2 \quad (4.10)$$

is often very useful. The propagators appearing in  $\hat{\Gamma}_A^{\mu\nu}$  can be expressed with  $x$  and  $y$ :

$$\begin{aligned}\frac{1}{1-y} &= \frac{q^2}{[(p_{\tilde{t}_1} + p_g)^2 - m^2]_+}, \\ \frac{1}{1-x} &= \frac{1}{-1+y+z} = \frac{q^2}{[(p_{\tilde{t}_1^*} - p_g)^2 - m^2]_+}.\end{aligned}\quad (4.11)$$

One can express the dependency of the integrand of the phase space integration using only  $y$  and  $z$ :

$$\begin{aligned}I^{(r)\mu}{}_\mu &= -C_F g_S^2 \int \underbrace{\delta_{11} + \delta_{12}}_{\text{I.R. divergences}} + \delta_{10} + \delta_{00} \text{dLIPS}_3(q), \\ \delta_{11} &= 2(\beta^4 - \beta^2) \frac{1}{(1-y)^2}, \\ \delta_{12} &= 2(\beta^4 + \beta^2) \frac{1}{(1-y)(-1+y+z)}, \\ \delta_{01} &= -8\beta^2 \frac{1}{1-y}, \\ \delta_{00} &= 2d.\end{aligned}\quad (4.12)$$

In the original integrand, there appear terms proportional to  $\frac{1}{(1-x)^2}$  and  $\frac{1}{1-x}$ , but in the phase space integral these are equivalent to  $\frac{1}{(1-y)^2}$  and  $\frac{1}{1-y}$  respectively. In (20.12) the three body phase space integral of a function depending on  $y$  and  $z$  is rewritten to an ordinary integral over  $y$  and  $z$ . Only the integrals containing divergences have to be carried out in  $d$  dimensions. Therefore, the integrals over  $\delta_{10}$  and  $\delta_{00}$  become simple. The four phase space integrals are carried out in the appendix and the results are given in (20.18), (20.22), (20.23) and (20.24). With this we obtain:

$$I^{(r)\mu}_{\mu} = -C_F g_S^2 F_3 \left\{ \frac{4\beta^3 + 2\beta^2(1 + \beta^2) \log(w)}{\epsilon_{IR}} + 6\beta + 14\beta^3 + (3 - 5\beta^2 + 12\beta^3) \log(w) \right. \\ \left. - 24\beta^3 \log(1 - w) + \beta^2(1 + \beta^2) \left[ -\frac{4\pi^2}{3} - \log(w) + \log(w)^2 \right] \right. \\ \left. + 8 \log(w) \log(1 + w) + 12Li_2(w) + 8Li_2(-w) \right\}. \quad (4.13)$$

$F_3$  is defined in (20.12). The leading order term in  $\beta$  is of  $O(\beta^5 \log(\beta))$ :

$$I^{(r)\mu}_{\mu} = -C_F g_S^2 F_3 \left[ -\frac{16}{3\epsilon_{IR}} - \frac{176}{5} + 32 \log(2) + 32 \log(\beta) \right] \beta^5 + O(\beta^7 \log(\beta)). \quad (4.14)$$

Therefore  $\sigma(e^+e^- \rightarrow \tilde{t}_1 \tilde{t}_1^* g)$  is also of  $O(\beta^5 \log(\beta))$ .

## 5. Result for the cross section at 1-loop order

For the total cross section at 1-loop order we obtain the same result as [8], where the I.R. divergences are not regulated by dimensional regularization but by introducing an infinitesimal gluon mass. Using the results in (3.24), (4.6) and (4.13) we obtain:

$$\sigma^{(1)} = \sigma^{(t)} + \delta\sigma^{(v)} + \sigma(e^+e^- \rightarrow \tilde{t}_1 \tilde{t}_1^* g) \\ = \sigma^{(t)} \left( 1 + C_F \frac{\alpha_S}{\pi} f(\beta) \right), \quad (5.1)$$

with

$$f(\beta) = \frac{1 + \beta^2}{\beta} \left[ \frac{3}{2\beta} + \log(w) \log(1 + w) + 2 \log(w) \log(1 - w) + 4Li_2(w) + 2Li_2(-w) \right] \\ - 4 \log(1 - w) - 2 \log(1 + w) + \left[ 3 + \frac{1}{\beta^3} \left( 2 - \frac{5}{4}(1 + \beta^2)^2 \right) \right] \log(w), \quad (5.2)$$

where  $\alpha_S = \frac{g_S^2}{4\pi}$ .  $\delta\sigma^{(v)}$  are the virtual corrections to the cross section.



## **Part II.**

### **Effective theory calculation**



## 6. Motivation

In the last part, we carried out a one-loop calculation for the total cross section of  $e^+e^- \rightarrow \tilde{t}_1\tilde{t}_1^*$ . If, however, the CMS energy  $\sqrt{s}$  of the  $e^+e^-$  pair is close to the threshold energy for the production of a  $\tilde{t}_1\tilde{t}_1^*$  pair, which means that  $\sqrt{s} \approx 2m$ , the perturbation series in orders of  $\alpha_S$  breaks down. The reason for this is that the corrections to the production vertex, which involve the exchange of  $n$  gluons, are enhanced by  $(1/\beta)^n$ . Thus if  $\beta \sim \alpha_S$  the size of those multi-loop contributions is actually of leading order and a one-loop calculation is thus not sufficiently close to threshold. The same problem arises for top-pair production close to threshold [28].

At one loop order we can see this explicitly by expanding (5.1) for  $\beta \sim \alpha_S \ll 1$ :

$$\begin{aligned} f(\beta) &= \frac{\pi^2}{2\beta} + O(\beta) \\ \sigma^{(1)} &= \sigma^{(t)} \left( 1 + \frac{C_F \pi \alpha_S}{2\beta} + O(\alpha_S \beta^0) \right) \end{aligned} \quad (6.1)$$

For  $\beta \sim \alpha_S$  the one-loop correction is therefore not suppressed with respect to the tree-order result. The single source of the  $O(\alpha_S/\beta)$  term is  $\delta F_{\triangle}$ , which is the virtual correction coming from the triangle diagram. Expanding (3.22) for  $\beta \ll 1$  we obtain:

$$2\text{Re } \delta F_{\triangle} = \frac{C_F \pi \alpha_S}{2\beta} + O(\alpha_S \beta^0) \quad (6.2)$$

We now define  $E$  as the energy above threshold, which means that  $\sqrt{s} = 2m + E$ .  $E$  can be calculated with the parameter  $v$ , via  $E = mv^2$ . This is understood as a definition for  $v$ . Up to corrections of  $O(v^3)$   $\beta$  and  $v$  are equivalent:

$$\beta = \sqrt{1 - \frac{4m^2}{s}} = \sqrt{1 - \frac{4m^2}{(2m + mv^2)^2}} = v - \frac{3v^3}{8} + O(v^5) \quad (6.3)$$

Therefore one could replace  $\beta$  by  $v$  within the expansions above.

The  $(1/v)^n$  enhancement of the loop integrals comes from the integration domain, where the gluons are potential. A gluon is potential if its momentum  $k = (k^0, \mathbf{k})$  is parametrically  $(mv^2, mv)$ .

As the contribution of these vertex corrections is even singular for  $v \rightarrow 0$ , one calls them "Coulomb singularities". But if  $mv^2$  was of  $O(\Lambda_{\text{QCD}})$  the behaviour of the system would not be Coulombic because of non-perturbative effects. However,  $v$  is bounded from below because of finite lifetime effects, which can be taken into account at leading order by the formal substitution [24]

$$v = \sqrt{\frac{E}{m}} = \sqrt{\frac{\sqrt{s} - 2m}{m}} \rightarrow \sqrt{\frac{\sqrt{s} - 2m + i\Gamma_{\tilde{t}_1}}{m}}. \quad (6.4)$$

$E = mv^2$  is the energy above threshold ( $\sqrt{s} = 2m + E$ ) and thus the kinetic energy of the squarks. For low values of  $E$ ,  $\Gamma_{\tilde{t}_1}$  therefore serves as an IR cut-off and one can ignore non-perturbative effects if  $\Gamma_{\tilde{t}_1} \gg \Lambda_{\text{QCD}}$ .

We will replace the power counting in powers of  $\alpha_S$  with a power counting in  $\alpha_S$  and  $v$ , where  $v \sim \alpha_S$ . This leads us to the application of "velocity non-relativistic QCD" (vNRQCD) for coloured scalars, which is an effective theory for non-relativistic squarks\* [29]. Originally vNRQCD was developed for non-relativistic bottom and top quark systems [34, 26].

---

\*To shorten notation we will often refer to "vNRQCD for coloured scalars" plainly as "vNRQCD".

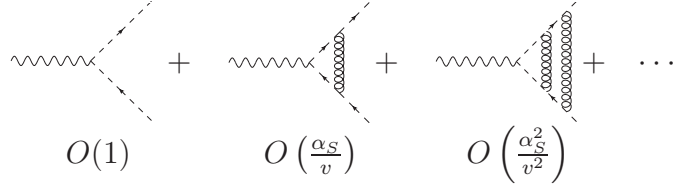


**Figure 2.:** This figure shows the order of the vertex corrections, which involve the exchange of a gluon. Close to threshold, when  $\alpha_S \sim v \ll 1$ , every gluon exchange gives a factor of  $\alpha_S/v$  at leading order. The diagrams are all of the same order and therefore the perturbative series in number of loops breaks down. The  $1/v$  enhancement comes from the integration domain, where the gluon is potential. We will later sum up all the diagrams with potential gluons, by using the Green's function of the Schrödinger equation.

There is an additional reason why it is important to switch to vNRQCD in order to describe the squarks in the non-relativistic regime. Without switching to an effective theory, the loop corrections will contain logarithms of ratios between the various scales appearing in the problem:

$$\begin{array}{lll}
 m & \text{(stop mass)} & \text{hard scale} \\
 \mathbf{p} \sim mv & \text{(momenta of the stops)} & \text{soft scale} \\
 E \sim mv^2 & \text{(kinetic energy)} & \text{ultrasoft scale}
 \end{array}$$

These logarithms can be large if  $v \ll 1$  and thus spoil the convergence of the perturbation series. By matching to an effective theory at the hard scale  $m$  we can avoid logarithms of the form  $\log(m/E)$  and  $\log(m/\mathbf{p})$ . However, the soft and the ultrasoft scale both have to be described in vNRQCD. If one does not do an additional matching to another EFT, one cannot avoid the large logarithms between the soft and ultrasoft scale by using only one renormalization scale.

Matching once more to another EFT and integrating out the soft scale is a possible approach to this problem. This additional matching has to be done at the soft scale and the theory, which only contains the ultrasoft modes, is known as potential NRQCD (pNRQCD). pNRQCD was proposed by Soto and Pineda in 1997 [41]. However, introducing two independent renormalization scales can lead to ill-defined RGEs.

The approach in vNRQCD is to introduce two renormalization scales. These scales however cannot be chosen independently but they have to be correlated in accordance with the quark equations of motion. The theory fixes the scale correlation [26] and one can parametrize the two renormalization scales in terms of the so-called *subtraction velocity*  $\nu$ :

$$\begin{aligned}
 \mu_S &= m\nu, \\
 \mu_U &= m\nu^2.
 \end{aligned} \tag{6.5}$$

Therefore, the matching for vNRQCD is done with  $\nu = 1$  and the calculation of matrix elements with  $\nu = v$ . The RGEs for  $\nu$  are called "velocity RGEs" (vRGEs) [34]. In this way one can sum up all the large logarithms. In a *fixed order perturbation theory*, where one sums up the Coulomb singularities, but not the large logarithms, the R ratio with respect to the production of a  $\mu^+\mu^-$  pair looks like [27]:

$$R = \frac{\sigma_{\tilde{t}_1\tilde{t}_1}}{\sigma_{\mu^+\mu^-}} = v^3 \sum_k \left(\frac{\alpha_S}{v}\right)^k \times \left\{ 1 \text{ (LO)}; \alpha_S, v \text{ (NLO)}; \alpha_S^2, \alpha_S, v, v^2 \text{ (NNLO)}; \dots \right\}, \tag{6.6}$$

for  $\alpha_S \sim v \ll 1$ . Here LO stands for leading order, NLO for next-to-leading order and NNLO for next-to-next-to-leading order. When the large logarithms are summed up through renormalization

group equations, one speaks of leading-logarithmic (LL), next-to-leading-logarithmic (NLL) and next-to-next-to-leading-logarithmic (NNLL) order [27]:

$$R = \frac{\sigma_{\tilde{t}_1 \tilde{t}_1}}{\sigma_{\mu^+ \mu^-}} = v^3 \sum_k \left( \frac{\alpha_S}{v} \right)^k \sum_i (\alpha_S \log(v))^i \times \left\{ 1 \text{ (LL); } \alpha_S, v \text{ (NLL); } \alpha_S^2, v^2 \text{ (NNLL); } \dots \right\}. \quad (6.7)$$

Before we introduce vNRQCD and apply it to our problem at hand we will briefly speak about the concept of effective field theories. We also need to introduce the optical theorem which gives a connection between  $\sigma_{\text{tot}}$  and the imaginary part of the forward scattering amplitude that can be calculated in vNRQCD.

## 7. Effective Field Theories

### 7.1. A short introduction to Effective Field Theories

The main idea of an effective field theory (EFT), such as vNRQCD, is that if one restricts the full theory to a certain kinematic domain, one should replace the full Lagrangian with one that is more appropriate for the description of the dynamics in this region. This new theory should describe the same physics more efficiently as long as one does not try to apply it for regions outside of its domain of validity.

This idea is not only applied in QFT, but also in other fields of physics like electrodynamics. There one for instance uses the multi-pole expansion of the electromagnetic field, to effectively describe the fields at large distances away from the source. If one probed the field at small distances to the source, the description of the multi-pole expansion would be no more valid and will even give an infinite value for fields, which in the full theory are well-behaved and finite.

In fact, a modern interpretation of Quantum field theories (QFTs), such as the standard model (SM), is to consider them as effective theories, that are only valid up to a certain energy scale. The interpretation of the infinities, that arise in loop integrals in perturbative calculations, is then that they are a consequence of the application of the SM Lagrangian for high energy modes that it can no more describe. However, if the momenta where the SM fails are much higher than the scales that appear in the loop integrals, it is justified to treat these integrals over high momenta, which showed up as infinities during the calculation, as constants. The infinities can thus be considered as constant terms, which are in fact finite but cannot be calculated with the SM. A regularization scheme makes it possible to calculate with the infinities as constant terms. One tries to absorb these terms in the coefficients of the operators that appear in the theory. A theory, where it is possible to absorb the infinities at all orders of perturbation theory without introducing an infinite number of additional operators, is called renormalizable in the classical sense. This is indeed the case for the SM\*.

However, a theory that is formally not renormalizable can still be sensible, if one can absorb the infinities at each order of a power counting scheme. The power counting is supposed to quantify the parametric size of contributions. If one is interested in the result up to a specific order in the power counting, all the contributions at higher orders, by which we mean finite terms as well as infinities, are suppressed and can thus be ignored. To understand that this is sensible one has to remember that the infinities should not be considered as large terms, but rather as finite terms, which cannot be calculated with the effective theory. Thus, it makes sense to say that infinities at a higher order in the power counting are suppressed and can thus be ignored.

One can take this interpretation one step further. By considering the integrals over high momenta, where the SM is no more valid, as constants, we are of course making an approximation. These integrals will depend on the scales that appear in our problem, although the dependency is weak, if the scale  $\Lambda_{\text{new}}$ , where new physics beyond the SM becomes relevant, is much bigger than the scales in our system. To get more accuracy one can however make an expansion in terms of the SM scales divided by  $\Lambda_{\text{new}}$ . A common strategy to search for physics beyond the SM is to match the effect of new models for processes at lower energies to local operators that are added to the SM. These operators are suppressed by  $1/\Lambda_{\text{new}}$ , therefore they are giving only small corrections at energies at the scale of the SM. These additional operators, however, spoil the renormalizability of the SM as they are generally of higher mass dimension ( $> 4$ ). It would of course be an advantage, if the SM

---

\*The proof of this is highly non-trivial. Veltman and 't Hooft solved a part of the problem, by proving that Yang-Mills theory is renormalizable [49]. This earned them the Nobel Prize in 1999.

already included such higher dimensional operators that gave us a hint about the new physics and in particular about the scale the SM breaks down.

The "Fermi Theory" [22, p. 314] is a famous example for an EFT. This was once the best available description for the weak force. The theory, however, is non-renormalizable. It includes an operator of the form:

$$O_1 = -\frac{4G_F}{\sqrt{2}}V_{ub}V_{ud}^*(\bar{u}\gamma^\mu P_L b)(\bar{d}\gamma_\mu P_L u). \quad (7.1)$$

$V_{ub}$  and  $V_{ud}$  are elements of the Cabibbo-Kobayashi-Maskawa (CKM) Matrix, which has to be determined experimentally.  $O_1$  is a four fermion operator of mass dimension 6. Nowadays we have a high energy description for the weak force as part of the SM, where it is mediated by the W and Z bosons, which are much heavier than the u, b and d quarks. As  $\frac{G_F}{\sqrt{2}} = \frac{g^2}{8M_W^2}$ , where  $M_W$  is the mass of the W boson,  $O_1$  is suppressed by  $1/M_W^2$ . In this case, the scale of the new physics  $\Lambda_{\text{new}}$  is represented by  $M_W$ . The Fermi Theory can be obtained from the SM and remains the appropriate description of the weak force for energies much smaller than  $M_W$ . Since  $O_1$  is part of a non-renormalizable theory, it already gives a hint about the scale, where the Fermi Theory breaks down. This once helped to discover the electroweak theory and in this sense it would be good if also the SM was non-renormalizable.

We want to emphasize that using the Fermi Theory instead of directly applying the full SM for processes at CMS energies  $E_{CM} \ll M_W$  is more appropriate. The reason is that by using the Fermi Theory one avoids large logarithms like  $\ln\left(\frac{M_W}{E_{CM}}\right)$  in the corrections, which could spoil the convergence of the perturbation series. In order to obtain the Fermi Theory from the SM one integrates out the high energy dynamics at the renormalization scale  $\mu = M_W$  by putting these contributions into local operators of the EFT. Then one scales the obtained theory down to  $\mu \sim E_{CM}$  via renormalization group (RG) evolution before carrying out loop integrals in the EFT. The loop integrals within the Fermi Theory contain only smaller scales and large logarithms are avoided if  $\mu$  is at the same order as these scales. This procedure eventually avoids large logarithms in the corrections, which means that they were summed up into the coefficients of local operators by the RG evolution!

Summing up the large logarithms is one of our reasons to use vNRQCD for the description of squarks production close to threshold in  $e^+e^-$  collisions. In addition the power counting of the effective theory in general quantifies the size of contributions much better than a simple expansion in the couplings. For instance we saw explicitly that the perturbation series in terms of  $\alpha_S$  did not converge in (6.1), as the one loop correction was of the same parametric size as the tree order result.

Another important EFT is called "Heavy Quark Effective Theory" (HQET), which is for instance used to describe the decay of the B mesons. HQET was constructed in 1990 by Georgi [20]. One can also obtain this theory from the SM and in this sense it contains only SM physics. But using HQET for the description of B meson systems yields much better results than a direct application of the SM. Other important EFTs include "Soft-collinear effective theory" (SCET) [7], "Chiral Perturbation Theory" (ChPT) [33] and of course "Non-relativistic QCD" (NRQCD) [12, 11]. We will use a variant of NRQCD for coloured scalars [29].

## 7.2. Matching and the threshold expansion

The Lagrangian of the EFT is a linear combination of operators where the coefficients are called *Wilson Coefficients*. These coefficients contain the dynamics of the off-shell degrees of freedom. One determines them by doing a measurement or a matching computation. As the off-shell modes are

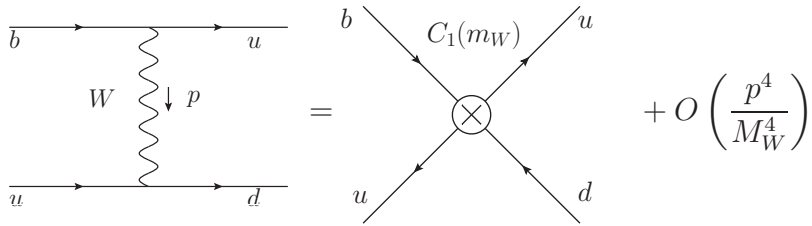


**Figure 3.:** The full theory diagram describing the exchange of the W boson can be expanded if  $p^2 \ll M_W^2$ . In the original Fermi Theory the leading order contribution is taken into account via the four fermion operator  $O_1$ .  $O_1$  was constructed such that at the matching scale  $C_1(\Lambda_{\text{new}} = M_W) = 1$ . However,  $C_1(\mu)$  will depend on the renormalization scale  $\mu$  because of renormalization group (RG) running. The reason for doing the matching at  $\mu \approx \Lambda_{\text{new}}$  is to avoid large logarithms like  $\log(\mu_{\text{match}}/M_W)$  for the matching of loop diagrams.

no more present in the EFT one often speaks about "integrating out"\* degrees of freedom in this context.

In order to match the EFT to the full theory it is crucial to define a power-counting scheme and to expand the full theory diagrams according to it. In vNRQCD we for instance expand in terms of  $\alpha_S$  and  $v$ . The brute force way for doing an expansion of a full theory Feynman diagram is to analytically calculate the diagram and to expand the result after doing the integrations. However, this is not very practical as it is usually very difficult to calculate loop diagrams analytically.

The threshold expansion is a tool to expand Feynman diagrams before doing the integration and was developed by Beneke and Smirnov [10] for the expansion of massive Feynman integrals near threshold. It is based on the method of regions with dimensional regularization and works as follows:

1. The scales in the integral have to be identified.
2. The integration domain for the loop momenta has to be split into regions in which each loop momentum is of the order of one of the scales in the problem.
3. In every region, the integrand has to be expanded in the parameters, which are small. The terms in the expansion will be integrals that are only giving contributions for the momenta in the given region (if one uses dimensional regularization, where scaleless integrals are zero).
4. After the expansion, the integrals have to be carried out over the entire integration domain in every region.

It is not easy to justify this procedure rigorously but loosely speaking it works because one uses dimensional regularization, where all integrals without scale vanish. There exist more rigorous arguments for special cases [14, 13].

A way to get a better understanding of how this method can possibly work is to do the same procedure without dimensional regularization in the cut-off scheme. One follows the same steps but introduces explicit intermediate cut-offs between the different regimes. In this case it should be clear that we obtain the correct result because with an explicit cut-off one can expand the integrand before doing the integration. If one adds the results of all the regimes, the intermediate cut-off terms will

---

\*Speaking of "integration" makes sense if one thinks in terms of the path-integral formalism.



have to disappear order by order and the final result will only depend on the cut-off of the entire integral.

The procedure using dimensional regularization works analogously. After doing the expansion in dimensional regularization, the integral will only contain scales for the given region and therefore the finite parts should be identical to the procedure where a cut-off is used. The cut-off terms will show up as divergences and dimensional regularization automatically throws away all of them, except for the logarithmic ones, which remain as  $1/\epsilon$  terms. When adding up all the regimes, the  $1/\epsilon$  terms corresponding to intermediate cut-offs will cancel, while the  $1/\epsilon$  terms corresponding to the divergences of the entire integral will remain.

Even if this analogy between the method of regions with an explicit cut-off and dimensional regularization is not at all proving that the procedure is always correct, it shows how the method is supposed to work. An explicit example for a simple one dimensional integral, which is expanded with both approaches, is given in [26].

One should always bear in mind that one has to strictly expand the integrand for the given region, if one uses the method with dimensional regularization. Otherwise one leaves scales in the integral that lead to a finite contribution from a different region. In this case one would have double counting. On the other hand, if one uses the method with explicit cut-offs, one is of course not obligated to expand the integrand.

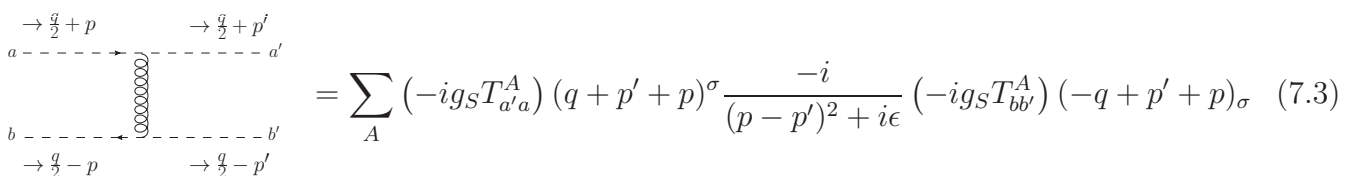
An important feature of the method is that each term in the expansion only contributes at a specific order in the power counting.

For the dynamics of a non-relativistic  $\tilde{t}_1 \bar{\tilde{t}}_1$  pair, there are four relevant regions for the loop momenta [10]:

$$\begin{aligned}
\text{hard: } (k^0, \mathbf{k}) &\sim (m, m) \\
\text{soft: } (k^0, \mathbf{k}) &\sim (mv, mv) \\
\text{potential: } (k^0, \mathbf{k}) &\sim (mv^2, mv) \\
\text{ultrasoft: } (k^0, \mathbf{k}) &\sim (mv^2, mv^2)
\end{aligned} \tag{7.2}$$

These are the relevant regions if the routing of the external momentum  $q$  is *canonical*. This means it is chosen such that it is equally split among the squarks at the production vertex and is then only routed through the squark lines. Other routings are of course possible but less practical. The relevant regimes for the loop momenta are a consequence of the pole structure of the propagators.

Up to this point we considered the threshold expansion as a purely mathematical tool for expanding Feynman diagrams. In practice, it is often helpful to do the threshold expansion before defining the fields and operators of the effective theory. By expanding the full theory diagrams one can get an idea about which are the relevant fields and interactions in the EFT. Let us for instance expand the following full theory diagram:



$$= \sum_A (-ig_s T_{a'a}^A) (q + p' + p)^\sigma \frac{-i}{(p - p')^2 + i\epsilon} (-ig_s T_{bb'}^A) (-q + p' + p)_\sigma \tag{7.3}$$

for the regime where  $p$ ,  $p'$  and  $p - p'$  are potential and  $q = (\sqrt{s}, \mathbf{0})$ . We then have:

$$\frac{-i}{(p - p')^2 + i\epsilon} = \frac{-i}{\underbrace{(p^0 - p'^0)^2}_{\ll (\mathbf{p} - \mathbf{p}')^2} - (\mathbf{p} - \mathbf{p}')^2 + i\epsilon} \approx \frac{i}{(\mathbf{p} - \mathbf{p}')^2 - i\epsilon},$$

$$(q + p' + p)^\sigma (-q + p' + p)_\sigma \approx -q^2 \approx -4m^2. \quad (7.4)$$

The leading order contribution in the potential regime therefore gives:

$$4m^2 \sum_A T_{a'a}^A T_{bb'}^A \frac{i4\pi\alpha_S}{(\mathbf{p} - \mathbf{p}')^2}. \quad (7.5)$$

In a propagator of a gluon with a potential momentum the  $i\epsilon$  is irrelevant as the momentum of a massless particle cannot get on-shell in this regime. As we can see the propagator of a gluon for the potential regime corresponds to the Fourier transform of the Coulomb potential. In vNRQCD the contributions of potential gluons at LO is also accounted for by the Coulomb potential.

The expanded diagrams of the full theory often correspond to EFT diagrams which are as well only contributing at a specific order in  $v$ . This motivates the identification of the propagators of particles in the EFT with the expanded propagators for the different regimes in the threshold expansion. In vNRQCD one for instance defines soft and ultrasoft gluons and potential squarks. We will also speak about potential gluons but in the EFT they will be represented as potentials and not as particles\*. However, one cannot strictly derive the Lagrangian of the EFT from the threshold expansion of the full theory diagrams.

---

\*They are represented as potentials because potential gluons cannot become on-shell.

## 8. Optical Theorem and Cutkosky rules

To calculate the total cross section  $\sigma_{\text{tot}}$  we will use the optical theorem, which states that the imaginary part of the forward scattering amplitude gives  $\sigma_{\text{tot}}$  up to some kinematic factors. The exact statement for a collision of two particles (e.g. an  $e^+e^-$  pair) is that

$$\sigma_{\text{tot}}(k_1, k_2 \rightarrow \text{anything}) = \frac{\text{Im}(\mathcal{M})}{2E_{\text{cm}}p_{\text{cm}}}, \quad (8.1)$$

where  $\mathcal{M}$  denotes the respective forward scattering amplitude. Here  $E_{\text{cm}} = \sqrt{s}$  and  $p_{\text{cm}}$  are the energy and momentum in the center of mass system (CMS). The optical theorem is a direct consequence of the unitarity of the S-matrix [40, p. 231].  $p_{\text{cm}}$  in our 2-particle system can be expressed with the function

$$\lambda(a, b, c) = a^2 + b^2 + c^2 - 2ab - 2ac - 2bc \quad (8.2)$$

as

$$p_{\text{cm}}^2 = \frac{1}{4s} \lambda(m_e^2, m_e^2, s) \approx \frac{s}{4}. \quad (8.3)$$

The approximation is possible as the colliding  $e^+e^-$  particles are highly relativistic. Therefore (8.1) simplifies to:

$$\sigma_{\text{tot}}(e^+e^- \rightarrow \text{anything}) = \frac{\text{Im}(\mathcal{M})}{s}. \quad (8.4)$$

In perturbative calculations unitarity manifests itself through cutting rules of Feynman diagrams [50]. With these cutting rules one can calculate  $2\text{Im}(\mathcal{M})$  (where  $\mathcal{M}$  is the matrix element of the diagram) as follows:

1. Identify the incoming and the outgoing side of the diagram.
2. Cut the diagram in all possible ways and replace each cut propagator by  $\text{Im}(2i*\text{Propagator})\theta(p_0)$ . Here  $p_0$  is the total energy that flows from the incoming to the outgoing side of the propagator. Due to  $\theta(p_0)$  the energy is only allowed to flow from the incoming to outgoing side through the cut. For a scalar propagator we therefore get the following replacement rule:

$$\frac{i}{p^2 - m^2 + i\epsilon} \rightarrow \text{Im} \left[ \frac{-2}{p^2 - m^2 + i\epsilon} \right] \theta(p^0) = 2\pi\delta(p^2 - m^2)\theta(p^0). \quad (8.5)$$

These replacements render the loop integral into a phase space integral. For our work we will need to cut through unstable (anti)stop EFT propagators:

$$\frac{i}{\frac{E}{2} \pm p_0 - \frac{\mathbf{p}^2}{2m} + i\frac{\Gamma_{\tilde{t}_1}}{2}} \rightarrow -2\text{Im} \left[ \frac{1}{\frac{E}{2} \pm p_0 - \frac{\mathbf{p}^2}{2m} + i\frac{\Gamma_{\tilde{t}_1}}{2}} \right] = \frac{i}{\frac{E}{2} \pm p_0 - \frac{\mathbf{p}^2}{2m} + i\frac{\Gamma_{\tilde{t}_1}}{2}} \Gamma_{\tilde{t}_1} \frac{-i}{\frac{E}{2} \pm p_0 - \frac{\mathbf{p}^2}{2m} - i\frac{\Gamma_{\tilde{t}_1}}{2}}. \quad (8.6)$$

Note that in this case the  $\theta$  function is always 1, as  $m + \frac{E}{2} \pm p_0$  is the total energy going through the propagators and  $E \pm p_0 \ll m$ . Therefore we have that  $\theta(m + \frac{E}{2} \pm p_0) = 1$ .

3. Conjugate the propagators at the outgoing side of the diagram.
4. Multiply the vertices at the outgoing side of the diagram by  $(-1)$ .
5. Sum over all cuts.

We want to point out that the cutting rules illustrate that there is a close connection between phase space and loop integrals.

## 9. Operators and fields in vNRQCD

In this section the fields and operators of vNRQCD are presented.

### 9.1. The label formalism of vNRQCD

The hard modes are integrated out in vNRQCD and are put into the Wilson coefficients of local operators. For the other contributions one needs a systematic way to separate the scales. To achieve this one splits the momenta of the squarks into three different parts:

$$(p^0, \mathbf{p}) = (m, 0) + (0, \mathbf{p}) + (k^0, \mathbf{k}). \quad (9.1)$$

Here we have  $\mathbf{p} \sim mv$  and  $k^0 \sim \mathbf{k} \sim mv^2$ . The  $(m, 0)$  part of the momentum is of no relevance for the dynamics. The idea is to divide the soft momentum space into quadratic boxes of length  $mv^2$  and to describe the modes of each box with a different field  $\psi_{\mathbf{p}}$ . These fields are labelled with the soft momentum, which is why the procedure is called the "label formalism". They are treated as different particles with different propagators and interactions.  $\psi_{\mathbf{p}}$  and  $\psi_{\mathbf{p}'}$  interact via the exchange of soft gluons and potentials but not via ultrasoft gluons. An illustration of the label-formalism is given in figure 4. The original non-relativistic squark field can be written as:

$$\psi(x) = e^{-imt} \sum_{\mathbf{p}} e^{i\mathbf{p}\cdot\mathbf{x}} \psi_{\mathbf{p}}(x). \quad (9.2)$$

$\mathbf{p}$  runs over soft momenta. This means that only the ultrasoft momentum in (9.1) remains a continuous variable. The ultrasoft momentum operator applied on  $\psi_{\mathbf{p}}(x)$  is therefore  $-i\nabla\psi_{\mathbf{p}}(x)$ .

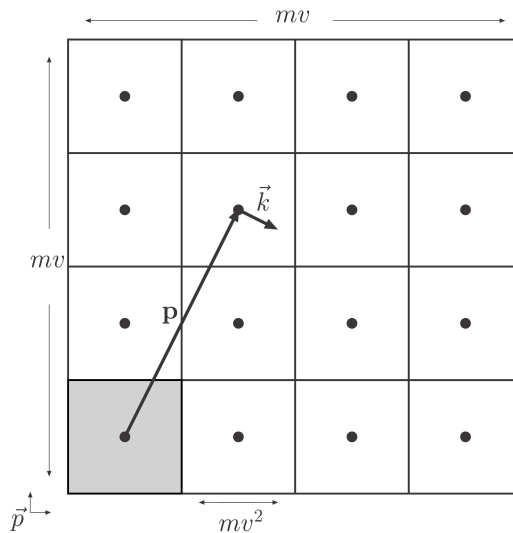


**Figure 4.:** The soft momentum space is split into quadratic boxes of length  $mv^2$ . In vNRQCD there is a separate squark field for each box, which describes the modes therein. The figure is taken from [47].

In vNRQCD one performs an analogous redefinition for the antisquark  $\chi_{\mathbf{p}}(x)$  and the soft gluon fields  $A_{\mathbf{p}}^{\mu}(x)$ . Technically the label formalism enables us to obtain a separation of the soft and ultrasoft scale, which is necessary for a consistent power-counting in  $v$  [47]. It was originally proposed to construct HQET [20].

## 9.2. $e^+e^-$ fields in the EFT

Because the effective theory needs to describe the  $\tilde{t}_1\tilde{t}_1$  production only in the threshold region and in the c.m. frame, the initial states  $a_{\tau'}^{c\dagger}(\mathbf{k}')a_{\tau}^{\dagger}(\mathbf{k})|0\rangle^*$  can be assumed to fulfil  $s = (k + k')^2 \approx 4m^2$  and  $\mathbf{k} = -\mathbf{k}'$ . Furthermore we can assume for simplicity that the  $e^+e^-$  pair collides along the  $z$ -axis and therefore the four momenta are determined for a given  $s$ :

$$\begin{aligned} k^{\mu} &= \left( \frac{\sqrt{s}}{2}, \frac{\sqrt{s}}{2}\hat{\mathbf{e}}_z \right), \\ k'^{\mu} &= \left( \frac{\sqrt{s}}{2}, -\frac{\sqrt{s}}{2}\hat{\mathbf{e}}_z \right), \end{aligned} \quad (9.3)$$

where  $\hat{\mathbf{e}}_z$  is the unit vector in  $z$ -direction. We can now define the fields  $e_-(x)$ ,  $e_+(x)$  that contain all the relevant modes of the  $e^+e^-$  particles:

$$\begin{aligned} e_-(x) &= \sum_{\tau, \sqrt{s}} a_{\tau}(\mathbf{k})u_{\tau}(\mathbf{k})e^{-ikx}, \\ e_+(x) &= \sum_{\tau, \sqrt{s}} a_{\tau'}^{c\dagger}(\mathbf{k}')v_{\tau}(\mathbf{k}')e^{ik'x}, \end{aligned} \quad (9.4)$$

where  $u_{\tau}$  and  $v_{\tau}$  are the electron, positron Dirac spinors. The sum over the c.m. energies denoted by  $\sqrt{s}$  is restricted to the threshold region. As we specified that the incoming  $e^+e^-$  pair is colliding along the  $z$ -axis, we can restrict ourselves to the momenta in (9.3) and do not need an integration over angles. In the phase factors one uses the 4-momenta relative to  $(m, \mathbf{0})$ :

$$\begin{aligned} \hat{k}^{\mu} &= \left( \frac{\sqrt{s}}{2} - m, \frac{\sqrt{s}}{2}\hat{\mathbf{e}}_z \right), \\ \hat{k}'^{\mu} &= \left( \frac{\sqrt{s}}{2} - m, -\frac{\sqrt{s}}{2}\hat{\mathbf{e}}_z \right). \end{aligned} \quad (9.5)$$

## 9.3. Operators in vNRQCD

A part of the operators and their Wilson coefficients presented here will not be calculated explicitly but will be important at higher order. Whenever this is the case the corresponding terms are coloured red.

The bilinear part of the Lagrangian contains the kinetic terms for the squarks (including an effective description of the decay of the squarks) and the coupling to the ultrasoft gluons:

$$\begin{aligned} \mathcal{L}_{\text{bilinear}} &= \sum_{\mathbf{p}} \left\{ \psi_{\mathbf{p}}^* \left[ iD^0 - \frac{(\mathbf{p} - i\mathbf{D})^2}{2m} + \frac{\mathbf{p}^4}{8m^3} \right. \right. \\ &\quad \left. \left. + \frac{i}{2}\Gamma_{\tilde{t}_1} \left( 1 - \frac{\mathbf{p}^2}{2m^2} \right) + \dots \right] \psi_{\mathbf{p}} + (\psi \rightarrow \chi, T \rightarrow \bar{T}) \right\}. \end{aligned} \quad (9.6)$$

The form of  $\mathcal{L}_{\text{bilinear}}$  is constrained by reparametrization and gauge invariance. Due to reparametrization invariance soft momenta always have to appear together with  $-i\nabla$  [34]. And one obtains manifest

---

\*  $a_{\tau'}^{c\dagger}$ ,  $a_{\tau}^{\dagger}(\mathbf{k})$  are the  $e^+$ ,  $e^-$  creation operators.

gauge invariance of  $\mathcal{L}_{\text{bilinear}}$  by substituting  $\partial^0$  and  $\nabla$  with covariant derivatives:

$$\begin{aligned} D^0 &= \partial^0 + igA^0(x), \\ \mathbf{D} &= \nabla - ig\mathbf{A}(x). \end{aligned} \quad (9.7)$$

Due to the partial Fourier transformation in (9.2)  $\psi_{\mathbf{p}}(x)$  and  $\chi_{\mathbf{p}}(x)$  only contain ultrasoft fluctuations. Therefore  $i\partial^0$  and  $-i\nabla$  refer to the ultrasoft energies and momenta relative to the soft momentum  $\mathbf{p}$ . For this reason the covariant derivative does also only contain the ultrasoft gluon field. The kinematic corrections which are coloured red are of NNLO.

The potential part contains the interactions due to the exchange of potential gluons:

$$\mathcal{L}_{\text{pot}} = - \sum_{\mathbf{p}, \mathbf{p}'} \tilde{\mu}_S^{2\epsilon} \tilde{V}(\mathbf{p}, \mathbf{p}') \psi_{\mathbf{p}'}^* \psi_{\mathbf{p}} \chi_{-\mathbf{p}'}^* \chi_{-\mathbf{p}} + \dots, \quad (9.8)$$

with

$$\begin{aligned} \tilde{V}(\mathbf{p}, \mathbf{p}') &= (T^A \otimes \bar{T}^A) \left[ \frac{\mathcal{V}_c^{(T)}}{\mathbf{k}^2} + \frac{\mathcal{V}_k^{(T)} \pi^2}{m|\mathbf{k}|} + \frac{\mathcal{V}_r^{(T)}(\mathbf{p}^2 + \mathbf{p}'^2)}{2m^2 \mathbf{k}^2} + \frac{\mathcal{V}_2^{(T)}}{m^2} + \dots \right] \\ &+ (1 \otimes 1) \left[ \frac{\mathcal{V}_c^{(1)}}{\mathbf{k}^2} + \frac{\mathcal{V}_k^{(1)} \pi^2}{m|\mathbf{k}|} + \frac{\mathcal{V}_2^{(1)}}{m^2} + \dots \right], \end{aligned} \quad (9.9)$$

where  $\mathbf{k} = \mathbf{p}' - \mathbf{p}$  and

$$\begin{aligned} \mathcal{V}_c^{(T)}(1) &= 4\pi\alpha_S(m), & \mathcal{V}_r^{(T)}(1) &= 4\pi\alpha_S(m), & \mathcal{V}_2^{(T)}(1) &= -\pi\alpha_S(m), \\ \mathcal{V}_c^{(1)}(1) &= 0, & \mathcal{V}_k^{(1)}(1) &= 0, \end{aligned}$$

$$\mathcal{V}_k^{(T)}(1) = \alpha_S^2(m) \left( \frac{7C_A}{8} - \frac{C_d}{8} \right), \quad \mathcal{V}_k^{(1)}(1) = \alpha_S^2(m) \frac{C_1}{2} \quad (9.10)$$

$$C_d = 8C_F - 3C_A, \quad C_1 = \frac{1}{2}C_F C_A - C_F^2, \quad (9.11)$$

$$C_F = \frac{4}{3}, \quad C_A = 3. \quad (9.12)$$

As discussed before the contribution of  $\mathcal{V}_c^{(T,1)}$  in scattering diagrams in figure 2 is of  $O(\alpha_S/v)$ . It is therefore important to sum up all these loop diagrams, which we do by using the respective Coulomb Green's function.  $\mathcal{V}_2^{(1,T)}$  and  $\mathcal{V}_r(T)$  contribute at  $O(\alpha_S v)$ . They are the analog of the Breit-Fermi potentials known from QED.  $\mathcal{V}_k^{(1,T)}$  are generated by one-loop diagrams and are therefore of  $O(\alpha_S^2 v^0)$ . For squark-antisquark scattering in a color singlet state only the linear combination of coefficients  $\mathcal{V}_i^{(s)} = -C_F \mathcal{V}_i^{(T)} + \mathcal{V}_i^{(1)}$  is relevant [29].

We need currents that describe the production and annihilation of a  $\bar{t}_1 \tilde{t}_1$  pair from/to an  $e^+ e^-$  pair. In the full theory the production/annihilation happens via the exchange of a photon or Z boson.

With the fields in the EFT we define the squarks production and annihilation currents as follows:

$$O_{\mathbf{p}}^j = \psi_{\mathbf{p}}^* 2p^j \chi_{-\mathbf{p}}^*, \quad (9.13)$$

$$O_{V,\mathbf{p}}^{(n)} = \left[ \bar{e}_+ \gamma_j (\hat{E}/m)^n e_- \right] O_{\mathbf{p}}^j, \quad (9.14)$$

$$O_{A,\mathbf{p}}^{(n)} = \left[ \bar{e}_+ \gamma_j \gamma_5 (\hat{E}/m)^n e_- \right] O_{\mathbf{p}}^j, \quad (9.15)$$

$$\mathcal{L}_{\text{cur}} = \sum_{\mathbf{p}} \tilde{\mu}_S^\epsilon \left[ C_V O_{V,\mathbf{p}} + C_A O_{A,\mathbf{p}} + C_V^{(1)} O_{V,\mathbf{p}}^{(1)} + C_A^{(1)} O_{A,\mathbf{p}}^{(1)} + \dots \right] + H.c., \quad (9.16)$$

where we use the notation  $O_{V/A,\mathbf{p}} \equiv O_{V/A,\mathbf{p}}^{(0)}$ .

At the matching scale the Wilson coefficients are:

$$C_V^{\text{Born}} = -\frac{2\pi\alpha}{m} \left[ \frac{\tilde{Q}_\gamma}{4m^2} - \frac{2}{\sin(2\theta_W)} v_e \frac{\tilde{Q}_Z}{4m^2 - m_Z^2} \right], \quad (9.17)$$

$$C_A^{\text{Born}} = \frac{2\pi\alpha}{m} \frac{2}{\sin(2\theta_W)} a_e \frac{\tilde{Q}_Z}{4m^2 - m_Z^2}, \quad (9.18)$$

$$C_{V/A}(\nu) = C_{V/A}^{\text{Born}} c(\nu) + C_{V/A}^{\text{loop}}. \quad (9.19)$$

$c(\nu)$  contains the hard matching conditions, which are in our case the contribution of the hard gluon loops at one loop level. In (3.23) we obtained  $Re\delta F$  which are the radiative corrections to the real part of the form factor of the full theory current at 1-loop level. One can show that in  $\delta F$  the  $O(\alpha_S\beta^0)$  terms without the I.R. divergences correspond to the NLO contribution from the hard gluon loops. Furthermore, the hard gluon loops do not contribute to the imaginary part of  $\delta F$  and therefore up to NLO  $c(\nu)$  is simply the  $O(\alpha_S\beta^0)$  part of  $Re\delta F$  without the  $1/\epsilon_{IR}$  terms:

$$c(\nu = 1) = 1 - \frac{\alpha_S(m)}{\pi} C_F. \quad (9.20)$$

$c(\nu)$  has a NLL running which is calculated in [29].  $\frac{\alpha_S(m)}{\pi} C_F$  is a correction of the order of 5% for  $m$  between 100 and 500 GeV.  $C_{V/A}^{\text{loop}}$  is a NNLO correction that accounts for hard electroweak contributions.  $C_{V/A}^{(1)}$  contains NNLO effects from the expansion of the full theory current.

## 9.4. Factorization formula

We want to calculate  $\sigma_{\text{tot}}$ , which is given by  $Im(\mathcal{M})/s$  due to the optical theorem. With spin averaging we obtain:

$$\frac{1}{4} \sum_{\text{spins}} \mathcal{M} = \left[ C_V(\nu)^2 L_{VV}^{lk} + C_A(\nu)^2 L_{AA}^{lk} + C_V(\nu) C_A(\nu) (L_{AV}^{lk} + L_{VA}^{lk}) \right] \mathcal{A}^{lk}(\nu), \quad (9.21)$$



with

$$\begin{aligned}
 \mathcal{A}^{lk} &= i \sum_{\mathbf{p}, \mathbf{p}'} \int d^d x e^{i\hat{q}x} \langle 0 | T O_{\mathbf{p}}^{l\dagger}(x) O_{\mathbf{p}'}^k(0) | 0 \rangle, \tag{9.22} \\
 L_{VV}^{lk} &= \frac{1}{4} \sum_{\tau, \tau'} [\bar{v}_{\tau'}(\mathbf{k}') \gamma^l u_{\tau}(\mathbf{k})] [\bar{u}_{\tau}(\mathbf{k}) \gamma^k v_{\tau'}(\mathbf{k}')], \\
 L_{AA}^{lk} &= \frac{1}{4} \sum_{\tau, \tau'} [\bar{v}_{\tau'}(\mathbf{k}') \gamma^l \gamma^5 u_{\tau}(\mathbf{k})] [\bar{u}_{\tau}(\mathbf{k}) \gamma^k \gamma^5 v_{\tau'}(\mathbf{k}')], \\
 L_{VA}^{lk} &= \frac{1}{4} \sum_{\tau, \tau'} [\bar{v}_{\tau'}(\mathbf{k}') \gamma^l u_{\tau}(\mathbf{k})] [\bar{u}_{\tau}(\mathbf{k}) \gamma^k \gamma^5 v_{\tau'}(\mathbf{k}')], \\
 L_{AV}^{lk} &= \frac{1}{4} \sum_{\tau, \tau'} [\bar{v}_{\tau'}(\mathbf{k}') \gamma^l \gamma^5 u_{\tau}(\mathbf{k})] [\bar{u}_{\tau}(\mathbf{k}) \gamma^k v_{\tau'}(\mathbf{k}')], \tag{9.23}
 \end{aligned}$$

where  $\hat{q} = (E, \mathbf{0})$ . Due to spin averaging we have  $L_{VV}^{lk} = L_{AA}^{lk}$  and  $L_{AV}^{lk} = L_{VA}^{lk} = 0$ . We define

$$\begin{aligned}
 L^{lk} &= L_{VV}^{lk} (= L_{AA}^{lk}) \\
 &= \frac{1}{2} (k + k')^2 (\delta^{lk} - \hat{e}_z^l \hat{e}_z^k) \\
 L^{ll} &= s. \tag{9.24}
 \end{aligned}$$

As  $\mathcal{A}^{lk}$  does only depend on  $E$ , we get

$$\mathcal{A}^{lk} = \mathcal{A}^{jj} \frac{\delta^{lk}}{3}, \tag{9.25}$$

where the sum over  $j$  is implied. Finally we obtain:

$$\begin{aligned}
 \sigma_{\text{tot}}(\nu) &= \frac{1}{4s} \sum_{\text{spins}} \text{Im}(\mathcal{M}) \\
 &= \frac{1}{3} \text{Im} [(C_V(\nu)^2 + C_A(\nu)^2) \mathcal{A}^{jj}(\nu)]. \tag{9.26}
 \end{aligned}$$

## 10. Greenfunction

In (6.1) we saw that the perturbation series in  $\alpha_S$  breaks down for  $v \sim \alpha_S$ . The diagrams in figure (2) are all of the same order and we need to sum up the leading order contribution of every diagram. The leading order contribution stems from the exchange of potential gluons. In the effective theory the contribution of potential gluons is taken into account by  $\mathcal{L}_{\text{pot}}$  given in (9.8). As we will see, we can make use of the Greenfunction of the Schrödinger equation to sum up the contribution of potential gluons in all the diagrams given in figure (2).

### 10.1. Definition of the Greenfunction and its Fourier transform

The Green operator  $G_C(E)$  of non-relativistic Quantum mechanics for an unstable squark antisquark pair that interact via a Coulomb potential is defined by the following operator equation:

$$\left( \hat{H} - (E + i\Gamma_{\tilde{t}_1}) \right) G_C(E) = \left( \frac{\hat{\mathbf{p}}^2}{m} + V_C(|\hat{\mathbf{x}}|) - (E + i\Gamma_{\tilde{t}_1}) \right) G_C(E) = \mathbf{1}, \quad (10.1)$$

where

$$V_C(r) \equiv -\frac{a}{r}. \quad (10.2)$$

The Greenfunction  $G(\mathbf{x}', \mathbf{x}, E)$  is defined as:

$$G_C(\mathbf{x}', \mathbf{x}, E) \equiv \langle \mathbf{x}' | G_C(E) | \mathbf{x} \rangle, \quad (10.3)$$

where  $|\mathbf{x}\rangle$  represents a two particle state of a squark and anti-squark that are separated by  $\mathbf{x}$ . The normalisation of these states is given by:

$$\langle \mathbf{x}' | \mathbf{x} \rangle = \delta^3(\mathbf{x}' - \mathbf{x}). \quad (10.4)$$

$G_C(\mathbf{x}', \mathbf{x}, E)$  therefore fulfils the following differential equation:

$$\left( -\frac{\nabla_{\mathbf{x}'}^2}{m} + V_C(x') - (E + i\Gamma_{\tilde{t}_1}) \right) G_C(\mathbf{x}', \mathbf{x}, E) = \delta^3(\mathbf{x}' - \mathbf{x}). \quad (10.5)$$

The Fourier transform of  $G_C(\mathbf{x}', \mathbf{x}, E)$ :

$$\tilde{G}_C(\mathbf{p}', \mathbf{p}, E) \equiv \int d^3\mathbf{x}' d^3\mathbf{x} e^{-i\mathbf{p}' \cdot \mathbf{x}'} G_C(\mathbf{x}', \mathbf{x}, E) e^{i\mathbf{p} \cdot \mathbf{x}} \quad (10.6)$$

satisfies the equation:

$$\left( \frac{\mathbf{p}'^2}{m} - (E + i\Gamma_{\tilde{t}_1}) \right) \tilde{G}_C(\mathbf{p}', \mathbf{p}, E) + \int \frac{d^3k}{(2\pi)^3} \tilde{V}_C(\mathbf{p}', \mathbf{k}) \tilde{G}_C(\mathbf{k}, \mathbf{p}, E) = (2\pi)^3 \delta^3(\mathbf{p}' - \mathbf{p}), \quad (10.7)$$

where  $\tilde{V}_C(\mathbf{p}', \mathbf{p})$  is the Fourier transform of  $V_C(x)$ :

$$\tilde{V}_C(\mathbf{p}', \mathbf{p}) \equiv \int d^3\mathbf{x}' d^3\mathbf{x} e^{-i\mathbf{p}' \cdot \mathbf{x}'} V_C(|\mathbf{x}' - \mathbf{x}|) e^{i\mathbf{p} \cdot \mathbf{x}} = \frac{-4\pi a}{(\mathbf{p} - \mathbf{p}')^2} \quad (10.8)$$

Solving this equation iteratively we obtain:

$$\tilde{G}_C^{(0)} = \frac{(2\pi)^3 \delta^3(\mathbf{p}' - \mathbf{p})}{\frac{\mathbf{p}^2}{m} - (E + i\Gamma_{\tilde{t}_1})}, \quad (10.9)$$

$$\left( \frac{\mathbf{p}'^2}{m} - (E + i\Gamma_{\tilde{t}_1}) \right) \tilde{G}_C^{(i+1)}(\mathbf{p}', \mathbf{p}, E) = - \int \frac{d^3k}{(2\pi)^3} \tilde{V}_C(\mathbf{p}', \mathbf{k}) \tilde{G}_C(\mathbf{k}, \mathbf{p}, E), \quad (10.10)$$

where  $\tilde{G}_C^{(i)}$  is the  $O(\alpha_S^i)$  contribution in  $\tilde{G}_C$ . For the  $O(\alpha_S)$  part we get:

$$\tilde{G}_C^{(1)}(\mathbf{p}', \mathbf{p}, E) = - \frac{1}{\frac{\mathbf{p}'^2}{m} - (E + i\Gamma_{\tilde{t}_1})} \tilde{V}_C(\mathbf{p}', \mathbf{p}) \frac{1}{\frac{\mathbf{p}^2}{m} - (E + i\Gamma_{\tilde{t}_1})}. \quad (10.11)$$

## 10.2. Connection between the Greenfunction and ladder diagrams

Via (10.10) it will be possible to establish a connection between  $\tilde{G}_C(\mathbf{p}', \mathbf{p}, E)$  and the following sum of diagrams in Fourier space\*:

$$\tilde{G}_D(p', p, E) \equiv \begin{array}{c} \begin{array}{ccccccc} \rightarrow \frac{q}{2} + p & & \rightarrow \frac{q}{2} + p & & \rightarrow \frac{q}{2} + p' & & \rightarrow \frac{q}{2} + p & & \rightarrow \frac{q}{2} + p' \\ \hline & & \text{---} & & \text{---} & & \text{---} & & \text{---} \\ & & \text{---} & & \text{---} & & \text{---} & & \text{---} \\ \hline \rightarrow \frac{q}{2} - p & & \rightarrow \frac{q}{2} - p & & \rightarrow \frac{q}{2} - p' & & \rightarrow \frac{q}{2} - p & & \rightarrow \frac{q}{2} - p' \end{array} \\ + \\ \begin{array}{ccccccc} \rightarrow \frac{q}{2} + p & & \rightarrow \frac{q}{2} + p & & \rightarrow \frac{q}{2} + p' & & \rightarrow \frac{q}{2} + p & & \rightarrow \frac{q}{2} + p' \\ \hline & & \text{---} & & \text{---} & & \text{---} & & \text{---} \\ & & \text{---} & & \text{---} & & \text{---} & & \text{---} \\ \hline \rightarrow \frac{q}{2} - p & & \rightarrow \frac{q}{2} - p & & \rightarrow \frac{q}{2} - p' & & \rightarrow \frac{q}{2} - p & & \rightarrow \frac{q}{2} - p' \end{array} \\ + \dots \end{array} \quad (10.12)$$

One calls these diagrams *ladder diagrams* for obvious reasons.  $G_D(p', p, E)$  includes the external propagators. To establish this connection we are following the ideas in [50, p. 62]. As we are only summing up the contribution of potential gluons, each gluon propagator corresponds to one insertion of the potential given in (9.9):

$$\begin{array}{c} \rightarrow \frac{q}{2} + p \\ \hline \text{---} \\ \hline \rightarrow \frac{q}{2} + p' \\ \hline \rightarrow \frac{q}{2} - p \\ \hline \text{---} \\ \hline \rightarrow \frac{q}{2} - p' \end{array} = -i\tilde{V}(\mathbf{p}, \mathbf{p}') = -i\tilde{V}(\mathbf{p}', \mathbf{p}). \quad (10.13)$$

In the following we will set  $a = \frac{C_F \mathcal{V}_c^{(T)}(\nu)}{4\pi}$  such that  $\tilde{V}_C(\mathbf{p}, \mathbf{p}')$  is the leading order of  $\tilde{V}(\mathbf{p}', \mathbf{p})$ . We denote the  $O(\alpha_S^i)$  contribution of  $\tilde{G}_D$  with  $\tilde{G}_D^{(i)}$ . Let us first look at the  $O(\alpha_S)$  contribution of  $\tilde{G}_D(p', p, E)$ :

$$\begin{aligned} \tilde{G}_D^{(1)}(p', p, E) &\equiv \begin{array}{c} \rightarrow \frac{q}{2} + p \\ \hline \text{---} \\ \hline \rightarrow \frac{q}{2} + p' \\ \hline \rightarrow \frac{q}{2} - p \\ \hline \text{---} \\ \hline \rightarrow \frac{q}{2} - p' \end{array} = h(p)(-i)\tilde{V}(\mathbf{p}', \mathbf{p})h(p'), \\ h(p) &\equiv \frac{i}{\frac{E}{2} + p^0 - \frac{\mathbf{p}^2}{2m} + i\frac{\Gamma_{\tilde{t}_1}}{2}} \frac{i}{\frac{E}{2} - p^0 - \frac{\mathbf{p}^2}{2m} + i\frac{\Gamma_{\tilde{t}_1}}{2}} \end{aligned} \quad (10.14)$$

\*For the definition of  $\tilde{G}_D$  the diagrams are understood to include the external propagators.

For  $i \geq 1$  we define  $\tilde{G}^{(i)}(\mathbf{p}', \mathbf{p}, E)$  as:

$$\begin{aligned}\tilde{G}^{(i)}(\mathbf{p}', \mathbf{p}, E) &= i \frac{\tilde{G}_D^{(i)}(p', p, E)}{f(p')f(p)}, \\ f(p) &\equiv \frac{i}{\frac{E}{2} + p^0 - \frac{\mathbf{p}^2}{2m} + i\frac{\Gamma_{\tilde{\epsilon}_1}}{2}} + \frac{i}{\frac{E}{2} - p^0 - \frac{\mathbf{p}^2}{2m} + i\frac{\Gamma_{\tilde{\epsilon}_1}}{2}} \\ &= (-i)h(p)(E + i\Gamma_{\tilde{\epsilon}_1} - \frac{\mathbf{p}^2}{m}).\end{aligned}\quad (10.15)$$

Here  $\tilde{G}^{(i)}(\mathbf{p}', \mathbf{p}, E)$  is already written as a function depending only on  $(\mathbf{p}', \mathbf{p}, E)$  and not on  $(p^0, p'^0)$ . This is obviously true for  $\tilde{G}^{(1)}$ , which apart from  $\tilde{V}_C \rightarrow \tilde{V}$  is identical to  $\tilde{G}_C^{(1)}$  given in (10.11). Using the following iteration formula we will prove by induction that  $\tilde{G}^{(i)}$  is independent of  $(p^0, p'^0)$  for  $i \geq 1$ :

$$\begin{array}{c} \begin{array}{ccccccc} \rightarrow \frac{q}{2} + p & & \rightarrow \frac{q}{2} + p' & & \rightarrow \frac{q}{2} + p & \rightarrow \frac{q}{2} + p' + k & \rightarrow \frac{q}{2} + p' \\ \vdots & \dots & \vdots & \dots & \vdots & \vdots & \vdots \\ \rightarrow \frac{q}{2} - p & & \rightarrow \frac{q}{2} - p' & & \rightarrow \frac{q}{2} - p & \rightarrow \frac{q}{2} - p' - k & \rightarrow \frac{q}{2} - p' \end{array} \\ = \\ \begin{array}{ccccccc} \rightarrow \frac{q}{2} + p & & \rightarrow \frac{q}{2} + p' & & \rightarrow \frac{q}{2} + p & \rightarrow \frac{q}{2} + p' + k & \rightarrow \frac{q}{2} + p' \\ \vdots & \dots & \vdots & \dots & \vdots & \vdots & \vdots \\ \rightarrow \frac{q}{2} - p & & \rightarrow \frac{q}{2} - p' & & \rightarrow \frac{q}{2} - p & \rightarrow \frac{q}{2} - p' - k & \rightarrow \frac{q}{2} - p' \end{array} \end{array} \cdot \quad (10.16)$$

Algebraically this means:

$$\tilde{G}_D^{(i+1)}(p', p, E) = \int \frac{d^4 k}{(2\pi)^4} (-i) \tilde{V}(\mathbf{p}', \mathbf{k}) \underbrace{\tilde{G}_D^{(i)}(k, p, E)}_{(-i)f(p)\tilde{G}^{(i)}f(k)} \frac{if(p')}{E + i\Gamma_{\tilde{\epsilon}_1} - \frac{\mathbf{p}'^2}{m}}. \quad (10.17)$$

If we now assume that  $\tilde{G}^{(i)}$  is independent of  $(p^0, p'^0)$  we can rewrite this equation as follows:

$$\begin{aligned}\left(\frac{\mathbf{p}'^2}{m} - (E + i\Gamma_{\tilde{\epsilon}_1})\right) \tilde{G}_D^{(i+1)}(p', p, E) &= \\ if(p) \int \frac{d^3 k}{2\pi} \tilde{V}(\mathbf{p}', \mathbf{k}) \tilde{G}^{(i)}(\mathbf{k}, \mathbf{p}, E) \underbrace{\int \frac{dk^0}{2\pi} f(k) f(p')}_{=1},\end{aligned}\quad (10.18)$$

where  $\int \frac{dk^0}{2\pi} f(k) = 1$  can easily be shown by an explicit computation. We obtain the following iteration formula for  $\tilde{G}^{(i)}$ :

$$\left(\frac{\mathbf{p}'^2}{m} - (E + i\Gamma_{\tilde{\epsilon}_1})\right) \tilde{G}^{(i+1)}(\mathbf{p}', \mathbf{p}, E) = - \int \frac{d^3 k}{2\pi} \tilde{V}(\mathbf{p}', \mathbf{k}) \tilde{G}^{(i)}(\mathbf{k}, \mathbf{p}, E). \quad (10.19)$$

This proves that  $\tilde{G}^{(i+1)}$  is independent of  $(p^0, p'^0)$  if this is the case for  $\tilde{G}^{(i)}$ . The key point is that except for  $\tilde{V}_C \rightarrow \tilde{V}$  this iteration formula is identical to (10.10). We still did not define  $\tilde{G}^{(0)}$  but this shows that for  $i \geq 1$  we have that  $\tilde{G}^{(i)} \rightarrow \tilde{G}_C^{(i)}$  for  $\tilde{V} \rightarrow \tilde{V}_C$ . It is now tempting to define:

$$\tilde{G}^{(0)}(\mathbf{p}', \mathbf{p}, E) \equiv \tilde{G}_C^{(0)}(\mathbf{p}', \mathbf{p}, E). \quad (10.20)$$

With this definition we have:

$$\tilde{G}(\mathbf{p}', \mathbf{p}, E) \equiv \sum_{i=0}^{\infty} \tilde{G}^{(i)}(\mathbf{p}', \mathbf{p}, E) \rightarrow \tilde{G}_C(\mathbf{p}', \mathbf{p}, E) \text{ for } \tilde{V} \rightarrow \tilde{V}_C. \quad (10.21)$$

This means that  $\tilde{G}_C$  gives the leading order contribution to  $\tilde{G}$ . If we wanted to calculate  $\tilde{G}$  beyond leading order we would need to solve (10.7) for  $\tilde{V}_C \rightarrow \tilde{V}$ .

However, if we also defined  $\tilde{G}^{(0)}$  via (10.15) we would get a slightly different result and therefore the equation:

$$\tilde{G}_D(p', p, E) = f(p')(-i)\tilde{G}(\mathbf{p}', \mathbf{p}, E)f(p) \quad (10.22)$$

is not entirely correct for this definition of  $\tilde{G}^{(0)}$ . For all the contributions from  $O(\alpha_S)$  onwards the equation is of course correct, there is only a subtle disagreement in the  $O(\alpha_S^0)$  term. Let us have a look at the 4-point function in position space corresponding to  $\tilde{G}_D^{(0)}(p', p, E)$ :

$$\begin{aligned} G_D^{(0)}(x'_1, x'_2, x_1, x_2) &\equiv \begin{array}{c} \xrightarrow{x_1} \quad \xrightarrow{x'_1} \\ \xleftarrow{x_2} \quad \xleftarrow{x'_2} \end{array} \\ &= \int \frac{d^4 p_1}{(2\pi)^4} \frac{d^4 p_2}{(2\pi)^4} e^{-ip_1(x'_1 - x_1)} e^{-ip_2(x'_2 - x_2)} \frac{i}{p_1^0 - \frac{\mathbf{p}_1^2}{2m} + i\frac{\Gamma_{\tilde{t}_1}}{2}} \frac{i}{p_2^0 - \frac{\mathbf{p}_2^2}{2m} + i\frac{\Gamma_{\tilde{t}_1}}{2}} \end{aligned} \quad (10.23)$$

If equation (10.22) was true for  $O(\alpha_S^0)$  we would have to get the same expression for  $G_D^{(0)}$  by interpreting

$$\tilde{G}_D^{(0)}(p', p, E) \equiv f(p')(-i)\tilde{G}^{(0)}(\mathbf{p}', \mathbf{p}, E)f(p) \quad (10.24)$$

as a 4-point Feynman diagram in the CMS and transforming it to the respective 4-point function in position space. To do this we first need to give an expression for  $\tilde{G}_D^{(0)}$  outside of the CMS:

$$\begin{aligned} \tilde{G}_D^{(0)}(p'_1, p'_2, p_1, p_2) &= \left( \frac{i}{p_1^0 - \frac{\mathbf{p}_1^2}{2m} + i\frac{\Gamma_{\tilde{t}_1}}{2}} + \frac{i}{p_2^0 - \frac{\mathbf{p}_2^2}{2m} + i\frac{\Gamma_{\tilde{t}_1}}{2}} \right) \frac{(-i)(2\pi)^3 \delta^3 \left( \frac{\mathbf{p}_1 - \mathbf{p}_2}{2} - \frac{\mathbf{p}'_1 - \mathbf{p}'_2}{2} \right)}{\frac{\mathbf{p}_1^2}{2m} + \frac{\mathbf{p}_2^2}{2m} - (p_1^0 + p_2^0 + i\Gamma_{\tilde{t}_1})} \\ &\quad \left( \frac{i}{p_1'^0 - \frac{\mathbf{p}_1'^2}{2m} + i\frac{\Gamma_{\tilde{t}_1}}{2}} + \frac{i}{p_2'^0 - \frac{\mathbf{p}_2'^2}{2m} + i\frac{\Gamma_{\tilde{t}_1}}{2}} \right). \end{aligned} \quad (10.25)$$

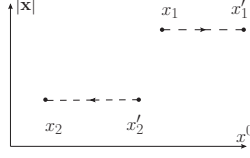
Doing the transformation of  $\tilde{G}_D^{(0)}$  into position space we obtain:

$$\begin{aligned} G_D^{(0)}(x'_1, x'_2, x_1, x_2) &\equiv \int \frac{d^4 p_1}{(2\pi)^4} \frac{d^4 p_2}{(2\pi)^4} \frac{d^4 p'_1}{(2\pi)^4} \frac{d^4 p'_2}{(2\pi)^4} e^{ip_1 x_1} e^{ip_2 x_2} e^{-ip'_1 x'_1} e^{-ip'_2 x'_2} \\ &\quad \tilde{G}_D^{(0)}(p'_1, p'_2, p_1, p_2) (2\pi)^4 \delta^4(p_1 + p_2 - p'_1 - p'_2) \\ &= \int \frac{d^4 p_1}{(2\pi)^4} \frac{d^4 p_2}{(2\pi)^4} e^{-ip_1(x'_1 - x_1)} e^{-ip_2(x'_2 - x_2)} \\ &\quad \frac{i}{p_1^0 - \frac{\mathbf{p}_1^2}{2m} + i\frac{\Gamma_{\tilde{t}_1}}{2}} \frac{i}{p_2^0 - \frac{\mathbf{p}_2^2}{2m} + i\frac{\Gamma_{\tilde{t}_1}}{2}} \theta(x'_2 - x_1^0) \theta(x'_1 - x_2^0). \end{aligned} \quad (10.26)$$

$G_D^{(0)}$  is identical to  $G_D^{(0)}$  except for the two  $\theta$  functions. Because of the pole structure of the propagators we could multiply  $G_D^{(0)}$  and  $G_D^{(0)}$  with the two  $\theta$  functions

$$\theta(x'_1 - x_1^0) \theta(x'_2 - x_2^0) \quad (10.27)$$

without changing these expressions. Therefore the difference in  $G_D^{(0)}$  and  $G_D^{(0)}$  is that  $G_D^{(0)} \neq 0$  only if  $x_1^0, x_2^0 < x_1', x_2'$ , while for  $G_D^{(0)} \neq 0$   $x_1^0 < x_1'$  and  $x_2^0 < x_2'$  suffices. This, for instance, means that the 4-point function corresponding to the following diagram:



is contained in  $\tilde{G}_D^{(0)}$  but not in  $\tilde{G}_D^{(0)}$ . However, as we need to close the *ladder diagrams* at one side\* the points for which  $G_D^{(0)}$  and  $G_D^{(0)}$  differ are anyway of no importance for our calculation. This means that we can use equation (10.22) without making a mistake.

With (10.22) we therefore found a connection between the sum of *ladder diagrams* involving potential gluons (10.12) and the Greenfunction of the Schrödinger equation (10.3). For the  $O(\alpha_S^0)$  contribution (10.22) is not entirely correct but the difference vanishes if we close the diagrams at one side. For summing up the leading order contribution we will use the Greenfunction of the Schrödinger equation for the Coulomb potential (10.5). For taking into account higher order corrections we would have to solve (10.10) for  $\tilde{V}_C \rightarrow \tilde{V}$ .

### 10.3. Solution for the Coulomb Greenfunction

In [35] the solution of (10.5) is given:

$$G_C(\mathbf{x}, \mathbf{y}, E) = \sum_{l=0}^{\infty} (2l+1)(xy)^l P_l(\mathbf{x} \cdot \mathbf{y}/(xy)) G_l(x, y, k), \quad (10.28)$$

where  $k \equiv -i\sqrt{m(E + i\Gamma_{\bar{t}})}$ .  $P_l(x)$  are the Legendre polynomials and

$$G_l(x, y, k) \equiv \frac{mk}{2\pi} (2k)^{2l} e^{-k(x+y)} \sum_{r=0}^{\infty} \frac{L_r^{2l+1}(2kx) L_r^{2l+1}(2ky) r!}{(r+l+1-\rho)(r+2l+1)!}. \quad (10.29)$$

The parameter  $\rho$  is defined as

$$\rho \equiv \frac{am}{2k}. \quad (10.30)$$

$L_r^k(x)$  are the associated Laguerre polynomials, which are defined as:

$$L_r^k(x) \equiv \frac{e^x x^{-k}}{r!} \left( \frac{d}{dx} \right)^r e^{-x} x^{r+k}. \quad (10.31)$$

---

\*As shown in figure 2.

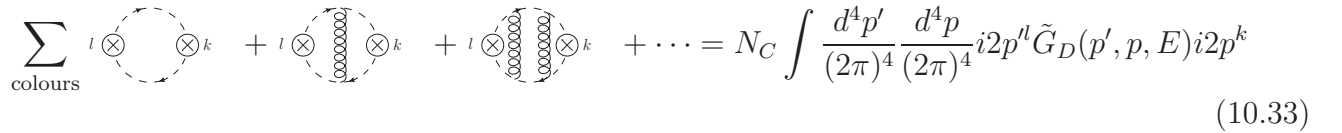
### 10.4. Calculating $\mathcal{A}^{lk}$ at leading order

We will close the sum of *ladder diagrams* with the P-wave squarks production vertex given by the operator  $O_p^j$  defined in (9.13) that generates the Feynman rule:



$$= i2p^j, \quad (10.32)$$

where  $j$  is a spatial index. The S-wave quark production vertex, which one would use in the calculation of  $\sigma(e^+e^- \rightarrow t\bar{t})$ , is constant in the momentum  $p$  and therefore diagrams with the S-wave production vertex will be less divergent for  $p \rightarrow \infty$ . We can therefore expect more UV divergences than in the case of top production [28]. Closing  $\tilde{G}_D$  on both sides with this vertex we obtain:



$$\sum_{\text{colours}} i \otimes \text{---} \otimes k + i \otimes \text{---} \otimes k + i \otimes \text{---} \otimes k + \dots = N_C \int \frac{d^4p'}{(2\pi)^4} \frac{d^4p}{(2\pi)^4} i2p^l \tilde{G}_D(p', p, E) i2p^k \quad (10.33)$$

We call the leading order contribution of this expression  $i\mathcal{A}_C^{lk}$  and calculate it via  $\tilde{G}_C$  by making use of (10.22):

$$\begin{aligned} i\mathcal{A}_C^{lk} &\equiv N_C \int \frac{d^4p'}{(2\pi)^4} \frac{d^4p}{(2\pi)^4} i2p^l f(p) (-i) \tilde{G}_C(\mathbf{p}', \mathbf{p}, E) f(p') i2p^k \\ &= i4N_C \underbrace{\int \frac{d^3p'}{(2\pi)^3} \frac{d^3p}{(2\pi)^3} p^l \tilde{G}_C(\mathbf{p}', \mathbf{p}, E) p^k}_{\equiv \tilde{G}_C^{P, lk}(E)}, \end{aligned} \quad (10.34)$$

where we used  $\int \frac{dp^0}{2\pi} f(p) = 1$ .  $i\mathcal{A}_C^{lk}$  is the leading order contribution of  $i\mathcal{A}^{lk}$  defined in (9.22). As the function  $\tilde{G}_C^{P, lk}(E)$  only depends on a scalar we can make the Ansatz:

$$\begin{aligned} \tilde{G}_C^{P, lk}(E) &= \tilde{G}_C^P \frac{\delta^{lk}}{3}, \\ \tilde{G}_C^P(E) &= \int \frac{d^3p'}{(2\pi)^3} \frac{d^3p}{(2\pi)^3} (\mathbf{p} \cdot \mathbf{p}') \tilde{G}_C(\mathbf{p}', \mathbf{p}, E). \end{aligned} \quad (10.35)$$

In [24] the result for  $\tilde{G}_C^P$  is given:

$$\begin{aligned} \tilde{G}_C^P(E) &= \frac{m^4}{4\pi} \left\{ iv^3 - av^2 \left[ \ln \left( \frac{-iv}{\nu} \right) - 1 + \ln 2 + \gamma_E + \Psi \left( 1 - \frac{ia}{2v} \right) \right] \right. \\ &\quad \left. + i \frac{va^2}{4} - \frac{a^3}{4} \left[ \ln \left( \frac{-iv}{\nu} \right) - \frac{7}{4} + \ln 2 + \gamma_E + \Psi \left( 1 - \frac{ia}{2v} \right) \right] \right\} \\ &\quad + \frac{m^4}{16\pi} \left( \frac{1}{\epsilon} + \frac{2}{3} \right) \left( v^2 a + \frac{a^3}{8} \right), \end{aligned} \quad (10.36)$$

where the *subtraction velocity*  $\nu$  is defined in (6.5),  $v = \sqrt{\frac{E+i\Gamma_{\tilde{t}_1}}{m}}$ ,  $\Gamma_E$  is the so-called Euler Gamma and  $\Psi(z) = \frac{\Gamma'(z)}{\Gamma(z)}$  is the Digamma function. The UV divergences in  $\tilde{G}_C^P$  were regularized by dimensional regularization with the renormalization scale  $\mu_S = m\nu$ .

In all the terms up to  $O(\alpha_S^3)$  there appear UV divergences. Although there are no  $\frac{1}{\epsilon}$  terms of  $O(\alpha_S^0)$  and  $O(\alpha_S^2)$  these contributions are nevertheless divergent, but dimensional regularization does not see them as it throws away power divergences and only keeps logarithmic ones as  $\frac{1}{\epsilon}$  terms. There is for instance a linear divergence in  $Im(\tilde{G}_C^P)$  at  $O(\alpha_S^0)$  which is invisible in dimensional regularization. Therefore we find divergences in the imaginary part of  $\tilde{G}_C^P(E)$  in the contributions up to  $O(\alpha_S)$ . For  $\Gamma_{\tilde{t}_1} \rightarrow 0$  the divergences in the imaginary part disappear.

This can be understood by calculating the imaginary part of  $\mathcal{A}_C^{lk}$  via the Cutkosky rules. For a finite value of  $\Gamma_{\tilde{t}_1}$  the cut squark propagators are not replaced by a  $\delta$ -function but the replacement rule given in (8.6) has to be used. This means that for a finite  $\Gamma_{\tilde{t}_1}$  one has to integrate over outgoing squark momenta that are far away from its mass-shell. The UV divergences in  $Im(\mathcal{A}_C^{lk})$  appear because vNRQCD is not a good description if the outgoing squark states are not close to on-shell. For  $\Gamma_{\tilde{t}_1} \rightarrow 0$  the outgoing squark momenta are set on-shell by the  $\delta$ -function and therefore vNRQCD is not used to predict the amplitudes to off-shell squark states. The divergences in  $Im(\mathcal{A}_C^{lk})$  are called *phase space (PS) divergences* as they are related to an unrestricted PS integration. The *PS divergences* do not appear if we use vNRQCD to calculate a cross section with kinematic cuts on the final states. In the next section we will define such an observable which we can calculate in vNRQCD itself. For calculating  $\sigma_{\text{tot}}$  additional high energy information is needed, even at leading order.

If we would not encounter divergences in  $Im(\mathcal{A}^{lk})$  at leading order the prediction of vNRQCD for amplitudes to off-shell squark states would still be insensible and divergences related to this can appear at higher orders. This for instance happens for  $e^+e^- \rightarrow \bar{t}t$ , where  $\tilde{G}_D$  is closed by the S-wave production vertex. In this case  $\tilde{G}_C^P(E)$  is replaced by

$$\tilde{G}_C^S(E) \equiv \int \frac{d^3p'}{(2\pi)^3} \frac{d^3p}{(2\pi)^3} \tilde{G}_C(\mathbf{p}', \mathbf{p}, E) = G_C(0, 0, E), \quad (10.37)$$

which has a finite imaginary part. Nevertheless one encounters *PS divergences* if one goes to higher orders [28].

## 10.5. Calculating the P-wave Coulomb vertex function

In the next section we will solve the problem of the phase space divergences encountered in (10.36) by introducing kinematic cuts on the final states. To do this we will make use of the following vertex function, which we obtain by closing the diagrams in  $\tilde{G}_D$  with the vertex given in (10.32) at one side:

$$j \otimes \left( \begin{array}{c} \nearrow \\ \searrow \end{array} \right) + \dots = \int \frac{d^4p}{(2\pi)^4} i2p^j \tilde{G}_D(p', p, E) \quad (10.38)$$



We call the leading order contribution of this expression  $\gamma_C$ . The imaginary part of  $\tilde{G}_C^P(E)$  can be obtained by using the optical theorem:

$$\begin{aligned}
2Im\left(\tilde{G}_C^P(E)\right) &= \\
&\int \frac{d^4k}{(2\pi)^4} \frac{\gamma_C^l(k, E)}{h(k)} \frac{i}{\frac{E}{2} + k^0 - \frac{\mathbf{k}^2}{2m} + i\frac{\Gamma_{\tilde{t}_1}}{2}} \Gamma_{\tilde{t}_1} \frac{-i}{\frac{E}{2} + k^0 - \frac{\mathbf{k}^2}{2m} - i\frac{\Gamma_{\tilde{t}_1}}{2}} \\
&\frac{i}{\frac{E}{2} - k^0 - \frac{\mathbf{k}^2}{2m} + i\frac{\Gamma_{\tilde{t}_1}}{2}} \Gamma_{\tilde{t}_1} \frac{-i}{\frac{E}{2} - k^0 - \frac{\mathbf{k}^2}{2m} - i\frac{\Gamma_{\tilde{t}_1}}{2}} \left(\frac{\gamma_C^l(k, E)}{h(k)}\right)^* = \\
&\int \frac{d^4k}{(2\pi)^4} \Gamma_{\tilde{t}_1}^2 \gamma_C^l(k, E) (\gamma_C^l(k, E))^*, \tag{10.39}
\end{aligned}$$

where the sum over  $l$  is implied. The advantage of this expression for  $Im\left(\tilde{G}_C^P(E)\right)$  is that we can restrict the loop momentum  $k$  to avoid the PS divergences. As we will see the restriction of integration domain for  $k$  corresponds to a kinematic cut on the final states.  $\gamma_C$  can be calculated via  $\tilde{G}_C$ :

$$\gamma_C^j(p', E) \equiv \int \frac{d^4p}{(2\pi)^4} i2p^j f(p) (-i) \tilde{G}_C(\mathbf{p}', \mathbf{p}, E) f(p') = 2 \underbrace{\int \frac{d^3p}{(2\pi)^3} p^j \tilde{G}_C(\mathbf{p}', \mathbf{p}, E) f(p')}_{\equiv \tilde{\mathbf{g}}_C^{P,j}(\mathbf{p}', E)}, \tag{10.40}$$

where we used  $\int \frac{dp^0}{2\pi} f(p) = 1$ .

$$\tilde{\mathbf{g}}_C^P(\mathbf{p}', E) = \int \frac{d^3p}{(2\pi)^3} \mathbf{p} \tilde{G}_C(\mathbf{p}', \mathbf{p}, E) = \int d^3x' d^3x \frac{d^3p}{(2\pi)^3} \underbrace{\mathbf{p} e^{i\mathbf{p}\cdot\mathbf{x}}}_{-i\nabla_{\mathbf{x}} e^{i\mathbf{p}\cdot\mathbf{x}}} G_C(\mathbf{x}', \mathbf{x}, E) e^{-i\mathbf{p}'\cdot\mathbf{x}'} \tag{10.41}$$

$$\begin{aligned}
&= \int d^3x' d^3x \underbrace{\frac{d^3p}{(2\pi)^3} e^{i\mathbf{p}\cdot\mathbf{x}}}_{\delta^3(\mathbf{x})} (+i) \nabla_{\mathbf{x}} G_C(\mathbf{x}', \mathbf{x}, E) e^{-i\mathbf{p}'\cdot\mathbf{x}'} \\
&= i \int d^3x' [\nabla_{\mathbf{x}} G_C(\mathbf{x}', \mathbf{x}, E)]_{\mathbf{x}=0} e^{-i\mathbf{p}'\cdot\mathbf{x}'}. \tag{10.42}
\end{aligned}$$

In (10.28) the partial wave decomposition of  $G_C$  is given. For  $[\nabla_{\mathbf{x}} G_C(\mathbf{x}', \mathbf{x}, E)]_{\mathbf{x}=0}$  only the  $l = 1$  term, which corresponds to the P-wave contribution, remains. The contributions for  $l \geq 2$  vanish because of the  $(xx')^l$  term that is multiplied with  $G_l$ : If one does not apply at least  $l$  derivatives in  $\mathbf{x}$  on  $(xx')^l$  the resulting term vanishes for  $\mathbf{x} = 0$ . The  $l = 0$  contribution of  $G_C(\mathbf{x}', \mathbf{x}, E)$  is independent of the direction of  $\mathbf{x}, \mathbf{x}'$  and can therefore be written as a function  $g(x', x, E)$ . Using (10.41) we obtain that the  $l = 0$  contribution is of the form:

$$\int d^3x' d^3x \underbrace{\frac{d^3p}{(2\pi)^3} \mathbf{p} e^{i\mathbf{p}\cdot\mathbf{x}} g(x', x, E)}_{=0} e^{-i\mathbf{p}'\cdot\mathbf{x}'} = 0. \tag{10.43}$$

The key point is that  $\int d^3x \frac{d^3p}{(2\pi)^3} \mathbf{p} e^{i\mathbf{p}\cdot\mathbf{x}} g(x', x, E)$  is a vector but only depends on scalars which means that the expression has to vanish. Applying the derivative on the  $l = 1$  term we get:

$$\tilde{\mathbf{g}}_C^P(\mathbf{p}', E) = 3i \int d^3x' e^{-i\mathbf{p}'\cdot\mathbf{x}'} \mathbf{x}' G_1(x', 0, k), \tag{10.44}$$

where  $G_l$  is defined in (10.29) and  $k \equiv i\sqrt{m(E + i\Gamma_{\tilde{t}_1})}$ . The function  $\tilde{\mathbf{g}}_C^P(\mathbf{p}', E)$  is a vector that only depends on  $\mathbf{p}'$  and we can therefore make the Ansatz:

$$\begin{aligned}\tilde{\mathbf{g}}_C^P(\mathbf{p}', E) &= \tilde{g}_C^P(|\mathbf{p}'|, E)\mathbf{p}', \\ \tilde{g}_C^P(|\mathbf{p}'|, E) &= \frac{3i}{\mathbf{p}'^2} \int d^3x' e^{-i\mathbf{p}'\cdot\mathbf{x}'} (\mathbf{x}' \cdot \mathbf{p}') G_1(x', 0, k).\end{aligned}\quad (10.45)$$

Using spherical coordinates and doing the angular integration we get:

$$\tilde{g}_C^P(p', E) = \frac{12\pi}{p'^2} \int_0^\infty dx' x'^2 \left( \frac{\sin(p'x')}{p'x'} - \cos(p'x') \right) G_1(x', 0, k). \quad (10.46)$$

For one argument set to zero  $G_l$  simplifies to [35]:

$$G_l(x, 0, k) = \frac{mk}{2\pi} (2k)^{2l} e^{-kx} \frac{\Gamma(l+1-\rho) U(l+1-\rho, 2l+2, 2kx)}{(2l+1)!}. \quad (10.47)$$

Where  $U(a, b, z)$  is the usual definition of the confluent hypergeometric function [4]. The last integral can be carried out using the relation 7.621.3 in [21, p. 822]. After several reformations one can express the result as a sum of derivatives of the hypergeometric function  ${}_2F_1(a, b, c, z)$ :

$$\begin{aligned}\tilde{g}_C^P(p, E) &= \frac{1}{2p^3} m \left\{ 2p + ik(1-\rho) \left[ {}_2F_1^{(1,0,0,0)} \left( 0, 2, 1-\rho, \frac{k+ip}{2k} \right) \right. \right. \\ &\quad \left. \left. - {}_2F_1^{(1,0,0,0)} \left( 0, 2, 1-\rho, \frac{k-ip}{2k} \right) \right] + ik \left[ {}_2F_1^{(1,0,0,0)} \left( 0, 3, 2-\rho, \frac{k-ip}{2k} \right) \right. \right. \\ &\quad \left. \left. - {}_2F_1^{(1,0,0,0)} \left( 0, 3, 2-\rho, \frac{k+ip}{2k} \right) \right] \right\},\end{aligned}\quad (10.48)$$

where

$$\begin{aligned}{}_2F_1(a, b, c, z) &\equiv \sum_{n=0}^{\infty} \frac{(a)_n (b)_n}{(c)_n} \frac{z^n}{n!}, \\ {}_2F_1^{(1,0,0,0)}(a, b, c, z) &\equiv \frac{d}{da} {}_2F_1(a, b, c, z).\end{aligned}\quad (10.49)$$

## 11. Concept of Phase Space Matching

### 11.1. Restricting the PS integrals to the domain of vNRQCD

In the last section we encountered divergences in the phase space (PS) integrals which appeared due to finite lifetime effects. In our power counting, where  $\Gamma_{\tilde{t}_1} = O(v^2)$ , these divergences are even of leading order. This problem arises because we have to restrict the PS integration to a domain where the expansions in NRQCD are still sensible. In the following this will be achieved by introducing kinematic cuts on the final states.

As the stop and antistop are not stable, we calculate the cross section to final states to which they can decay. Depending on the point in the parameter space of the "minimal supersymmetric standard model" (MSSM) the decay to different final states will be dominant. The following processes can have a significant contribution to the total cross section:

$$\begin{aligned}
 e^+e^- &\rightarrow b\tilde{\chi}_i^+\bar{b}\tilde{\chi}_j^-, \\
 e^+e^- &\rightarrow t\tilde{\chi}_i^0\bar{t}\tilde{\chi}_j^0, \\
 e^+e^- &\rightarrow b\tilde{\chi}_i^+\bar{t}\tilde{\chi}_j^0, \\
 e^+e^- &\rightarrow t\tilde{\chi}_i^0\bar{b}\tilde{\chi}_j^-.
 \end{aligned} \tag{11.1}$$

Here  $\tilde{\chi}_i^\pm$   $i = 1, 2$  are charginos and  $\tilde{\chi}_i^0$   $i = 1, 2, 3, 4$  are neutralinos. We define what we call the invariant mass of the stop and antistop squarks  $M_{\tilde{t}_1, \tilde{\bar{t}}_1}$  through the reconstructed masses of the systems coming from their decays, e.g.:

$$\begin{aligned}
 M_{\tilde{t}_1}^2 &= p_{\tilde{t}_1}^2 = (p_b + p_{\tilde{\chi}_1^+})^2, \\
 M_{\tilde{\bar{t}}_1}^2 &= p_{\tilde{\bar{t}}_1}^2 = (p_{\bar{b}} + p_{\tilde{\chi}_1^-})^2.
 \end{aligned} \tag{11.2}$$

The selection prescriptions are cuts on the (anti)stop invariant masses of the form:

$$(m - \Delta M) \leq M_{\tilde{t}_1, \tilde{\bar{t}}_1} \leq (m + \Delta M). \tag{11.3}$$

This is a constraint on the off-shellness in the (anti)stop propagators. In vNRQCD the (anti)squark propagator is given as:

$$\frac{i}{p_0 - \frac{\mathbf{p}^2}{2m} + i\frac{\Gamma_{\tilde{t}_1}}{2}}. \tag{11.4}$$

Ignoring relativistic NNLL corrections (11.3) means that the off-shellness in the propagators must fulfill:

$$-\Delta M \leq p_0 - m - \frac{\mathbf{p}^2}{2m} \leq \Delta M. \tag{11.5}$$

This means that phase space integrations are limited by the scales  $\Delta M$  for  $p^0$  and  $\Lambda \equiv \sqrt{2m\Delta M}$  for  $\mathbf{p}$ . In the power counting we will take  $\Lambda \sim m\sqrt{v}$ , which implies  $\Delta M \sim mv$ . Numerically the scales  $\Delta M$  and  $\sqrt{2m\Delta M}$  have to be sufficiently below  $m$ , such that for all the  $\tilde{t}_1\tilde{\bar{t}}_1$  phase space configurations that pass the constraint (11.3) the NRQCD expansions are valid.

In vNRQCD the final states to which the (anti)stop particles can decay are integrated out. But cuts on the invariant mass of the system of decay products of the (anti)stop can be implemented in

vNRQCD itself although it is an unstable-particle EFT [9, p. 11]. For reproducing the phase space integrals over these final states one needs to cut the (anti)stop propagators via (8.6) and in order to restrict these phase space integrals to a domain, where vNRQCD is still a valid approximation, we have to apply invariant mass cuts according to (11.3) on the (anti)stop propagators. We will refer to these as "phase space cuts" (PS cuts) and call (anti)stop propagators, which pass the PS cuts, "resonant". In figure 5 we illustrate the meaning of the cut of a simple vNRQCD diagram as a phase space integration.

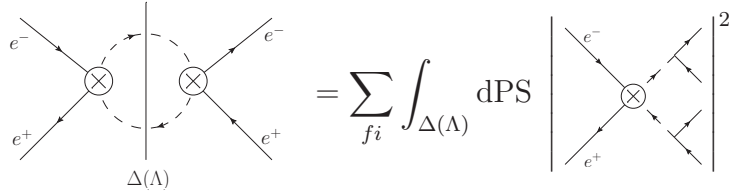


**Figure 5.:** Here the meaning of a cut through the unstable (anti)stop propagators is illustrated.  $\sum_{fi}$  sums over all the possible final states to which stop and antistop can decay to.

## 11.2. Power Counting

As we count  $\frac{\Lambda}{m}$  as  $O(\sqrt{v})$  we will get terms that are of some half integer power of  $v$  in the power counting. We will encounter terms that are parametrically enhanced by  $v^{-1/2}$  with respect to LO or NLO terms and call them  $LO_+$  or  $NLO_+$  respectively. In (10.36) we encountered divergences in  $\text{Im}\tilde{G}_C^P$ . After introducing an invariant mass cut-off these divergences disappear but, as we will see explicitly in section 13.1, they are replaced by PS corrections that are partly of  $LL_+$  order.

Dimensional regularization for instance throws away the linear divergence in  $\text{Im}\tilde{G}_C^P$ . After introducing an invariant mass cut-off we get a term which is of  $LO_+$  instead of this linear divergence, as we will see in (13.8). The  $\frac{1}{\epsilon}$  divergence corresponds to a  $LL_+$  term.

It should be noted that the corrections due to the introduction of cut-off can be parametrically bigger than the result in dimensional regularization.

## 11.3. Analysis of the cut propagator

The Cutkosky cut of the NRQCD propagator  $\frac{i}{\frac{E}{2} \pm p_0 - \frac{\mathbf{p}^2}{2m} + i\frac{\Gamma_{\tilde{t}}}{2}}$  corresponds to a PS integral in the full theory. By understanding this correspondence in more detail one can restrict the PS integral to a specific final state and include relativistic corrections. The full relativistic version of this propagator that is also including loop corrections is:

$$\frac{2mi}{\left(\frac{q}{2} \pm p\right)^2 - m^2 + \Pi\left(\left(\frac{q}{2} \pm p\right)^2\right)}, \quad (11.6)$$

where  $q = (2m + E, \mathbf{0})$ .  $i\Pi$  is the sum of all self-energy diagrams. When cutting this propagator via the Cutkosky rules we obtain:

$$\frac{2mi}{\left(\frac{q}{2} \pm p\right)^2 - m^2 + \Pi} \rightarrow -2\text{Im} \left( \frac{2m}{\left(\frac{q}{2} \pm p\right)^2 - m^2 + \Pi} \right) = \frac{2mi}{\left(\frac{q}{2} \pm p\right)^2 - m^2 + \Pi} \left( \frac{2\text{Im}\Pi}{2m} \right) \left( \frac{2mi}{\left(\frac{q}{2} \pm p\right)^2 - m^2 + \Pi} \right)^*. \quad (11.7)$$

For simplicity we did not write the  $\left(\frac{q}{2} \pm p\right)^2$  dependence of  $\Pi$ . Instead of calculating the total cross section, we can choose to restrict ourselves to the imaginary part coming from a single final state. This is also what we will do eventually. If we for instance want to calculate  $e^+e^- \rightarrow b \tilde{\chi}_i^+ \bar{b} \tilde{\chi}_j^-$  we will replace  $\text{Im}\Pi$  at the cuts by the imaginary part stemming only from the self-energy diagram with a  $\tilde{\chi}_i^+$  and a b-quark in the loop:

$$2\text{Im}\Pi(k^2) \rightarrow 2\text{Im}\tilde{\Pi}(k^2) \equiv 2\text{Im} \left[ (-i) \begin{array}{c} k \rightarrow \\ \tilde{t}_1 \end{array} \begin{array}{c} \curvearrowright \\ \tilde{\chi}_i^+ \\ \curvearrowleft \\ b \end{array} \rightarrow - \right] = \begin{array}{c} \curvearrowright \\ \curvearrowleft \end{array} \rightarrow - \quad (11.8)$$

The  $\Pi$  in the denominator of the propagators corresponds to virtual corrections and there one has to sum up all the self-energy contributions, even if one calculates the cross section to some specific final state. The partial decay width  $\tilde{\Gamma}_{\tilde{t}_1}$  is closely related to  $\text{Im}\tilde{\Pi}(m^2)$ :

$$\text{Im}\tilde{\Pi}(m^2) = m\tilde{\Gamma}_{\tilde{t}_1} \quad (11.9)$$

Replacing  $\frac{\text{Im}\tilde{\Pi}(k^2)}{m}$  at the cut by  $\tilde{\Gamma}_{\tilde{t}_1}$  is therefore a leading order approximation:

$$\frac{\text{Im}\tilde{\Pi}(k^2)}{m} = \tilde{\Gamma}_{\tilde{t}_1} \left( 1 + \underbrace{O\left(\frac{k^2 - m^2}{m^2}\right)}_{O(v^2)} \right). \quad (11.10)$$

We define  $\tilde{\Gamma}_{\tilde{t}_1}(k^2)$  as a function that depends on the invariant mass of the ingoing  $\tilde{t}_1$  propagator:

$$\tilde{\Gamma}_{\tilde{t}_1}(k^2) \equiv \frac{\text{Im}\tilde{\Pi}(k^2)}{\sqrt{k^2}}. \quad (11.11)$$

At higher orders the  $k^2$  dependence in the  $\frac{\text{Im}\tilde{\Pi}(k^2)}{m}$  term at the cut has to be taken into account. If we include the next term in the expansion, we obtain:

$$\frac{\text{Im}\tilde{\Pi}(k^2)}{m} = \tilde{\Gamma}_{\tilde{t}_1} - \frac{\text{Im}(\delta\tilde{Z})(k^2 - m^2)}{m} + \tilde{\Gamma}_{\tilde{t}_1} O(v^4). \quad (11.12)$$

Where  $\delta Z$  is the wave-function renormalization in the on-shell scheme, which is related to  $\Pi$  as given in (3.7).  $\delta\tilde{Z}$  is the contribution of the wave function renormalization due to  $\tilde{\Pi}$ . The imaginary part of  $\delta Z$  will be called  $\delta Z^{\text{abs}}$  in the following:

$$\begin{aligned} \text{Im}(\delta\tilde{Z}_{\text{abs}}) &\equiv \text{Im}(\delta\tilde{Z}), \\ \delta\tilde{Z}_{\text{abs}} &= -i \frac{1}{2m^2} \left( \tilde{\Gamma}_{\tilde{t}_1} + 2m^2 \left. \frac{d\tilde{\Gamma}_{\tilde{t}_1}}{dk^2} \right|_{k^2=m^2} \right). \end{aligned} \quad (11.13)$$

If we are interested in the cross section to some specific final state at leading order (11.7) becomes

$$\frac{i}{\frac{E}{2} \pm p_0 - \frac{\mathbf{p}^2}{2m} + i\frac{\Gamma_{\tilde{t}_1}}{2}} \rightarrow \frac{i}{\frac{E}{2} \pm p_0 - \frac{\mathbf{p}^2}{2m} + i\frac{\Gamma_{\tilde{t}_1}}{2}} \tilde{\Gamma}_{\tilde{t}_1} \frac{-i}{\frac{E}{2} \pm p_0 - \frac{\mathbf{p}^2}{2m} - i\frac{\Gamma_{\tilde{t}_1}}{2}}. \quad (11.14)$$

Except for  $\Gamma_{\tilde{t}_1} \rightarrow \tilde{\Gamma}_{\tilde{t}_1}$  this is identical to the substitution (8.6), which is used for calculating the total cross section. If we want to go to higher orders there are two different corrections that we need to consider: The first comes from the expansion of the propagators left and right of the cut in (11.7). Corrections to the propagator are dealt with by introducing 2-point insertions into the EFT. This means that the non-relativistic propagator in the EFT remains unchanged but one adds 2-point vertices, which include kinematic effects and self-energy corrections. Unlike in (11.12) also the real part of the self energy contributes to these corrections.

These 2-point vertices are suppressed by  $O(v^2)$  if  $\mathbf{k} \sim mv$ . However, as  $\Lambda$ , which represents the cut-off on the three momenta, is counted as  $O(m\sqrt{v})$ ,  $\mathbf{k}$  can be of  $O(m\sqrt{v})$ . Therefore the corrections due to the expansion of the propagator left and right of the cut are of  $\text{NLO}_+$ . If we would not implement an invariant mass cut-off the corrections due to these 2-point vertices would be of NNLO in dimensional regularization.

The second effect is due to the  $k^2$  dependence of  $Im\tilde{\Pi}(k^2)$  at the cut and can be taken into account via the expansion we did in (11.12). From this expression it is clear that the effect is proportional to  $\delta\tilde{Z}_{\text{abs}}$ . It can be shown that doing this expansion at one cut is equivalent to using (11.14) and multiplying the connected vertices with  $(1 + \delta\tilde{Z}_{\text{abs}}/2)$ . In this way the connected vertices obtain an imaginary part. For instance the creation and annihilation currents in the process  $e^+e^- \rightarrow b\tilde{\chi}_i^+ \bar{b}\tilde{\chi}_j^-$  are both multiplied by  $(1 + \delta\tilde{Z}_{\text{abs}})$  as they are both connected to two squark propagators\*. The PS corrections to this effect is also of  $\text{NLO}_+$ .

## 11.4. Phase Space Matching formalism

One possibility to calculate  $\sigma_{\text{incl}}(\Lambda)$  is to use only the vNRQCD operators and to evaluate the PS integrals with cuts. We already calculated the Coulomb corrections to the vertex function in section 10.4. The remaining phase space integral with cut could now be carried out numerically. We are however going to follow a different approach where we will match the selection prescription on the final states to local operators. This is possible if  $\Lambda$  is considered to be a hard scale, which corresponds to high energy dynamics and can be integrated out at the matching scale  $\nu_{\text{match}} \approx \frac{\Lambda}{m}$ . In [28, 43] a similar approach was followed for the description of  $e^+e^- \rightarrow t\bar{t}$ , where the angular momentum state is a S-wave. In our case the angular momentum state is a P-wave state and this is also the first time the PS matching formalism is applied for a P-wave angular momentum state.

The advantage of matching the selection prescriptions into local operators is that by the RG evolution we will sum up large logarithms of the form  $\log\left(\frac{\Lambda}{mv}\right)$ .

In our effective theory  $Im(\mathcal{M})/s$  will then not correspond to  $\sigma_{\text{tot}}$  but to  $\sigma_{\text{incl}}(\Lambda)$ , which is the cross section to final states that fulfil the selection prescriptions we described above. This will later give the matching condition for the EFT.

The invariant mass cut-off  $\Delta M$  should be below  $m$  such that the PS integrals are restricted to a domain where vNRQCD is still sensible. We choose  $\Lambda \sim m\sqrt{v}$  as it is then hard with respect to the soft scale but at the same time the expansions in vNRQCD are still valid for  $\mathbf{p} \sim \Lambda$ . We will match to the effective theory with PS matching at the matching scale  $\nu_{\text{match}} \approx \frac{\Lambda}{m}$ .

---

\*There is no complex conjugation of  $\delta\tilde{Z}_{\text{abs}}$  at the annihilation current, as this is a non-hermitian effect.

In addition to the contribution of these cut diagrams, which we can reproduce in vNRQCD by introducing invariant mass cuts, there exist also numerous background diagrams that contribute to the same cross section (see figure 6 for an example of such a diagram). However, in the regime where the  $\tilde{t}_1, \tilde{\bar{t}}_1$  propagators are resonant, we expect the vNRQCD diagrams to be the dominant ones. For large  $\Delta M$  we therefore not only have the problem that the diagrams including the  $\tilde{t}_1, \tilde{\bar{t}}_1$  propagators are no more adequately described in vNRQCD, but also that their contribution in the kinematic regime, where  $\tilde{t}_1, \tilde{\bar{t}}_1$  propagators are less resonant, will become subleading to the background contributions. Our approach is therefore limited to some maximal value for  $\Delta M$  for these two reasons. By using the program Madgraph [6] to numerically calculate the cross section for some parameter point in the full MSSM, we will check in section 15 that the background contributions at tree order are small for the  $\Delta M$  values we use in our analysis. It is possible to match the background contributions into the Wilson coefficients of our EFT.

A different approach would be to match only to phase space integrals calculated in the full theory which is carried out for top production in [9]. If the matching is done in the full theory, we do not rely on NRQCD expansions and can therefore choose bigger values for  $\Lambda$ . However, if we want to investigate  $\tilde{t}_1, \tilde{\bar{t}}_1$  production the regime where  $\mathbf{p}_{\tilde{t}_1} \gg mv$  is also less interesting, as the diagrams where the final states are produced over the decay of  $\tilde{t}_1, \tilde{\bar{t}}_1$  are only resonant for  $\mathbf{p}_{\tilde{t}_1} \sim mv$ . The effect of raising  $\Lambda$  beyond  $m\sqrt{v}$ , which corresponds to our power-counting, is to introduce more of the regime, where the  $\tilde{t}_1, \tilde{\bar{t}}_1$  propagators are less resonant and the background contributions therefore become more important. Raising  $\Lambda$  will in any case render the background contributions more important, which means that one also needs to invest more work for calculating them at higher precision. For us the assumption that we can ignore most of the background contributions is crucial and we will test it in section 15 via a Monte Carlo simulation in Madgraph. We will see that if we choose  $\Lambda$  smaller, the background is also getting less important. In order to match the effect of the cut-off  $\Lambda$  into local operators, we only need that it is large compared to the soft-scale, this is therefore also possible if the matching calculations are only carried out in the full theory. However, in [9] the effect of the cut-off  $\Lambda$  was not integrated out.

Therefore  $\sigma_{\text{incl}}(\Lambda) = \text{Im}(\mathcal{M})/s$  consists of two contributions:

$$\sigma_{\text{incl}}(\Lambda) = \sigma_{\text{NRQCD}}(\Lambda) + \sigma_{\text{rem}}(\Lambda), \quad (11.15)$$

where  $\sigma_{\text{NRQCD}}(\Lambda)$  is the cross section computed in vNRQCD with the invariant mass cuts on the intermediate (anti)stop propagators applied.  $\sigma_{\text{rem}}(\Lambda)$  contains for instance diagrams with no (anti)stop propagators as intermediate states. We call diagrams with only one (anti)stop propagator single-resonant and diagrams with a stop and an antistop as intermediate states double-resonant. The interference between single and double-resonant diagrams has to be taken into account in  $\sigma_{\text{NRQCD}}(\Lambda)$  at NLO<sub>+</sub> order\*. Figure 6 shows examples for double- and single-resonant diagrams. It also shows a pure background diagram, which contains no (anti)stop as an intermediate state.

---

\*The interference contributions lead to a divergence which corresponds to a NLO<sub>+</sub> PS correction. The finite part in dimensional regularization contributes only at NNLL.

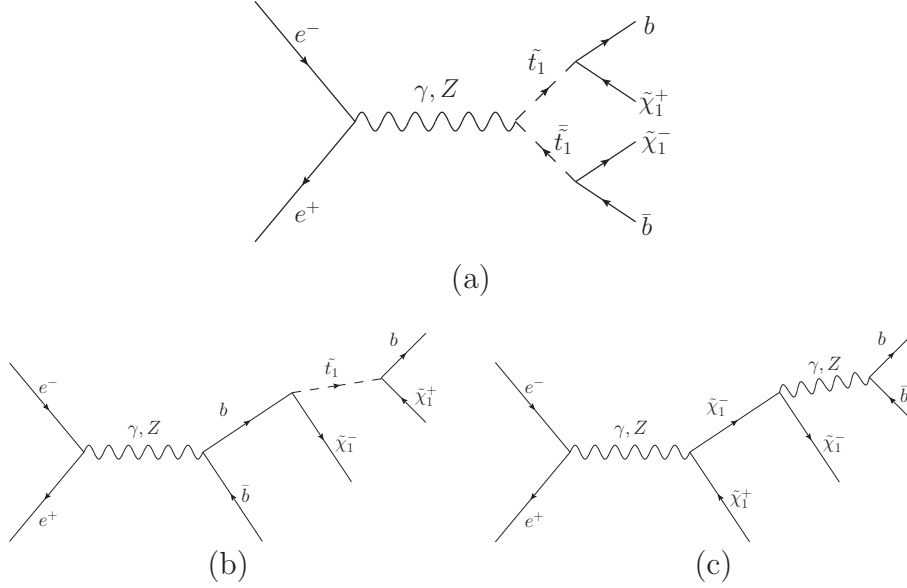


**Figure 6.:** (a) Double-resonant full theory diagram ( $e^+e^- \rightarrow \tilde{t}_1\tilde{t}_1^- \rightarrow b\tilde{\chi}_1^+\bar{b}\tilde{\chi}_1^-$ ). (b) Single-resonant full theory diagram ( $e^+e^- \rightarrow \tilde{t}_1\bar{b}\tilde{\chi}_1^- \rightarrow b\tilde{\chi}_1^+\bar{b}\tilde{\chi}_1^-$ ). (c) Pure background diagram that contains no (anti)stop as an intermediate state.

## 12. Additional Operators for the Phase Space Matching

Besides the operators of vNRQCD we will have to include additional ones in order to account for  $\sigma_{\text{rem}}(\Lambda)$  to do the renormalization and to carry out the "phase space matching", where we will absorb the selection prescriptions on the final states into the Wilson coefficients of our theory. Again contributions that are not calculated explicitly in our work will be coloured red. Eventually, a factorization formula for calculating  $\sigma_{\text{incl}}(\Lambda)$  in the effective theory will be presented.

### 12.1. Additional Operators

The  $e^+e^-$  forward scattering operators are needed for phase space matching contributions (which encode selection prescriptions on the final states, that are part of the definition of the inclusive cross section), to renormalize the phase space divergences (which arise due to finite lifetime effects) and to account for the background diagrams, which contribute to the same process [28]. We define the following  $e^+e^-$  forward scattering operators:

$$\tilde{O}_V^{(n)} = - [\bar{e}_- \gamma^j e_+] [\bar{e}_- \gamma_j (\hat{E}/m)^n e_+], \quad (12.1)$$

$$\tilde{O}_A^{(n)} = - [\bar{e}_- \gamma^j \gamma^5 e_+] [\bar{e}_- \gamma_j \gamma^5 (\hat{E}/m)^n e_+], \quad (12.2)$$

$$\mathcal{L}_{\text{fsc}} = \sum_{n=0}^1 \tilde{C}_V^{(n)} \tilde{O}_V^{(n)} + \tilde{C}_A^{(n)} \tilde{O}_A^{(n)} + \sum_{n=2} \tilde{C}_V^{(n)} \tilde{O}_V^{(n)} + \tilde{C}_A^{(n)} \tilde{O}_A^{(n)}. \quad (12.3)$$

We will use the notation  $\tilde{O}_{V/A} \equiv \tilde{O}_{V/A}^{(0)}$ . If we wanted to include polarization effects, we had to include two additional forward scattering operators in order to absorb the contributions of diagrams, where there is one axial vector and one vector current [43, p. 24]. For the spin averaged cross section these diagrams are averaged to 0.



One includes interference contributions between single and double resonant diagrams (via  $C_{V/A}^{\text{int}}$ ) and PS Cut contributions that cannot be absorbed into the forward scattering  $e^+e^-$  operators (via  $\delta\tilde{c}(\Lambda)$  and  $\delta\tilde{c}^{\text{int}}(\Lambda)$ ) into the Wilson coefficients of the current operators given in (15.8) (in [28] this has been carried out for top production).  $C_{V/A}^{\text{loop}}$  accounts for hard electroweak contributions.  $C_{V/A}$  is now  $\Lambda$  dependent and looks as follows:

$$C_{V/A}(\Lambda, \nu) = C_{V/A}^{\text{Born}} c(\nu)(1 + i\delta\tilde{c}(\Lambda)) + iC_{V/A}^{\text{int}}(1 + \delta\tilde{c}^{\text{int}}(\Lambda)) + C_{V/A}^{\text{loop}}. \quad (12.4)$$

$C_{V/A}^{\text{loop}}$  gives a NNLO<sub>+</sub>,  $\delta\tilde{c}^{\text{int}}$  a N<sup>3</sup>LO<sub>+</sub> and  $C_{V/A}^{\text{int}}$  a NLO<sub>+</sub> effect. Hermitian conjugation in (15.8) does not act on the imaginary part of  $C_{V/A}(\Lambda, \nu)$  as they correspond to finite lifetime effects which are non-hermitian.

## 12.2. Factorization formula

We want to calculate  $\sigma_{\text{incl}}(\Lambda)$ , where  $\Lambda$  refers to the appropriate selection prescription on the final states. In the effective theory we have  $\sigma_{\text{incl}}(\Lambda) = \text{Im}(\mathcal{M})/s$ , where  $\mathcal{M}$  is the  $e^+e^-$  forward scattering amplitude. In the full theory  $\text{Im}(\mathcal{M})/s$  gives the total  $e^+e^-$  cross section. In the effective theory  $\text{Im}(\mathcal{M})$  is matched to the respective phase space integrals with cuts, which implement the selection prescription on the final states. The only difference to the expression given in (9.21) is that we now also include the contribution of the  $e^+e^-$  forward scattering operators:

$$\begin{aligned} \frac{1}{4} \sum_{\text{spins}} \mathcal{M} &= [C_V(\nu)^2 L_{VV}^{lk} + C_A(\nu)^2 L_{AA}^{lk} + C_V(\nu)C_A(\nu) (L_{AV}^{lk} + L_{VA}^{lk})] \mathcal{A}^{lk}(\nu) \\ &+ \sum_{n=0}^1 \left(\frac{E}{m}\right)^n \left[ \tilde{C}_V^{(n)}(\Lambda, \nu) L_{VV}^{ll} + \tilde{C}_A^{(n)}(\Lambda, \nu) L_{AA}^{ll} \right]. \end{aligned} \quad (12.5)$$

Finally we obtain:

$$\begin{aligned} \sigma_{\text{incl}}(\Lambda, \nu) &= \frac{1}{4s} \sum_{\text{spins}} \text{Im}(\mathcal{M}) \\ &= \frac{1}{3} \text{Im} [(C_V(\nu)^2 + C_A(\nu)^2) \mathcal{A}^{jj}(\nu)] \\ &+ \sum_{n=0}^1 \left(\frac{E}{m}\right)^n \text{Im} \left[ \tilde{C}_V^{(n)}(\Lambda, \nu) + \tilde{C}_A^{(n)}(\Lambda, \nu) \right]. \end{aligned} \quad (12.6)$$

## 13. Phase space matching

As mentioned earlier, we construct an effective theory, where  $\sigma_{\text{incl}}(\Lambda) = \frac{Im(\mathcal{M})}{s}$ .  $\mathcal{M}$  is the  $e^+e^-$  forward scattering amplitude in the effective theory. The selection prescriptions on the final states are absorbed into the Wilson coefficients of the  $e^+e^-$  forward scattering operators and the currents. As we will see, at the order we are working the forward scattering operators will be sufficient to absorb the phase space (PS) matching contributions. We will first calculate the cut diagrams at  $O(\alpha_S^0)$  and  $O(\alpha_S)$  in vNRQCD. Then we will match them to  $Im(\mathcal{M})$  in the EFT to obtain the Wilson coefficients and anomalous dimensions. We will do the matching at the renormalization scale  $\nu_{\text{match}} \approx \frac{\Lambda}{m}$  to avoid large logarithms of the form  $\ln\left(\frac{\Lambda}{mv}\right)$ .

### 13.1. Calculation of cut diagrams in vNRQCD

#### Prerequisites

We replace the loop momentum at the cut  $k$  with the variables:

$$t_1 = 2m \left( \frac{E}{2} + k^0 - \frac{\mathbf{k}^2}{2m} \right), \quad t_2 = 2m \left( \frac{E}{2} - k^0 - \frac{\mathbf{k}^2}{2m} \right). \quad (13.1)$$

The kinematic cuts in (11.5) for the (anti)squark propagators imply simple integration limits for  $t_1, t_2$ :

$$-\Lambda^2 \leq t_1, t_2 \leq \Lambda^2, \quad (13.2)$$

where  $\Lambda = \sqrt{2m\Delta M}$ . In addition  $t_1, t_2$  can only have values such that  $\mathbf{k}^2 > 0$ . To express the integrand with  $t_1, t_2$  we can use:

$$k^0 = \frac{t_1 - t_2}{4m}, \quad k = |\mathbf{k}| = \sqrt{Em - \frac{1}{2}(t_1 + t_2)}. \quad (13.3)$$

The integrand is independent of the direction of  $\mathbf{k}$ , and we obtain:

$$d^4k = 4\pi \mathbf{k}^2 d|\mathbf{k}| dk^0 = \frac{\pi}{2m} \sqrt{Em - \frac{1}{2}(t_1 + t_2)} dt_1 dt_2. \quad (13.4)$$

We will rewrite all the integrals as a linear combination of the following basis integrals :

$$\begin{aligned} I_k^{p_1 q_1 p_2 q_2, x} &\equiv \underbrace{\int_{\mathbb{R}^2} dt_1 dt_2 \theta(\Lambda^2 - |t_1|) \theta(\Lambda^2 - |t_2|) \theta\left(mE - \frac{1}{2}(t_1 + t_2)\right)}_{= \int_{\Delta(\Lambda)} dt_1 dt_2} \\ &\times \frac{k P_k^x(t_1, t_2)}{(t_1 + im\Gamma_{\tilde{t}_1})^{p_1} (t_1 - im\Gamma_{\tilde{t}_1})^{q_1} (t_2 + im\Gamma_{\tilde{t}_1})^{p_2} (t_2 - im\Gamma_{\tilde{t}_1})^{q_2}}, \end{aligned} \quad (13.5)$$

where

$$\begin{aligned}
P_0^x(t_1, t_2) &\equiv 1, \\
P_1^x(t_1, t_2) &\equiv \frac{1}{k} i \ln \frac{V_x + k}{V_x - k}, \\
P_2^x(t_1, t_2) &\equiv \frac{1}{t_1 + t_2 + 2im\Gamma_{\tilde{t}_1}}, \\
V_x &\equiv \sqrt{mE + xim\Gamma_{\tilde{t}_1}}, \\
x \in \{0, 1\}, \quad p_1, p_2, q_1, q_2 &\in \mathbb{N}_0.
\end{aligned} \tag{13.6}$$

For  $I_{0/2}^{p_1 q_1 p_2 q_2}$  we omit the  $x$ . We took the results for these integrals as an expansion in  $\frac{\Gamma_{\tilde{t}_1}}{m}, \frac{E}{m}$  from the appendix of [43].

With  $Im\left(\mathcal{A}_C^{(m)lk}\right)(\Lambda)$  we denote the  $O(\alpha_S^m)$  contribution to  $Im\left(\mathcal{A}_C^{lk}\right)$  calculated with a kinematic cut specified by  $\Lambda$ .

$$Im\left(\mathcal{A}_C^{(0)lk}\right)(\Lambda)$$

For the  $O(\alpha_S^0)$  contribution we obtain:

$$\begin{aligned}
2Im\left(\mathcal{A}_C^{(0)lk}\right)(\Lambda) &= \sum_{\text{colours}} \text{Diagram} = \\
&N_C \int_{\Delta(\Lambda)} \frac{d^4 k}{(2\pi)^4} i 2k^l \frac{i}{\frac{E}{2} + k^0 - \frac{\mathbf{k}^2}{2m} + i\frac{\Gamma_{\tilde{t}_1}}{2}} \Gamma_{\tilde{t}_1} \frac{-i}{\frac{E}{2} + k^0 - \frac{\mathbf{k}^2}{2m} - i\frac{\Gamma_{\tilde{t}_1}}{2}} \\
&\frac{i}{\frac{E}{2} - k^0 - \frac{\mathbf{k}^2}{2m} + i\frac{\Gamma_{\tilde{t}_1}}{2}} \Gamma_{\tilde{t}_1} \frac{-i}{\frac{E}{2} - k^0 - \frac{\mathbf{k}^2}{2m} - i\frac{\Gamma_{\tilde{t}_1}}{2}} (-i) 2k^k = \\
2Im\left(\mathcal{A}_C^{(0)jj}\right)(\Lambda) &\frac{\delta^{lk}}{3},
\end{aligned} \tag{13.7}$$

where the sum over  $j = 1, 2, 3$  is implied. Using  $t_1, t_2$  as integration variables we get:

$$\begin{aligned}
2Im \left( \mathcal{A}_C^{(0)jj} \right) (\Lambda) = & \\
N_C \int_{\Delta(\Lambda)} dt_1 dt_2 \frac{2m^3 \Gamma_{\tilde{t}_1}^2}{\pi^3} \frac{k \left[ Em - \frac{1}{2}(t_1 + t_2) \right]}{(t_1 + im\Gamma_{\tilde{t}_1})(t_1 - im\Gamma_{\tilde{t}_1})(t_2 + im\Gamma_{\tilde{t}_1})(t_2 - im\Gamma_{\tilde{t}_1})} = & \\
\frac{2N_C m^3 \Gamma_{\tilde{t}_1}^2}{\pi^3} \left( -I_0^{1101} + m(E + i\Gamma_{\tilde{t}_1}) I_0^{1111} \right) = & \\
2Im \left( \mathcal{A}_C^{(0)jj} \right) + 4N_C m^4 \left[ \underbrace{\frac{1}{\sqrt{2}\pi^2} \frac{\Gamma_{\tilde{t}_1} \Lambda}{m^2}}_{\text{LO}_+} - \underbrace{\frac{3}{\sqrt{2}\pi^2} \frac{E\Gamma_{\tilde{t}_1}}{m\Lambda} - \frac{1}{\pi^3} \frac{\Gamma_{\tilde{t}_1}^2}{m\Lambda} + \frac{3\text{arsinh}(1)}{\sqrt{2}\pi^3} \frac{\Gamma_{\tilde{t}_1}^2}{m\Lambda}}_{\text{NLO}_+} \right. & \\
\left. - \underbrace{\frac{1}{2\sqrt{2}\pi^2} \frac{E^2\Gamma_{\tilde{t}_1}}{\Lambda^3} + \frac{1}{\pi^3} \frac{E\Gamma_{\tilde{t}_1}^2}{\Lambda^3} + \frac{11}{24\sqrt{2}\pi^2} \frac{\Gamma_{\tilde{t}_1}^3}{\Lambda^3} + \frac{\text{arsinh}(1)}{\sqrt{2}\pi^3} \frac{E\Gamma_{\tilde{t}_1}^2}{\Lambda^3}}_{\text{NNLO}_+} + O(v^{11/2}) \right], & \quad (13.8)
\end{aligned}$$

where  $\mathcal{A}_C^{(0)jj}$  is the  $O(\alpha_S^0)$  contribution of  $\mathcal{A}_C^{jj}$  calculated in (10.34) in dimensional regularization:

$$\mathcal{A}_C^{(0)jj} = i \frac{N_C m^4}{\pi} v^3, \quad (13.9)$$

where  $v = \sqrt{\frac{E+i\Gamma_{\tilde{t}_1}}{m}}$ . Note that the leading order term of  $2Im \left( \mathcal{A}_C^{(0)jj} \right) (\Lambda)$  is not  $\mathcal{A}_C^{(0)jj}$  but  $\frac{4N_C m^2 \Gamma_{\tilde{t}_1} \Lambda}{\sqrt{2}\pi^2}$ , which is of  $O(v^{5/2})$  and therefore of  $\text{LO}_+$ . This is one example that the corrections due to the kinematic cut  $\Lambda$  can be formally bigger than the vNRQCD result for the cross section without a kinematic cut on the final states.

$$Im \left( \mathcal{A}_C^{(1)lk} \right) (\Lambda)$$

For the  $O(\alpha_S)$  contribution of  $Im \left( \mathcal{A}_C^{lk} \right) (\Lambda)$  we obtain:

$$2Im \left( \mathcal{A}_C^{(1)lk} \right) (\Lambda) = \sum_{\text{colours}} \left[ \text{Diagram 1} + \text{Diagram 2} \right] = \sum_{\text{colours}} 2\text{Re} \left[ \text{Diagram 3} \right]. \quad (13.10)$$

Using the Coulomb vertex function  $\gamma_C$  (10.40) and  $h(k)$  (10.14) we get:

$$\begin{aligned}
\sum_{\text{colours}} \left[ \text{Diagram 1} \right] &= N_C \int_{\Delta(\Lambda)} \frac{d^4k}{(2\pi)^4} \frac{\gamma_C^{(1)l}(k, E)}{h(k)} \frac{i}{\frac{E}{2} + k^0 - \frac{\mathbf{k}^2}{2m} + i\frac{\Gamma_{\tilde{t}_1}}{2}} \Gamma_{\tilde{t}_1} \\
&\quad \frac{-i}{\frac{E}{2} + k^0 - \frac{\mathbf{k}^2}{2m} - i\frac{\Gamma_{\tilde{t}_1}}{2}} \frac{i}{\frac{E}{2} - k^0 - \frac{\mathbf{k}^2}{2m} + i\frac{\Gamma_{\tilde{t}_1}}{2}} \Gamma_{\tilde{t}_1} \frac{-i}{\frac{E}{2} - k^0 - \frac{\mathbf{k}^2}{2m} - i\frac{\Gamma_{\tilde{t}_1}}{2}} (-i2k^k), \quad (13.11)
\end{aligned}$$

where  $\gamma_C^{(m)}$  is the  $O(\alpha_S^m)$  contribution of  $\gamma_C$ . In section 10.4 we calculated  $\gamma_C$  to all orders in  $\alpha_S$ . The  $O(\alpha_S)$  contribution of  $\frac{\gamma_C^{(k,E)}}{h(k)}$  is:

$$\begin{aligned} \frac{\gamma_C^{(1)l}(k, E)}{h(k)} &= \int \frac{d^4p}{(2\pi)^4} (i2p^l) \frac{i}{\frac{E}{2} + p^0 - \frac{\mathbf{p}^2}{2m} + i\frac{\Gamma_{\tilde{t}_1}}{2}} i \frac{4\pi a}{(\mathbf{k} - \mathbf{p})^2} \frac{i}{\frac{E}{2} - p^0 - \frac{\mathbf{p}^2}{2m} + i\frac{\Gamma_{\tilde{t}_1}}{2}} \\ &= \frac{ma}{2\mathbf{k}^2} \left[ 2V_+ + \frac{\mathbf{k}^2 + V_+^2}{|\mathbf{k}|} \ln \left( \frac{V_+ - |\mathbf{k}|}{V_+ + |\mathbf{k}|} \right) \right] k^l. \end{aligned} \quad (13.12)$$

Inserting this expression in (13.11) and using  $t_1, t_2$  as integration variables we get:

$$\begin{aligned} \sum_{\text{colours}} \text{Diagram} &= N_C \int_{\Delta(\Lambda)} dt_1 dt_2 \frac{-iam^4 \Gamma_{\tilde{t}_1}^2}{2\pi^3} \\ &\quad k \left[ 2V_+ + \frac{\mathbf{k}^2 + V_+^2}{|\mathbf{k}|} \ln \left( \frac{V_+ - |\mathbf{k}|}{V_+ + |\mathbf{k}|} \right) \right] \frac{\delta^{lk}}{3} = \\ &= \frac{N_C am^4 \Gamma_{\tilde{t}_1}^2}{\pi^3} \left( -iV_+ I_0^{1111} + mEI_1^{1111,1} - \frac{I_1^{1011,1}}{2} \right) \frac{\delta^{lk}}{3}, \end{aligned} \quad (13.13)$$

and finally:

$$\begin{aligned} 2Im \left( \mathcal{A}_C^{(1)jj} \right) (\Lambda) &= 2Im \left( \mathcal{A}_C^{(1)jj} \right) - \frac{4N_C am^3 \Gamma_{\tilde{t}_1}}{\pi} \left[ \underbrace{\frac{1}{8\epsilon} - \frac{1}{2} \ln \left( \frac{\Lambda}{m\nu} \right)}_{\text{LL}_+} + \underbrace{\frac{1}{3} + \frac{\ln(2)}{4}}_{\text{LO}} \right. \\ &\quad \left. + \underbrace{\frac{Em}{\Lambda^2} - \frac{\Gamma_{\tilde{t}_1} m}{2\pi\Lambda^2}}_{\text{NLO}} + O(v^2) \right], \end{aligned} \quad (13.14)$$

where  $\left( \mathcal{A}_C^{(1)jj} \right)$  is the  $O(\alpha_S)$  contribution of  $\mathcal{A}_C^{jj}$  calculated in (10.34) in dimensional regularization:

$$\mathcal{A}_C^{(1)jj} = \frac{N_C am^3 (E + i\Gamma_{\tilde{t}_1})}{12\pi} \left[ \frac{3}{\epsilon} + 14 - 12 \ln(2) - 12 \ln \left( \frac{-i\nu}{\nu} \right) \right]. \quad (13.15)$$

Note that because the divergences in  $Im \left( \mathcal{A}_C^{(1)jj} \right) (\Lambda)$  are regularized by the cut-off  $\Lambda$  the  $1/\epsilon$  as well as the  $\nu$  dependent terms cancel in  $Im \left( \mathcal{A}_C^{(1)jj} \right) (\Lambda)$ .

## Calculating $Im(\mathcal{A}_C^{lk})(\Lambda)$ numerically using $\gamma_C^l$

With the expression for  $\gamma_C^l$  calculated in section 10.4 we can write  $2Im(\mathcal{A}_C^{lk})(\Lambda)$  as follows:

$$\begin{aligned}
2Im(\mathcal{A}_C^{lk})(\Lambda) &\equiv \sum_{m=0}^{\infty} 2Im(\mathcal{A}_C^{(m)lk})(\Lambda) = \\
&N_C \int_{\Delta(\Lambda)} \frac{d^4k}{(2\pi)^4} \frac{\gamma_C^l(k, E)}{h(k)} \frac{i}{\frac{E}{2} + k^0 - \frac{\mathbf{k}^2}{2m} + i\frac{\Gamma_{\tilde{t}_1}}{2}} \Gamma_{\tilde{t}_1} \frac{-i}{\frac{E}{2} + k^0 - \frac{\mathbf{k}^2}{2m} - i\frac{\Gamma_{\tilde{t}_1}}{2}} \\
&\frac{i}{\frac{E}{2} - k^0 - \frac{\mathbf{k}^2}{2m} + i\frac{\Gamma_{\tilde{t}_1}}{2}} \Gamma_{\tilde{t}_1} \frac{-i}{\frac{E}{2} - k^0 - \frac{\mathbf{k}^2}{2m} - i\frac{\Gamma_{\tilde{t}_1}}{2}} \left( \frac{\gamma_C^k(k, E)}{h(k)} \right)^* = \\
&N_C \int_{\Delta(\Lambda)} \frac{d^4k}{(2\pi)^4} \Gamma_{\tilde{t}_1}^2 \gamma_C^l(k, E) (\gamma_C^k(k, E))^*, \tag{13.16}
\end{aligned}$$

where the function  $h(k)$  is defined in (10.14). Carrying out the remaining integral numerically we can obtain  $Im(\mathcal{A}_C^{lk})(\Lambda)$  at all orders in  $\alpha_S$  with arbitrary precision.

## Convergence of the expansion

We check the convergence of the expansion of  $Im(\mathcal{A}_C^{jj})(\Lambda)$  in  $\frac{E, \Gamma_{\tilde{t}_1}}{\Lambda}$  by comparing it to the numerically evaluated integral (13.16) at various orders in  $\alpha_S$ . Instead of  $Im(\mathcal{A}_C^{jj})(\Lambda)$  we plot  $\sigma_{\text{incl}}(\Lambda, \nu = 1)$  which we can easily obtain from  $Im(\mathcal{A}_C^{jj})(\Lambda)$  via:

$$\sigma_{\text{incl}}(\Lambda, \nu) = \frac{1}{3} Im[(C_V(\nu)^2 + C_A(\nu)^2) \mathcal{A}^{jj}(\Lambda, \nu)], \tag{13.17}$$

which is an immediate generalization of (9.26). Divergences appear only in the  $O(\alpha_S^0)$  and the  $O(\alpha_S)$  part of  $\mathcal{A}_C^{jj}$ . For the contributions of  $Im(\mathcal{A}_C^{jj})(\Lambda)$  which are of  $O(\alpha_S^{n \geq 2})$  we did not calculate an analytic expression. However, beyond  $O(\alpha_S)$  there are no infinities in  $Im(\mathcal{A}_C^{jj})$ , and therefore the  $O(\alpha_S^{n \geq 2})$  part of  $Im(\mathcal{A}_C^{jj})(\Lambda)$  converges to the  $O(\alpha_S^{n \geq 2})$  part in  $Im(\mathcal{A}_C^{jj})$  for  $\Lambda \rightarrow \infty$ . At each additional order in  $\alpha_S$  the PS corrections parametrically decrease by  $O(\frac{\alpha_S m}{\Lambda}) = O(\sqrt{v})$  and therefore the PS corrections become small at high orders in  $\alpha_S$ . Nevertheless the  $O(\alpha_S^2)$  and  $O(\alpha_S^3)$  PS corrections to  $Im(\mathcal{A}_C^{jj})$  are formally still of NLO<sub>+</sub> and NLO respectively. We can take these corrections into account numerically by using (13.16).

We show plots for fixed values of  $E$  and  $\Delta M$ . We use  $\Gamma_{\tilde{t}_1} = 1.4\text{GeV}$ ,  $m = 400\text{GeV}$  and  $\alpha_S = 0.094$ . Figures 7 and 8 show plots for  $E = 5\text{GeV}$  and  $E = -5\text{GeV}$ . Figures 9 and 10 show plots for  $\Delta M = 21\text{GeV}$  and  $\Delta M = 11\text{GeV}$ . For plotting the  $O(\alpha_S)$  term of  $Im(\mathcal{A}_C^{jj})$  we set  $\nu = 1$  and ignore the  $\frac{1}{\epsilon}$  divergences, which means that we plot the  $\overline{MS}$  renormalized result without PS matching corrections.

In figure 7 and 8 it can be seen clearly that the convergence improves for larger  $\Delta M$ . In figure 7 we see that for  $E = 5\text{GeV}$  there is already very good convergence for  $\Delta M \sim 10\text{GeV}$ . The NLO<sub>+</sub> effect of the  $O(\alpha_S^2)$  PS correction (which we did not compute analytically) is already only a 20% effect to the cross section for  $\Delta M \sim 10\text{GeV}$  and  $E = 5\text{GeV}$ . For  $\Delta M \sim 20\text{GeV}$  and  $\Delta \sim 35\text{GeV}$  the relative corrections due to this NLO<sub>+</sub> effect decrease to 10% and 5%.

In figure 8 we see that for  $E = -5\text{GeV}$  the cross section is much smaller. For  $E = -5\text{GeV}$  and  $\Delta M \sim 35\text{GeV}$  the NLO<sub>+</sub> PS correction at  $O(\alpha_S^2)$  is a 50% effect.

In figure 9 and 10 we see that the cross section is enhanced significantly if we increase the energy in the threshold region. However as the  $\tilde{t}_1\tilde{\bar{t}}_1$  state is produced as a P-Wave angular momentum state the enhancement is suppressed with respect to  $t\bar{t}$  production, where the  $t\bar{t}$  pair is produced as a S-Wave angular momentum state.

It can be said that the convergence of the PS corrections is very good for  $\Delta M \geq 15\text{GeV}$ .

## 13.2. Matching to the EFT

Graphically the matching condition at  $O(\alpha_S^0)$  reads:

$$\begin{aligned}
 & \text{Diagram 1: } e^- e^+ \text{ annihilation into } e^- e^+ \text{ via a } \Delta(\Lambda) \text{ state.} \\
 & = 2Im \left[ -i \left( \text{Diagram 2: } e^- e^+ \text{ annihilation into } e^- e^+ \text{ via a } \tilde{t}_1\tilde{\bar{t}}_1 \text{ loop.} + \sum_{n=0}^1 \tilde{C}_{V/A,\text{bare}}^{(0,n)}(\Lambda) \text{Diagram 3: } e^- e^+ \text{ annihilation into } e^- e^+ \text{ via a } t\bar{t} \text{ loop.} \right) \right] \\
 & = \text{Diagram 1} + 2Im \left[ -i \sum_{n=0}^1 \left( \tilde{C}_{V/A}^{(0,n)}(\Lambda, \nu_{\text{match}}) + \delta\tilde{C}_{V/A}^{(0,n)}(\nu_{\text{match}}) \right) \text{Diagram 3} \right]. \quad (13.18)
 \end{aligned}$$

Note that we could also have put a phase space matching coefficient for the production and annihilation currents, which is however not necessary here. Here we are computing the  $O(\alpha_S^0)$  part of the phase space matching coefficients. Generally we will denote the  $O(\alpha_S^m)$  part of the Wilson coefficient  $\tilde{C}_{V/A}^{(n)}$  as  $\tilde{C}_{V/A}^{(m,n)}$ . With this we obtain:

$$\begin{aligned}
 \tilde{C}_{V/A}^{(0,0)}(\Lambda, \nu_{\text{match}}) &= -i \frac{2C_{V/A}(\nu_{\text{match}})^2 N_C m^3 \Gamma_{\tilde{t}_1}}{3} \left[ -\frac{1}{\sqrt{2}\pi^2} \frac{\Lambda}{m} + \frac{1}{\pi^3} \frac{\Gamma_{\tilde{t}_1}}{\Lambda} - \frac{3\text{arsinh}(1)}{\sqrt{2}\pi^3} \frac{\Gamma_{\tilde{t}_1}}{\Lambda} \right], \\
 \tilde{C}_{V/A}^{(0,1)}(\Lambda, \nu_{\text{match}}) &= -i \frac{2C_{V/A}(\nu_{\text{match}})^2 N_C m^3 \Gamma_{\tilde{t}_1}}{3} \left[ \frac{3}{\sqrt{2}\pi^2} \frac{m}{\Lambda} \right], \\
 \delta\tilde{C}_{V/A}^{(0,0)}(\nu) &= \delta\tilde{C}_{V/A}^{(0,1)}(\nu) = 0. \quad (13.19)
 \end{aligned}$$

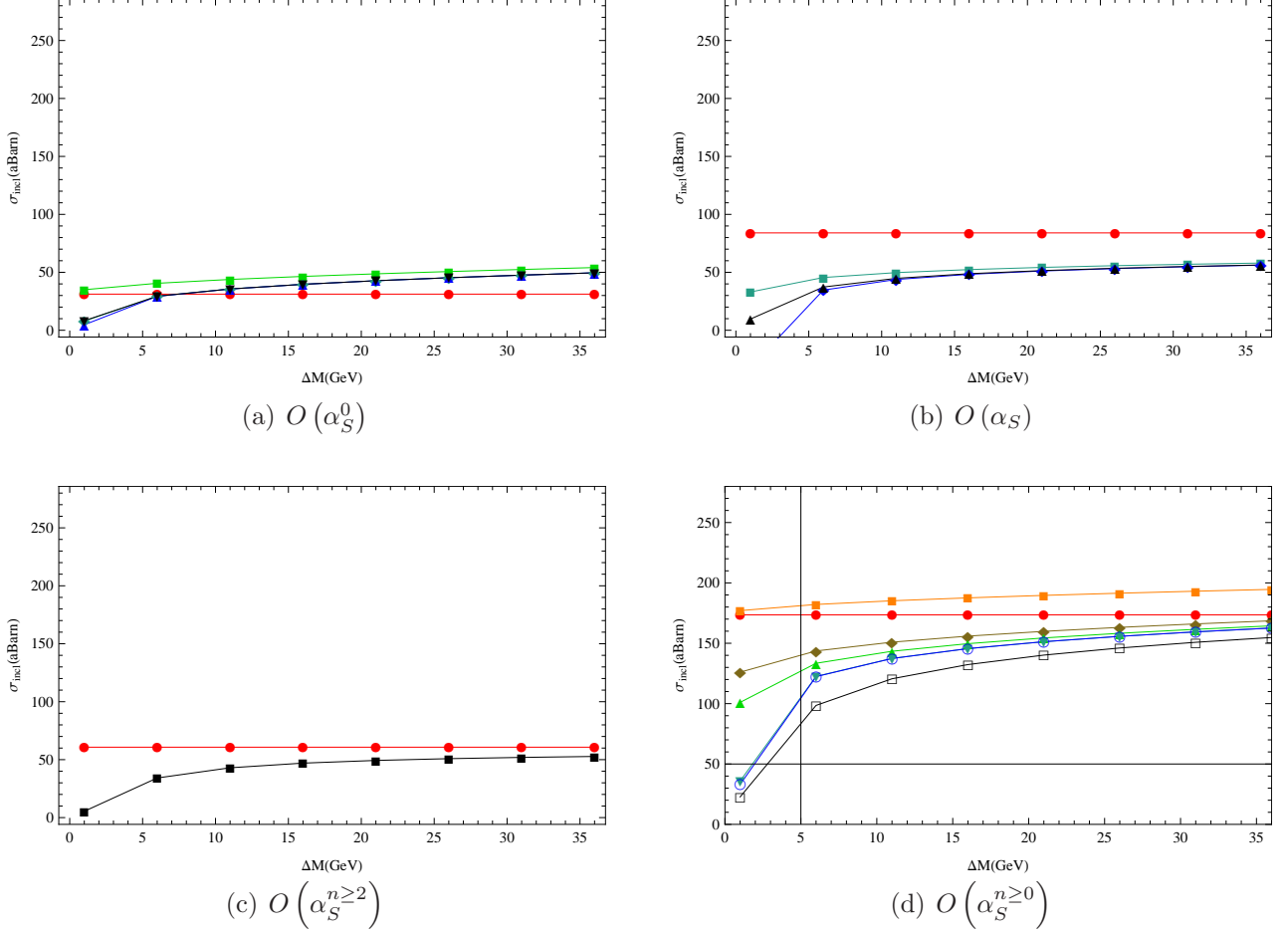


**Figure 7.:** These plots show  $\sigma_{\text{incl}}(\Lambda)$  for  $E = 5\text{GeV}$  for different orders of  $\alpha_S$ . The red curve corresponds to the  $\overline{MS}$  renormalized result without PS matching corrections. The black curve is obtained by doing the integral in (13.16) numerically. The blue, turquoise, green, brown and orange curves show different orders of the expansions (13.8) and (13.14). For the blue curve all the PS corrections calculated are taken into account, while for the other colours PS corrections are gradually omitted. In our power-counting the corrections in plot (a) and (b) should decrease by  $O\left(\frac{Em}{\Lambda}\right) = O(v)$ , while in plot (d) they decrease by  $O(\sqrt{v})$ . In plot (a) the blue, turquoise and green curves contain PS corrections of the expansion (13.8) up to NNLO<sub>+</sub>, NLO<sub>+</sub> and LO<sub>+</sub>. In plot (b) the blue and turquoise curves contain PS corrections of the expansion (13.14) up to NLO and LO. In plot (d) the blue, turquoise, green, brown and orange curves contain PS corrections of the expansions (13.8) and (13.14) up to NNLO<sub>+</sub>, NLO, NLO<sub>+</sub>, LO and LO<sub>+</sub>. The  $O(\alpha_S^2)$  PS correction is parametrically of NLO<sub>+</sub>. As we did not calculate PS corrections of  $O(\alpha_S^2)$  analytically the difference between the blue and the black curve in plot (d) is approximately the  $O(\alpha_S^2)$  PS correction.



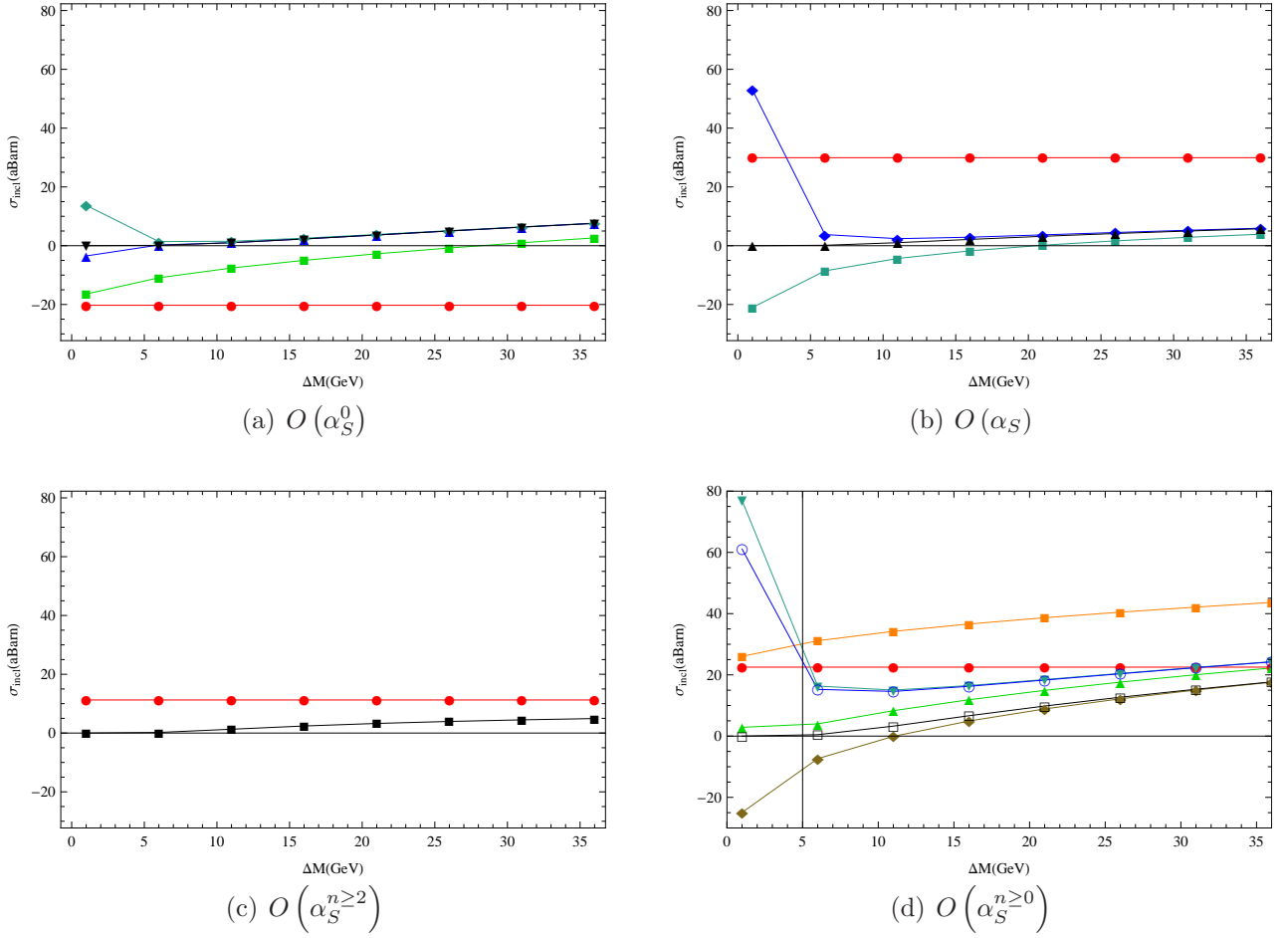


**Figure 8.:** These plots show  $\sigma_{\text{incl}}(\Lambda)$  for  $E = -5\text{GeV}$  for different orders of  $\alpha_S$ . For the meaning of the curves see figure 7.

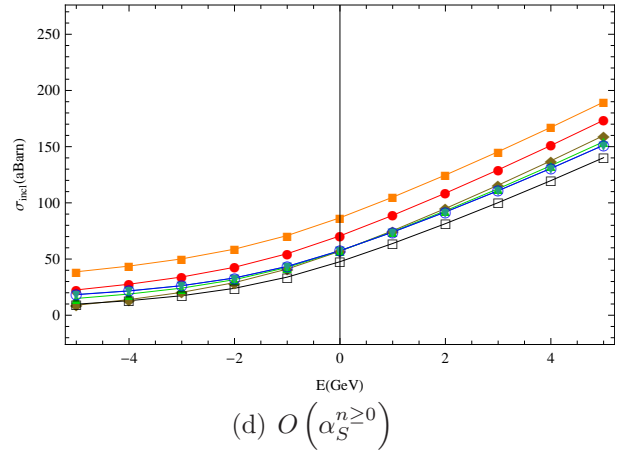
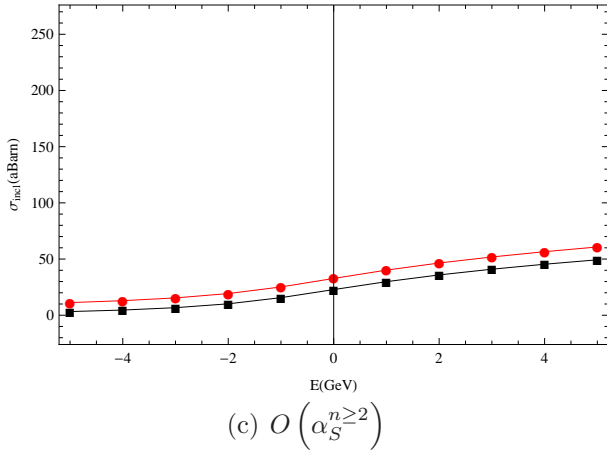
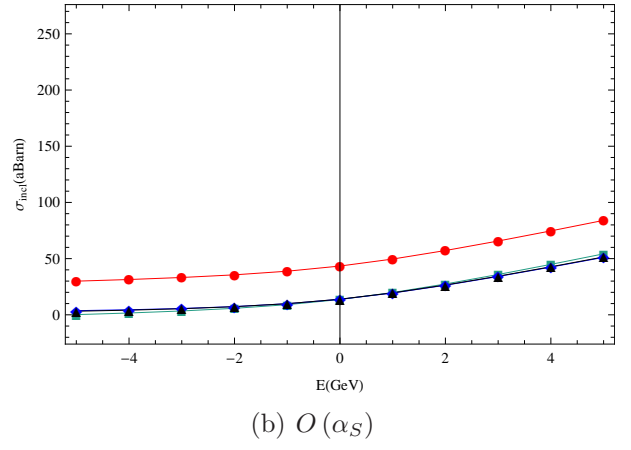
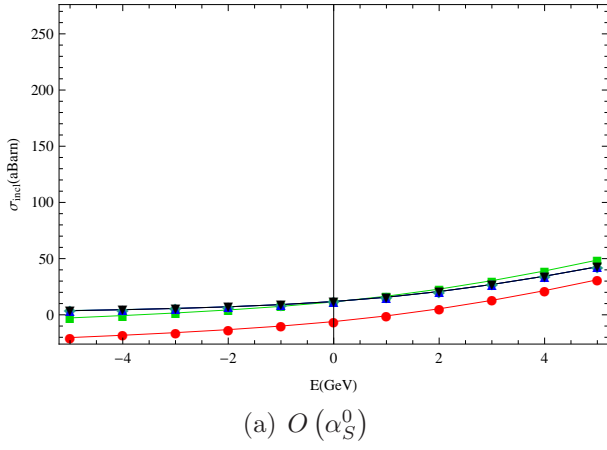


**Figure 9.:** These plots show  $\sigma_{\text{incl}}(\Lambda)$  for  $\Delta M = 21\text{GeV}$  for different orders of  $\alpha_S$ . For the meaning of the curves see figure 7.

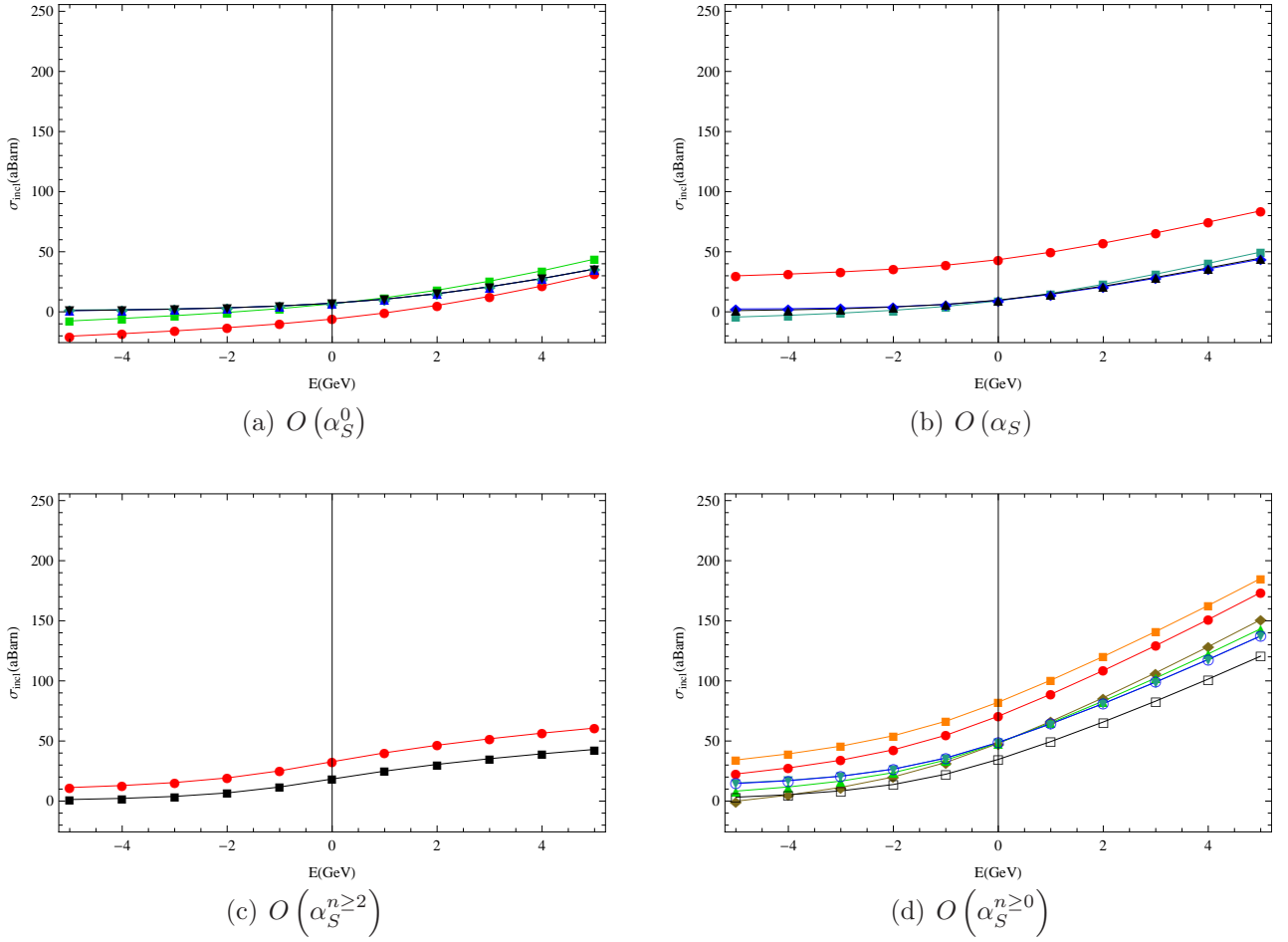


**Figure 10.:** These plots show  $\sigma_{\text{incl}}(\Lambda)$  for  $\Delta M = 11\text{GeV}$  for different orders of  $\alpha_S$ . For the meaning of the curves see figure 7.

Here we ignored the NNLO<sub>+</sub> PS corrections in (13.8). The matching condition at  $O(\alpha_S)$  reads:

$$\begin{aligned}
& \text{Diagram 1} + \text{Diagram 2} \\
&= 2Im \left[ -i \left( \text{Diagram 3} + \sum_{n=0}^1 \tilde{C}_{V/A,\text{bare}}^{(1,n)}(\Lambda) \text{Diagram 4} \right) \right] \\
&= \text{Diagram 5} + \text{Diagram 6} + \\
& 2Im \left[ -i \sum_{n=0}^1 \left( \tilde{C}_{V/A}^{(1,n)}(\Lambda, \nu_{\text{match}}) + \delta \tilde{C}_{V/A}^{(1,n)}(\nu_{\text{match}}) \right) \text{Diagram 7} \right]. \tag{13.20}
\end{aligned}$$

Again we do not put a phase space matching coefficient for the production and annihilation currents, although for the  $O(\alpha_S)$  phase space matching this would become necessary if we worked at a higher order. For this matching condition we obtain:

$$\begin{aligned}
\tilde{C}_{V/A}^{(1,0)}(\Lambda, \nu_{\text{match}}) &= -i \frac{2C_{V/A}(\nu_{\text{match}})^2 N_C a(\nu_{\text{match}}) m^3 \Gamma_{\tilde{t}_1} \left[ \frac{1}{3} + \frac{\ln(2)}{4} - \frac{1}{2} \ln \left( \frac{\Lambda}{m\nu_{\text{match}}} \right) - \frac{\Gamma_{\tilde{t}_1} m}{2\pi\Lambda^2} \right]}{3\pi}, \\
\tilde{C}_{V/A}^{(1,1)}(\Lambda, \nu_{\text{match}}) &= -i \frac{2C_{V/A}(\nu_{\text{match}})^2 N_C a(\nu_{\text{match}}) m^3 \Gamma_{\tilde{t}_1} m^2}{3\pi \Lambda^2}, \\
\delta \tilde{C}_{V/A}^{(1,0)}(\nu) &= -i \frac{2C_{V/A}(\nu)^2 N_C a(\nu) m^3 \Gamma_{\tilde{t}_1} 1}{3\pi 8\epsilon}, \\
\delta \tilde{C}_{V/A}^{(1,1)}(\nu) &= 0, \tag{13.21}
\end{aligned}$$

where  $\delta \tilde{C}_{V/A}^{(1,0)}(\nu)$  has to be chosen such that it absorbs the corresponding PS divergence for all values of  $\nu$  in the effective theory.

## 14. RG evolution due to PS divergences

In (13.21) we absorbed the  $\frac{1}{\epsilon}$  PS Divergence into a local four fermion operator. This leads to a non-trivial renormalization group equation (RGE) for  $C_{V/A}(\nu)$  which we will solve in this section. The RGE that we obtain from (13.21) sums up logarithms at  $LL_+$  order as the divergence absorbed is of LO. The RGE is obtained by requiring:

$$\frac{d\tilde{C}_{V/A,\text{bare}}}{d\ln(\nu)} = 0, \quad (14.1)$$

where

$$\tilde{C}_{V/A,\text{bare}} = \tilde{C}_{V/A}(\nu) + \delta\tilde{C}_{V/A}(\nu). \quad (14.2)$$

Therefore we get:

$$\frac{d\tilde{C}_{V/A}(\nu)}{d\ln(\nu)} = -\frac{d\delta\tilde{C}_{V/A}(\nu)}{d\ln(\nu)}. \quad (14.3)$$

In (13.21) we obtained:

$$\delta\tilde{C}_{V/A} = -i\frac{2C_{V/A}(\nu)^2 N_C a(\nu) m^3 \Gamma_{\tilde{t}_1}}{3\pi} \frac{1}{8\epsilon} [1 + O(\alpha_S, v)]. \quad (14.4)$$

As we can see the running of  $\tilde{C}_{V/A}(\nu)$  depends on the running of  $a(\nu)$  and  $C_{V/A}(\nu)$  through mixing. We have that  $a(\nu) = \frac{C_F \mathcal{V}_c^{(T)}(\nu)}{4\pi}$ , where  $\mathcal{V}_c^{(T)}(\nu)$  is the Wilson coefficient of the leading order potential in (9.8). We need the RGE for  $\mathcal{V}_c^{(T)}(\nu)$  which we obtain via  $\mathcal{V}_{c,\text{bare}}^{(T)}$ :

$$\mathcal{V}_{c,\text{bare}}^{(T)} = \tilde{\mu}_S^{2\epsilon} (\mathcal{V}_c^{(T)}(\nu) + \delta\mathcal{V}_c^{(T)}(\nu)). \quad (14.5)$$

For obtaining  $\frac{d\delta\tilde{C}_{V/A}}{d\ln(\nu)}$  at LO we only need to consider the LO expression of  $\frac{d\mathcal{V}_c^{(T)}(\nu)}{d\ln(\nu)}$ :

$$\frac{d\mathcal{V}_c^{(T)}(\nu)}{d\ln(\nu)} = \mathcal{V}_c^{(T)}(\nu) [-2\epsilon + O(\alpha_S)]. \quad (14.6)$$

Analogously we get:

$$\frac{dC_{V/A}(\nu)}{d\ln(\nu)} = -\epsilon C_{V/A}(\nu). \quad (14.7)$$

Therefore the RGE for  $\tilde{C}_{V/A}$  at  $LL_+$  reads:

$$\frac{d\tilde{C}_{V/A}(\nu)}{d\ln(\nu)} = 4\epsilon\delta\tilde{C}_{V/A}(\nu) = -i\frac{C_{V/A}(\nu)^2 N_C a(\nu) m^3 \Gamma_{\tilde{t}_1}}{3\pi}. \quad (14.8)$$

Although we derived this RGE at  $LL_+$  and ignored terms of higher order it remains valid at LL order, as there are no additional divergences at LO.

At  $NLL_+$  we encounter diagrams with an additional gluon loop like the one shown in figure 11, which render  $\frac{1}{\epsilon^2}$  divergences which are absorbed by  $\delta\tilde{C}_{V/A}$ . But these divergences only have the effect

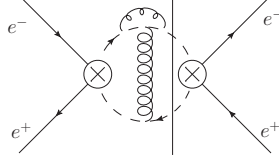


**Figure 11.:** This diagram renders a  $\frac{1}{\epsilon^2}$  divergence that is absorbed by  $\delta\tilde{C}_{V/A}$ . The effect of this kind of  $\frac{1}{\epsilon^2}$  divergences is that the RGE for  $\tilde{C}_{V/A}$  remains finite at NLL<sub>+</sub>.

that the RGE for  $\tilde{C}_{V/A}(\nu)$  remains finite at NLL<sub>+</sub> order. However, at NLL<sub>+</sub> the Wilson coefficient  $C_{V/A}(\Lambda, \nu)$  obtains an imaginary part, as shown in (12.4). In this way one gets sensible to the real part of  $\tilde{G}_C^P$  (10.36) which has different divergences than its imaginary part. At NLL<sub>+</sub> the running of  $\tilde{C}_{V/A}$  is therefore changed.

For solving the RGE at LL<sub>+</sub> we need to use  $a(\nu)$  at LL order.  $C_{V/A}(\nu)$  does not have a LL running and can thus be considered as constant\*. We have that:

$$a(\nu) = \frac{C_F \mathcal{V}_c^{(T)}(\nu)}{4\pi} = C_F \alpha_S(m\nu). \quad (14.9)$$

Using the LL RGE for  $\alpha_S(m\nu)$ :

$$\frac{d\alpha_S(m\nu)}{d\ln(\nu)} = -\frac{\beta_0}{2\pi} \alpha_S(m\nu)^2, \quad \beta_0 = 11 - \frac{2}{3}n_f \quad (14.10)$$

to substitute  $d\ln(\nu)$  by  $d\alpha_S(m\nu)$  we obtain [42]:

$$\frac{d\tilde{C}_{V/A}(\nu)}{d\alpha_S(m\nu)} = i \frac{2C_{V/A}(\nu_{\text{match}})^2 N_C C_F m^3 \Gamma_{\tilde{t}_1}}{3\beta_0 \alpha_S(m\nu)}, \quad (14.11)$$

where  $n_f = 3$  is the number of quark flavours. Finally we get:

$$\tilde{C}_{V/A}(\nu) = \tilde{C}_{V/A}(\nu_{\text{match}}) + i \frac{2C_{V/A}(\nu_{\text{match}})^2 N_C C_F m^3 \Gamma_{\tilde{t}_1}}{3\beta_0} \ln \left( \frac{\alpha_S(m\nu)}{\alpha_S(m\nu_{\text{match}})} \right). \quad (14.12)$$

$\nu_{\text{match}}$  is the scale where we do the PS matching. It should be chosen such that  $m\nu_{\text{match}} \approx \Lambda$ .

---

\* $C_{V/A}(\nu)$  has a NLL running [29].

## 15. Numerical comparison to a Madgraph simulation

Madgraph is a Monte Carlo simulator which is able to numerically evaluate the amplitudes and cross sections in several models at tree level [6]. We compared our analytical results to the results of Madgraph for the process  $e^+e^- \rightarrow b\tilde{\chi}_1^+\bar{b}\tilde{\chi}_1^-$  for the *Minimal Supersymmetric Standard Model* (MSSM) where we used the kinematic cut (11.3) on the final states. Unlike in our treatment Madgraph also takes into account non resonant diagrams like the one shown in figure 6(c) and we can therefore give an estimate of how sizeable these contributions are. We could also account for these effects by matching the non resonant contributions to the local 4 fermion operators and the single resonant diagrams to the  $\tilde{t}_1\tilde{t}_1$  production/annihilation operators in our treatment. However, the matching computations would require the evaluation of many diagrams in the MSSM and the relevant contributions are strongly dependent on the chosen values for the MSSM parameters. Another strategy would be to match the Wilson coefficients of local operators in our effective treatment to the tree level results from Madgraph.

As Madgraph only computes tree-level contributions it does not involve any  $O(\alpha_S)$  corrections. As we have seen in (6.1) and (10.36) the  $O(\alpha_S^n)$  corrections are of the same parametric size as the tree level results if the CMS energy of the colliding  $e^+e^-$  pair is close to threshold. This is why the Madgraph result is not appropriate for this regime but we can nevertheless use it to check the quality of our result at  $O(\alpha_S^0)$ . In contrast to the double and single-resonant contributions we also expect the non resonant diagrams to be more suppressed at higher orders in  $\alpha_S$  as the resonance of the  $\tilde{t}_1, \tilde{t}_1$  propagators was the reason for the proliferation of scales.

We did two separate Madgraph simulations: In  $e^+e^- \rightarrow \tilde{t}_1\tilde{t}_1 \rightarrow b\tilde{\chi}_1^+\bar{b}\tilde{\chi}_1^-$  Madgraph only takes into account the double resonant diagrams where a  $\tilde{t}_1\tilde{t}_1$  pair is produced and decays into a  $b\tilde{\chi}_1^+\bar{b}\tilde{\chi}_1^-$  final state. An example for such a diagram is given in figure 6(a). For the process  $e^+e^- \rightarrow b\tilde{\chi}_1^+\bar{b}\tilde{\chi}_1^-$  Madgraph also evaluates single and non resonant diagrams. Examples for such diagrams are shown in figure 6(b) and (c).

For doing the comparison with Madgraph we have to specify a point in the MSSM parameter space. The *Snowmass Points and Slopes* (SPS) are a set of benchmark points and parameter lines in the MSSM parameter space [5]. We use the so-called SPS1a point. In our treatment we are not sensible to all but only to the following parameters specified for the SPS1a point:

$$\begin{aligned} m &= 399.7\text{GeV}, & m_{\tilde{\chi}_1} &= 181.8\text{GeV}, & m_Z &= 91.19\text{GeV}, \\ \Gamma_{\tilde{t}_1} &= 2.02\text{GeV}, & \tilde{\Gamma}_{\tilde{t}_1} &= 1.37\text{GeV}, & \Gamma_Z &= 2.41\text{GeV}, \\ \cos\theta_t &= 0.554, & \alpha_S(m_Z) &= 0.118, & \alpha(m_Z) &= 1/127.93, \end{aligned} \quad (15.1)$$

where  $\cos\theta_t$  determines the mixing of the mass eigenstates  $\tilde{t}_1, \tilde{t}_2$  and the flavour eigenstates. This for instance affects the interaction vertex between a Z-Boson and  $\tilde{t}_1, \tilde{t}_1$  particles (2.1).  $\tilde{\Gamma}_{\tilde{t}_1}$  is the decay width from  $\tilde{t}_1$  to  $\tilde{\chi}_1^+b$  calculated at tree level. We are sensible on  $m_{\tilde{\chi}_1}$  because, as we will see later,  $\delta Z^{\text{abs}}$  depends on it.

For our treatment the power counting of the parameters is important. We need to have that  $\Gamma_{\tilde{t}_1} \sim E \sim mv^2$  with  $v \ll 1$ . If we choose  $E$  between  $-5$  and  $5$  GeV this is the case for the SPS1a parameter point.

### 15.1. Madgraph simulation for $e^+e^- \rightarrow \tilde{t}_1\tilde{t}_1 \rightarrow b\tilde{\chi}_1^+\bar{b}\tilde{\chi}_1^-$

For the simulation where Madgraph only takes into account double resonant diagrams it should in principle be possible to reach a perfect agreement with our results as the Madgraph result involves no

single and non resonant diagrams that we have to account for via matching to the full MSSM. To show that we have good convergence we also computed the kinematic corrections from the propagators, the kinematic cut and the matching to the squarks production/annihilation vertices as well as the corrections due to imaginary part of the wave function renormalization  $\delta Z^{\text{abs}}$  discussed in section 11.3 at NNLO\*. We discuss how we take these effects into account and show plots for the comparison for  $\Delta M = 21\text{GeV}$ ,  $\Delta M = 11\text{GeV}$  and  $\Delta M = 31\text{GeV}$  in figures 12, 13 and 14. Without these corrections the difference between the cross section computed in Madgraph and our analytic result is around 5 % for  $\Delta M = 11\text{GeV}$ , 10% for  $\Delta M = 21\text{GeV}$  and 15% for  $\Delta M = 31\text{GeV}$ . Including the corrections our result lies within the statistical error bars of the Madgraph result. This means that the  $O(\alpha_S^0)$  result for the description of double-resonant diagrams shows good convergence.

### Effects due to $\delta Z^{\text{abs}}$

In (11.13) we expressed  $\delta Z^{\text{abs}}$  with the decay width for  $\tilde{t}_1 \rightarrow b\tilde{\chi}_1^+$  which we call  $\tilde{\Gamma}_{\tilde{t}_1}$ .  $\tilde{\Gamma}_{\tilde{t}_1}(k^2)$  is understood as the expression for the decay width depending on the invariant mass of the ingoing  $\tilde{t}_1$  propagator. In [17] in equation (3) the tree order result for  $\tilde{\Gamma}_{\tilde{t}_1}$  is given. If we ignore  $m_b^2$  in  $(m^2 - m_b^2 + m_{\tilde{\chi}_1}^2)$  and  $\lambda^{1/2}(m^2, m_b^2, m_{\tilde{\chi}_1}^2)$  we obtain:

$$\left. \frac{d\tilde{\Gamma}_{\tilde{t}_1}}{dk^2} \right|_{k^2=m^2} \approx \frac{(m^2 + 3m_{\tilde{\chi}_1}^2)}{2m^2(m^2 - m_{\tilde{\chi}_1}^2)} \Gamma_{\tilde{t}_1}. \quad (15.2)$$

Using (11.13) we get:

$$\delta Z^{\text{abs}} = -i \frac{m^2 + m_{\tilde{\chi}_1}^2}{m(m^2 - m_{\tilde{\chi}_1}^2)} \tilde{\Gamma}_{\tilde{t}_1}. \quad (15.3)$$

As discussed in section 11.3 we can take into account the  $k^2$  dependence of  $\frac{Im\tilde{\Pi}(k^2)}{m}$  at the cut propagator at NNLO by using the replacement rule

$$\frac{i}{\frac{E}{2} \pm p_0 - \frac{\mathbf{p}^2}{2m} + i\frac{\Gamma_{\tilde{t}_1}}{2}} \rightarrow \frac{i}{\frac{E}{2} \pm p_0 - \frac{\mathbf{p}^2}{2m} + i\frac{\Gamma_{\tilde{t}_1}}{2}} \left( \tilde{\Gamma}_{\tilde{t}_1} - \frac{Im(\delta Z^{\text{abs}})(k^2 - m^2)}{m} \right) \frac{-i}{\frac{E}{2} \pm p_0 - \frac{\mathbf{p}^2}{2m} - i\frac{\Gamma_{\tilde{t}_1}}{2}} \quad (15.4)$$

instead of (11.14) for the cut propagator. The PS corrections of this effect are of NLO<sub>+</sub>. For  $\Delta M = 21\text{GeV}$  and  $\Delta M = 31\text{GeV}$  this is the NNLO effect with the biggest PS corrections, as can be observed in figure 12 and 14.

### Kinematic effects from expanding the $\tilde{t}_1, \tilde{\bar{t}}_1$ propagators

The expansion of the squark propagator in the potential regime at NNLO gives:

$$\frac{2mi}{\left(\frac{q}{2} + p\right)^2 - m^2 + \Pi\left(\left(\frac{q}{2} + p\right)^2\right)} = \frac{i}{\frac{E}{2} + p^0 - \frac{\mathbf{p}^2}{2m} + i\frac{\Gamma_{\tilde{t}_1}}{2}} + \frac{i}{\frac{E}{2} + p^0 - \frac{\mathbf{p}^2}{2m} + i\frac{\Gamma_{\tilde{t}_1}}{2}} i \left[ \frac{E^2 + 4p^0(E + p^0)}{8m} + \left(\frac{E}{2} + p^0 - \frac{\mathbf{p}^2}{2m}\right) \frac{\partial}{\partial p^2} \Pi \right]_{p^2=m^2} \frac{i}{\frac{E}{2} + p^0 - \frac{\mathbf{p}^2}{2m} + i\frac{\Gamma_{\tilde{t}_1}}{2}}, \quad (15.5)$$

---

\*The phase space matching corrections of these NNLO corrections are partly of NLO<sub>+</sub>.



where  $q = (2m + E, \mathbf{0})$ .  $i\Pi$  is the sum of all self-energy diagrams. The corrections can be dealt with by introducing 2-point vertices in the the EFT. Madgraph uses the propagator

$$\frac{2mi}{\left(\frac{q}{2} + p\right)^2 - m^2 + im\Gamma_{\tilde{t}_1}} \quad (15.6)$$

with a constant decay width  $\Gamma_{\tilde{t}_1}$ . Therefore it does not take into account the corrections due to  $\frac{\partial}{\partial p^2}\Pi\Big|_{p^2=m^2}$  which we therefore omit for this numerical comparison. The NNLO corrections to the  $\tilde{t}_1, \bar{\tilde{t}}_1$  propagators give PS corrections which are of NLO<sub>+</sub>.

### Relativistic effects when matching to the $O_{V/A,p}$ operators

When matching the diagrams



$$(15.7)$$

on the squarks production/annihilation operators we made a non-relativistic approximation. If we use

$$C_V^{\text{Born}} = -\frac{2\pi\alpha}{m} \left[ \frac{\tilde{Q}_\gamma}{q^2} - \frac{2}{\sin(2\theta_W)} v_e \frac{\tilde{Q}_Z}{q^2 - m_Z^2} \right], \quad (15.8)$$

$$C_A^{\text{Born}} = \frac{2\pi\alpha}{m} \frac{2}{\sin(2\theta_W)} a_e \frac{\tilde{Q}_Z}{q^2 - m_Z^2} \quad (15.9)$$

instead of  $C_V^{\text{Born}}, C_A^{\text{Born}}$  when evaluating the factorization formula (13.17), we take into account the relativistic corrections\*. For matching these effects at NNLO we would have to use the operators  $O_{V/A,p}^{(1)}$  defined in (9.14) to absorb them.

### Relativistic effects from the invariant mass cut-off

By using the variable  $t_1, t_2$  defined in (13.1) and the integration measure:

$$\int_{\Delta(\Lambda)} dt_1 dt_2 = \int_{\mathbb{R}^2} dt_1 dt_2 \theta(\Lambda^2 - |t_1|) \theta(\Lambda^2 - |t_2|) \theta\left(mE - \frac{1}{2}(t_1 + t_2)\right), \quad (15.10)$$

we implemented a cut on the non-relativistic approximation of the invariant mass of the  $\tilde{\chi}_1^+ b$  and  $\tilde{\chi}_1^- \bar{b}$  systems in the final state. The non-relativistic approximations given by  $t_1$  and  $t_2$  ignore effects that are suppressed by  $\frac{k^2}{m^2}$  with respect to  $t_1$  and  $t_2$ .

In order to get better agreement with the Madgraph simulation there are two possible ways to proceed. One possibility is to cut on the non-relativistic approximation of the invariant mass in the Madgraph simulation. The reason for implementing invariant mass cuts is that vNRQCD can

---

\*To consider the effect of the decay width  $\Gamma_Z$  we would have to change the imaginary part of  $C_{V/A}^{\text{Born}}$  at NNLO which would only give a N<sup>4</sup>LO effect for  $\sigma_{\text{incl}}(\Lambda)$ . Therefore we can ignore  $\Gamma_Z$  at NNLO.

only predict the transition amplitude to final states where the invariant mass of the  $\tilde{\chi}_1^+ b$  or the  $\tilde{\chi}_1^- \bar{b}$  systems is close to  $m$ . This is also achieved by cutting on the non-relativistic approximation of the invariant mass.

However, we will go a different way and implement a relativistic invariant mass cut in our calculation by using the variables

$$r_1 = \left(m + \frac{E}{2} + k^0\right)^2 - \mathbf{k}^2, \quad r_2 = \left(m + \frac{E}{2} - k^0\right)^2 - \mathbf{k}^2, \quad (15.11)$$

where  $k$  is the momentum through the  $\tilde{t}_1, \bar{\tilde{t}}_1$  propagators at the cut.  $r_1, r_2$  correspond directly to the square of the invariant masses of the  $\tilde{\chi}_1^+ b$  and  $\tilde{\chi}_1^- \bar{b}$  systems. Therefore the relativistic invariant mass cut is equivalent to

$$(m - \Delta M)^2 \leq r_1, r_2 \leq (m + \Delta M)^2. \quad (15.12)$$

To express the integrand with  $r_1, r_2$  we need to invert (15.11) which gives:

$$k^0 = \frac{r_1 - r_2}{2(E + 2m)} \quad (15.13)$$

and a rather cumbersome expression for  $|\mathbf{p}|$ . We can rewrite the loop integration over  $k$  via:

$$d^4k = 4\pi \mathbf{k}^2 d|\mathbf{k}| dk^0 = \frac{\pi |\mathbf{k}|}{E + 2m} dr_1 dr_2. \quad (15.14)$$

We did the integration over  $r_1, r_2$  numerically. As we can see for instance in the plots for  $\Delta M = 31\text{GeV}$  shown in figure 14, the effect of this correction is numerically of similar size as the correction discussed in section 15.1.

## 15.2. Madgraph simulation for $e^+e^- \rightarrow b \tilde{\chi}_1^+ \bar{b} \tilde{\chi}_1^-$

Finally we compare our results to a Madgraph simulation for  $e^+e^- \rightarrow b \tilde{\chi}_1^+ \bar{b} \tilde{\chi}_1^-$  where the single and non-resonant diagrams contributing to the same process are taken into account at  $O(\alpha_S^0)$ . The agreement with our results is of course worse than before, when Madgraph only considered the double-resonant diagrams. If we now include the NNLO effects discussed in the last subsection the agreement is getting worse. This can happen because there are now effects of similar order that we did not include. We expect that the main difference is due to the interference effects between single and double-resonant diagrams. They can be taken into account via an imaginary part of  $C_{V/A}$  as shown in (12.4). This correction is very similar to the one due to  $\delta Z^{\text{abs}}$  which is also absorbed via the imaginary part of  $C_{V/A}$ . We also expect the size of these effects to be similar.

The comparison shows that the dominant contribution to the process is taken into account by our treatment if we restrict ourselves to  $\Delta M$  values that are below 30GeV. For an invariant mass cut of  $\Delta M = 11\text{GeV}$  the difference between our results and the Madgraph simulation is around 5% and for  $\Delta M = 21\text{GeV}$  it is still around 10%\*. Figures 15, 16 and 17 show plots for the comparison for  $\Delta M = 21\text{GeV}$ ,  $\Delta M = 11\text{GeV}$  and  $\Delta M = 31\text{GeV}$ .

---

\*To be exact the difference between the results for  $E = -5\text{GeV}$  is more than 10%. This is because the cross section reduces significantly for energies below threshold, while the absolute value of the difference between our result and the one of the Madgraph simulation only depends mildly on  $E$ . With a difference of  $\sim 10\%$  we therefore mean that the difference is  $\sim 10\%$  for  $E \sim 5\text{GeV}$

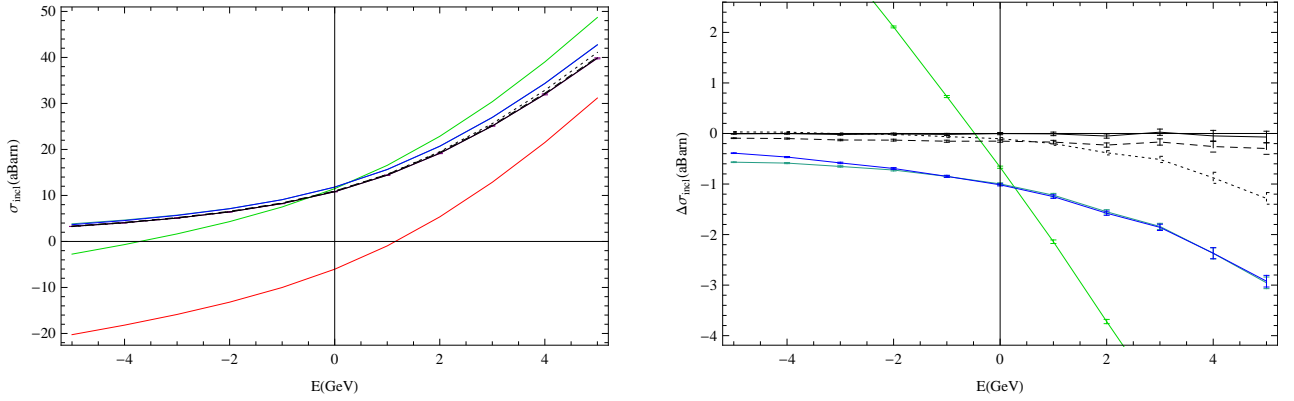


**Figure 12.:** These plots show the Madgraph result for the cross section of the process  $e^+e^- \rightarrow \tilde{t}_1\tilde{t}_1 \rightarrow b\tilde{\chi}_1^+\bar{b}\tilde{\chi}_1^-$  and our results at  $O(\alpha_S^0)$  for  $\Delta M = 21\text{GeV}$ . We do not take into account the hard gluon correction in (9.20) as they are also not contained in the Madgraph simulation. The red curve corresponds to the  $\overline{MS}$  renormalized result without PS matching corrections. The blue, turquoise and green curves show the NNLO<sub>+</sub>, NLO<sub>+</sub> and LO result of the expansion in (13.8). The dotted, dashed and solid black curves include all the PS corrections contained in the blue line and in addition the effects discussed in section 15.1 are added. The dotted black curve includes the NLO<sub>+</sub> corrections due to  $\delta Z^{\text{abs}}$ , in the dashed one the NLO<sub>+</sub> relativistic effects discussed in section 15.1 and 15.1 are added. Finally the solid black line adds the effects due to a relativistic invariant mass cut-off. The result of the Madgraph simulation is shown as a purple line, but it is difficult to see because it is covered by the black curves. The left plot shows the absolute values for  $\sigma_{\text{incl}}(\Lambda)$  while the right one shows the Madgraph result minus the results of our computations. Madgraph evaluates a statistical error for its results which is indicated by error bars in the plots. The black curve lies within these error bars.

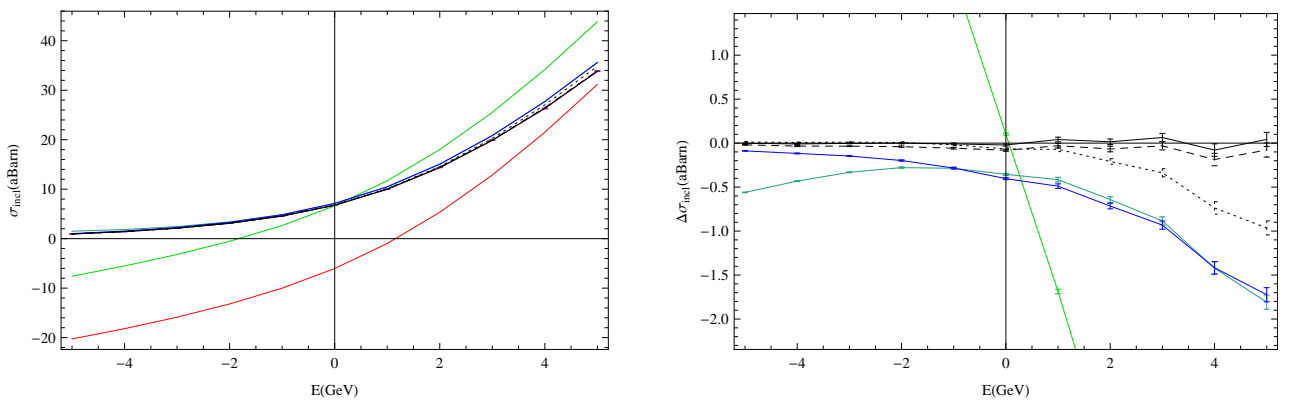


**Figure 13.:** These plots show the Madgraph result for the cross section of the process  $e^+e^- \rightarrow \tilde{t}_1\tilde{t}_1 \rightarrow b\tilde{\chi}_1^+\bar{b}\tilde{\chi}_1^-$  and our results at  $O(\alpha_S^0)$  for  $\Delta M = 11\text{GeV}$ . For the meaning of the curves see figure 12.

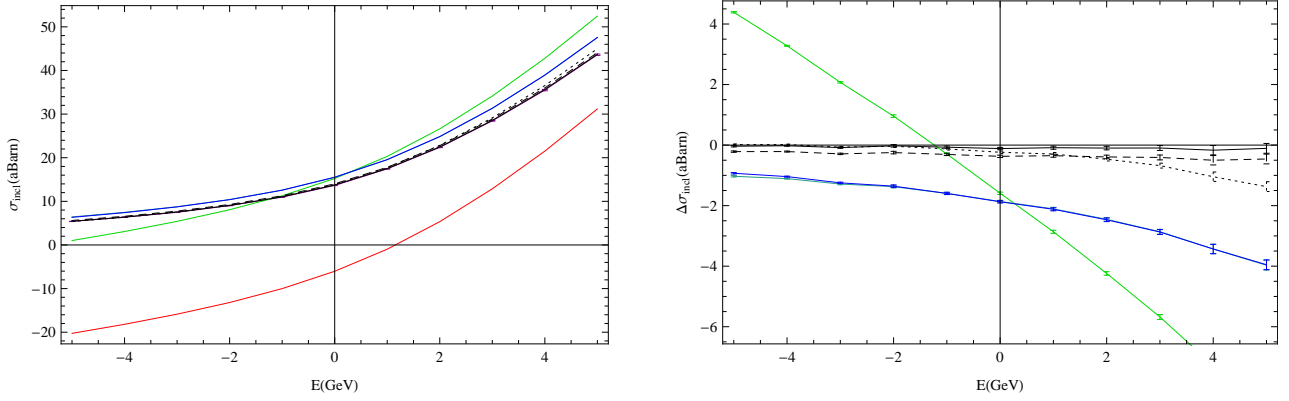


**Figure 14.:** These plots show the Madgraph result for the cross section of the process  $e^+e^- \rightarrow \tilde{t}_1 \tilde{t}_1^{\bar{}} \rightarrow b \tilde{\chi}_1^+ \bar{b} \tilde{\chi}_1^-$  and our results at  $O(\alpha_S^0)$  for  $\Delta M = 31\text{GeV}$ . For the meaning of the curves see figure 12.

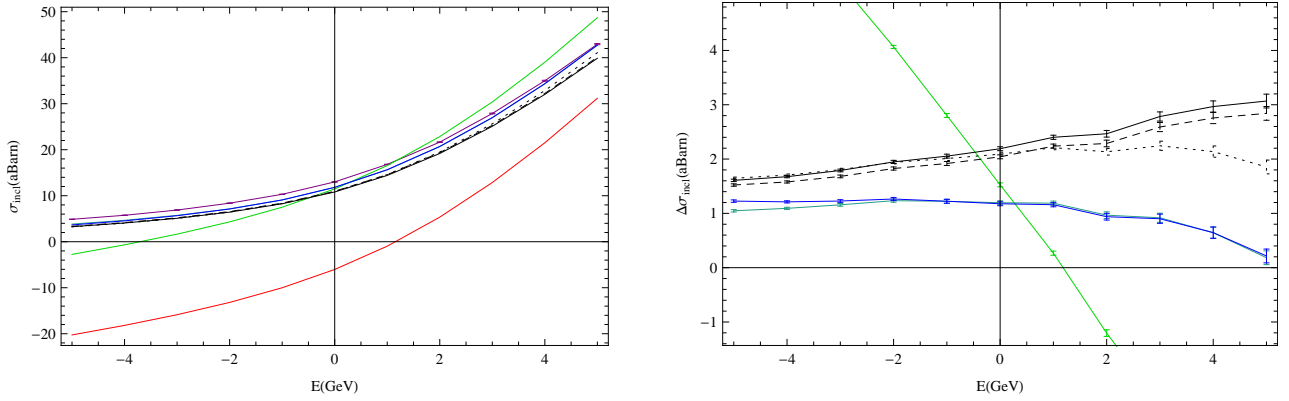


**Figure 15.:** These plots show the Madgraph result for the cross section of the process  $e^+e^- \rightarrow b \tilde{\chi}_1^+ \bar{b} \tilde{\chi}_1^-$  and our results at  $O(\alpha_S^0)$  for  $\Delta M = 21\text{GeV}$ . We do not take into account the hard gluon correction in (9.20) as they are also not contained in the Madgraph simulation. The red curve corresponds to the  $\overline{MS}$  renormalized result without PS matching corrections. The blue, turquoise and green curves show the NNLO<sub>+</sub>, NLO<sub>+</sub> and LO result of the expansion in (13.8). The dotted, dashed and solid black curves include all the PS corrections contained in the blue line and in addition the effects discussed in section 15.1 are added. The dotted black curve includes the NLO<sub>+</sub> corrections due to  $\delta Z^{\text{abs}}$ , in the dashed one the NLO<sub>+</sub> relativistic effects discussed in section 15.1 and 15.1 are added. Finally the solid black line adds the effects due to a relativistic invariant mass cut-off. The purple line corresponds to the result of the Madgraph simulation. The left plot shows the absolute values for  $\sigma_{\text{incl}}(\Lambda)$  while the right one shows the Madgraph result minus the results of our computations. Madgraph evaluates a statistical error for its results which is indicated by error bars in the plots.

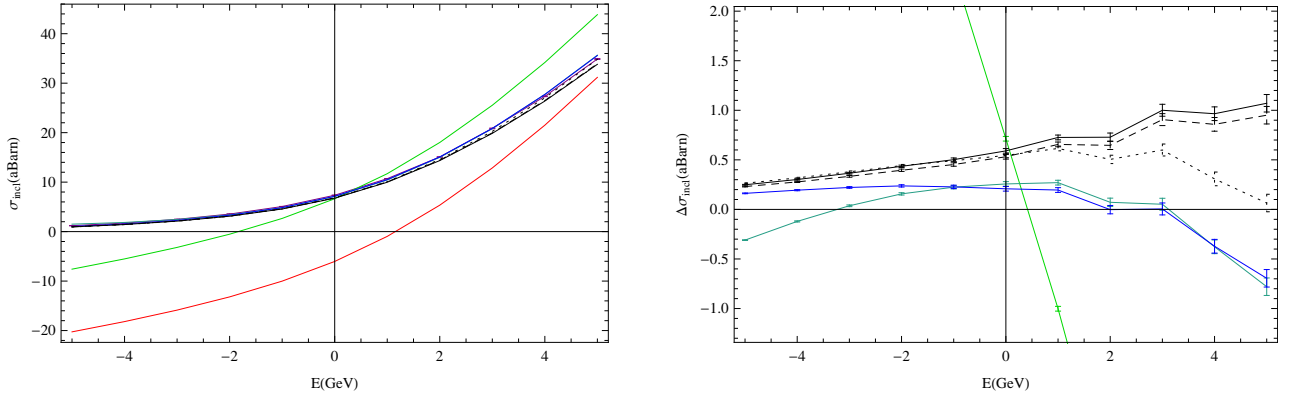


**Figure 16.:** These plots show the Madgraph result for the cross section of the process  $e^+e^- \rightarrow b \tilde{\chi}_1^+ \bar{b} \tilde{\chi}_1^-$  and our results at  $O(\alpha_S^0)$  for  $\Delta M = 11\text{GeV}$ . For the meaning of the curves see figure 15.

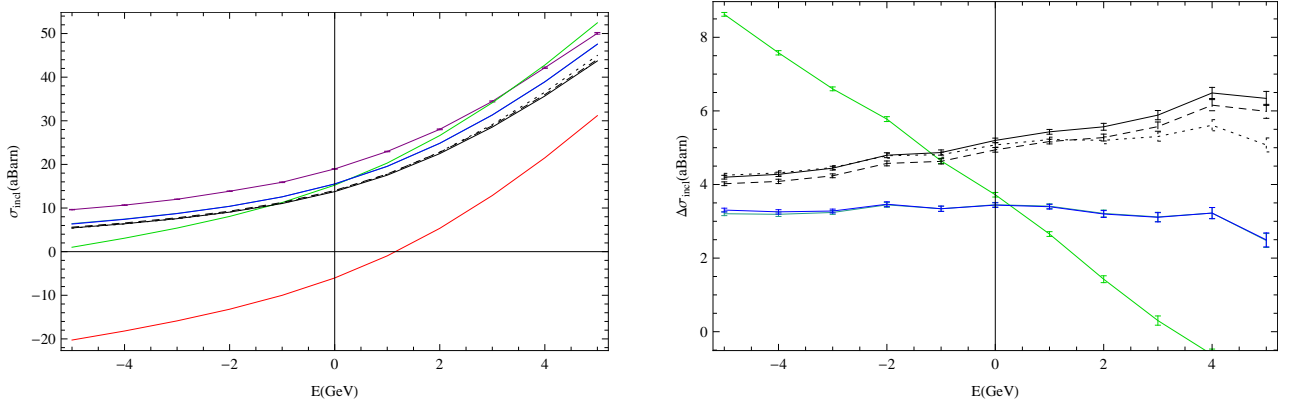


**Figure 17.:** These plots show the Madgraph result for the cross section of the process  $e^+e^- \rightarrow b \tilde{\chi}_1^+ \bar{b} \tilde{\chi}_1^-$  and our results at  $O(\alpha_S^0)$  for  $\Delta M = 31\text{GeV}$ . For the meaning of the curves see figure 15.

## 16. Preliminary result

In the last section we observed that when calculating the cross section of the process  $e^+e^- \rightarrow b \tilde{\chi}_1^+ \bar{b} \tilde{\chi}_1^-$  for an invariant mass cut-off of  $15 \leq \Delta M \leq 25 \text{ GeV}$  we can expect a precision of around 10% if we neglect the background contributions and the relativistic corrections. In this section we show a preliminary result for the cross section, where we take into account the running due to the PS-divergences discussed in section 14 but neglect the relativistic corrections and the background contributions. We also neglect the corrections to the Coulomb potential which have to be taken into account at NLO.

To avoid large logarithms we do a 2-stage matching. The matching to vNRQCD is carried out for  $\mu = m$ . Although vNRQCD is an unstable-particle EFT we can implement kinematic cuts on the invariant mass of the system of decay products of the (anti)stop [9, p.11]. At  $\nu_{\text{match}} = \Lambda/m$  we match the effect of the invariant mass cut-off on the local operators of our EFT with PS matching which is introduced in section 12. In section 13.1 we analytically calculated the  $O(\alpha_S^0)$  and  $O(\alpha_S)$  PS corrections to  $Im(\mathcal{A}_C^{jj})(\Lambda)$  up to NNLO<sub>+</sub>. However, the  $O(\alpha_S^2)$  PS-correction is formally still of NLO<sub>+</sub>. We determine the PS corrections numerically using (13.16). Although we do this calculation numerically the analytical expansion was important as a *proof of concept*, to see that it is possible to absorb the effect of the invariant mass cut-off in the local operators of the EFT with PS matching\*. Finally we obtain our result by applying the EFT with PS matching for  $\nu = v$ . In figure 18 we show the result of this calculation. In this plot we also show results for different choices of matching and renormalization scales.

In figure 18 we can see that the logarithms between  $\Lambda$  and the soft scale are sizeable as the difference between the result with (solid black curve) and without PS matching (blue curve) is about 10% for  $E > -1 \text{ GeV}$  and even larger for smaller energies. We can also see that doing the PS matching for  $\nu_{\text{match}} = 1$  (dashed black curve) instead of  $\nu_{\text{match}} = \frac{\Lambda}{m}$  leads to a difference of at least 5%. It is important to apply the EFT for  $\nu \sim v$ , as applying the theory for  $\nu \sim \frac{\Lambda}{m}$  (green curve) renders a difference of 50%. This means that the logarithms between the hard, soft and ultrasoft scale are very important. It is surprising that the result without an invariant mass cut-off (orange curve) also lies within an interval of 10% around the solid black curve. However, the orange curve is independent of the invariant mass cut-off and simply ignores the PS divergences. Therefore we interpret the small difference between the orange and the black curve as a coincidence.

---

\*It is wrong to assume that the PS corrections can always be absorbed into four-fermion operators. As illustrated in (12.4) it is for instance necessary to absorb them partly in the squarks production/annihilation currents.

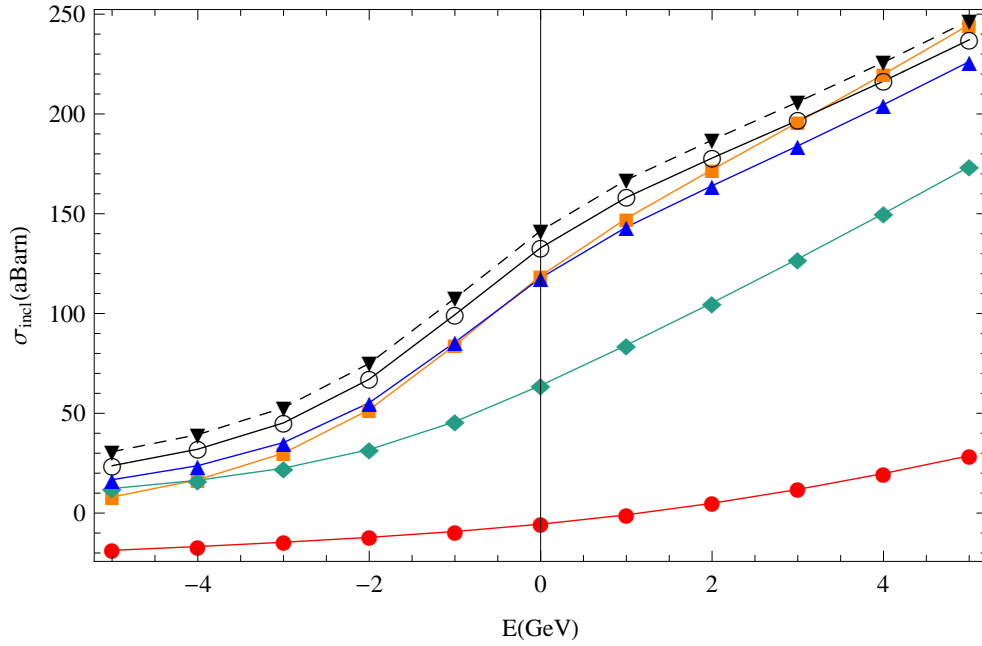


**Figure 18.:** This plot shows our preliminary result for the cross section of the process  $e^+e^- \rightarrow b\tilde{\chi}_1^+\bar{b}\tilde{\chi}_1^-$  with a kinematic cut of  $\Delta M = 21\text{GeV}$ . The red and orange curves correspond to the  $\overline{MS}$  renormalized result for  $\nu = v$  without PS matching corrections. The orange curve represents the result for  $\tilde{G}_C^P$  in (10.36) which includes the Coulomb-resummation, while the red curve is the  $O(\alpha_s^0)$  part of it. For the blue and green curve we introduced an invariant-mass cut-off but did not match its effect into local operators. For the green curve we take  $\nu = \frac{\Lambda}{m}$  and for the blue  $\nu = v$ . Finally for the black curves we matched the effect of the invariant-mass cut-off  $\Lambda$  onto the Wilson coefficients of our EFT with PS matching. For the dashed curve we did the PS matching for  $\nu_{\text{match}} = 1$  and for the solid curve for  $\nu_{\text{match}} = \frac{\Lambda}{m}$ . In both cases the EFT with PS matching is applied for  $\nu = v$ .

## 17. Conclusion

When calculating the cross section  $\sigma(e^+e^- \rightarrow \tilde{t}_1\tilde{t}_1)$  at 1-loop order in the first part of this work we have seen explicitly that the expansion in orders of  $\alpha_S$  breaks down close to threshold and it was therefore necessary to do a double expansion in  $\alpha_S$  and  $v$ . For doing this expansion we used vNRQCD which has also allowed us to sum up large logarithms between the hard, soft and ultrasoft scale. Applying the optical theorem we could calculate the total cross section  $\sigma(e^+e^- \rightarrow \tilde{t}_1\tilde{t}_1)$  by taking the imaginary part of the vacuum polarization function  $\mathcal{A}^{lk}$ . In chapter 10 we established that there is a close connection between the Greenfunction of the Schrödinger equation with the Coulomb potential and  $\mathcal{A}^{lk}$  at LO. However, when calculating  $\mathcal{A}^{lk}$  in this way, we encountered divergences in the imaginary part of  $\mathcal{A}^{lk}$  even at LO. These divergences are related to the finite lifetime of the produced  $\tilde{t}_1, \tilde{t}_1$  particles and can be avoided by restricting the invariant mass of the decay products of the (anti)stop, as explained in chapter 11.

Eventually we calculated the cross section from  $e^+e^-$  to some particles the stops can decay to (e.g.  $b\tilde{\chi}_1^+\bar{b}\tilde{\chi}_1^-$ ), with a PS cut applied on the final states. By adjusting the invariant mass cut-off we were able to restrict ourselves to a PS domain, where on the one hand the expansions of vNRQCD work well, and on the other the contribution of background diagrams are small compared to the contribution of the double-resonant diagrams described in vNRQCD. We chose the scale of the invariant mass cut-off  $\Lambda$  in between the soft and the hard scale. To sum up large logarithms between the soft scale and  $\Lambda$  we applied the PS matching formalism, where we matched the effect of the invariant mass cut-off into the operators of our effective theory. The concept of PS matching is described in chapter 11 and 12.

It has been important to check that it is possible to choose an invariant mass cut-off that is large enough such that its effect can be absorbed into local operators of our EFT and small enough such that the contribution of background diagrams to the inclusive cross section  $\sigma(e^+e^- \rightarrow b\tilde{\chi}_1^+\bar{b}\tilde{\chi}_1^-)$  is small with respect to the double-resonant ones. We checked this in chapter 15 by carrying out a tree level Monte Carlo simulation that takes the background diagrams into account. When comparing the results of this simulation to the  $O(\alpha_S^0)$  part of our analytic expression, we obtained that an invariant mass cut-off  $\Delta M$  of less than 30GeV is appropriate to achieve a precision of around 20%. For  $\Delta M \sim 20\text{GeV}$  the difference between the Monte Carlo simulation and our tree level result is about 10%. In chapter 13 we have seen that an invariant mass cut-off of about 10GeV is already large enough such that we have good convergence when putting the effect of the invariant mass cut-off into local operators\*.

We expect that the most important background contribution comes from the interference of single and double-resonant diagrams. This contribution could be taken into account in our analysis by matching it to the imaginary part of the stop production vertex. A result at NLL should take this and the effect of a NLO correction to the Coulomb potential into account.

In the LL result, which we presented in chapter 16, we have seen that the summation of logarithms between  $\Lambda$  and the soft scale, which is achieved due to the PS matching formalism, is a sizeable effect of about 10%.

---

\*In our analysis we concentrated on a specific point in the MSSM parameter space (namely the SPS1a point). At a different parameter point the outcome of this analysis might be different.



**Part III.**  
**Appendix**



## 18. Scalar $n$ -point Integrals

### 18.1. Prerequisites

The  $n$ -point integrals are carried out in  $d = 4 - 2\epsilon$  dimensions using dimensional regularisation [48]. In the results we will ignore factors of  $O(\epsilon)$ . We will often need the integration measure in polar coordinates:

$$\begin{aligned} d^d k &= |k|^{d-1} d|k| d\Omega_d, \\ d\Omega_d &= d \cos(\theta) \sin(\theta)^{d-3} d\Omega_{d-1}, \\ \Omega_d &\equiv \int d\Omega_d = 2 \frac{\pi^{\frac{d}{2}}}{\Gamma(\frac{d}{2})}, \end{aligned} \quad (18.1)$$

where  $\Gamma(x)$  refers to the gamma function. When carrying out the scalar-integrals we will often use the following formula [46, p. 102]:

$$\int d^d k \frac{(k^2)^\beta}{(k^2 - a + i\epsilon)^\alpha} = \frac{(-1)^\beta i \Gamma(\beta + \frac{d}{2}) \Gamma(\alpha - \beta - \frac{d}{2})}{(-1)^\alpha (4\pi)^{\frac{d}{2}} \Gamma(\alpha) \Gamma(\frac{d}{2})} (a - i\epsilon)^{\frac{d}{2} + \beta - \alpha}. \quad (18.2)$$

For rewriting the scalar integral to a form, where we can apply the formula above, we will introduce Feynman parameters [45].

By using a factor  $\tilde{\mu}^{2\epsilon}$  in the definition of the scalar integrals and rewriting the results in terms of  $\mu = \tilde{\mu} \exp\left(\frac{\ln(4\pi) - \gamma_E}{2}\right)$ , one gets rid of terms containing  $\ln(4\pi)$  and  $\gamma_E^*$ .

Sometimes it might be important to remember that the  $\epsilon$  in the propagators and the  $\epsilon$  referring to the  $d$  of dimensional regularisation are not equivalent. One first calculates the result for a general  $d$  with the  $\epsilon$  of the propagator going to 0 and only then analytically continues the result to  $d \rightarrow 4$ .

The scalar integrals are all depending on some mass parameter. Usually it is clear which mass is meant and therefore we will omit the mass dependency of the scalar integrals when using them in the other sections.

### 18.2. 1-point integral

For this integral we do not need to introduce Feynman parameters, but immediately get the result applying (18.2):

$$\begin{aligned} A_0(m^2) &\equiv \int d^d k \frac{\tilde{\mu}^{2\epsilon}}{[k^2 - m^2]_+} = \\ &= -i \frac{\Gamma(-1 + \epsilon) \tilde{\mu}^{2\epsilon}}{(4\pi)^{2-\epsilon}} (m^2 - i\epsilon)^{1-\epsilon} \\ &= \frac{im^2}{(4\pi)^2} \left( \frac{1}{\epsilon} + \ln\left(\frac{\mu^2}{m^2}\right) + 1 \right) + O(\epsilon). \end{aligned} \quad (18.3)$$

---

\* $\gamma_E$  is the so-called Euler gamma

### 18.3. 2-point integral

The general scalar 2-point integral is defined as:

$$\begin{aligned} B_0((p_1, m_1^2), (p_2, m_2^2)) &\equiv \int d^d k \frac{\tilde{\mu}^{2\epsilon}}{[(k+p_1)^2 - m_1^2]_+ [(k+p_2)^2 - m_2^2]_+} \\ &= B_0((p_1 - p_2, m_1^2), (0, m_2^2)). \end{aligned} \quad (18.4)$$

We need this integral in two different special cases, to which we refer to as  $\hat{B}_0$  and  $\tilde{B}_0$ :

$$\begin{aligned} \hat{B}_0(p^2, m^2) &\equiv \int d^d k \frac{\tilde{\mu}^{2\epsilon}}{k_+^2 [(k+p)^2 - m^2]_+} \\ &= \int_0^1 dx \int d^d k \frac{\tilde{\mu}^{2\epsilon}}{[(k+xp)^2 + (p^2 - m^2)x - x^2 p^2]_+}. \end{aligned} \quad (18.5)$$

We have introduced Feynman parameters. We can now substitute  $k+xp \rightarrow k$  and use (18.2):

$$\hat{B}_0(p^2, m^2) = \frac{i\tilde{\mu}^{2\epsilon}}{(4\pi)^{2-\epsilon}} \Gamma(\epsilon) \int_0^1 dx ((m^2 - p^2)x + p^2 x^2 - i\epsilon)^{-\epsilon}. \quad (18.6)$$

For the remaining integrand we can make an expansion in  $\epsilon$  because the integral is finite. We have to do the expansion up to  $O(\epsilon)$  as  $\Gamma(\epsilon)O(\epsilon) = O(1)$ .

$$\begin{aligned} \hat{B}_0(p^2, m^2) &= \frac{i\tilde{\mu}^{2\epsilon}}{(4\pi)^{2-\epsilon}} \Gamma(\epsilon) \int_0^1 dx [1 - \epsilon \ln((m^2 - p^2)x + p^2 x^2 - i\epsilon)] + O(\epsilon) \\ &= \frac{i}{(4\pi)^2} \left[ \frac{1}{\epsilon} + \ln\left(\frac{\mu^2}{m^2}\right) + 2 + \frac{m^2 - p^2}{p^2} \ln\left(\frac{m^2 - p^2}{m^2} - i\epsilon\right) \right] + O(\epsilon). \end{aligned} \quad (18.7)$$

For computing  $\frac{\partial \hat{B}_0}{\partial p^2}$  one has to be careful: Deriving by  $p^2$  introduces an I.R. divergence and one thus cannot use (18.7). We derive (18.6), where we have not yet expanded in  $\epsilon$ , by  $p^2$  and get:

$$\frac{\partial \hat{B}_0}{\partial p^2} = \frac{i\tilde{\mu}^{2\epsilon}}{(4\pi)^{2-\epsilon}} \Gamma(\epsilon) (-\epsilon) \int_0^1 dx ((m^2 - p^2)x + p^2 x^2 - i\epsilon)^{-1-\epsilon} (x^2 - x). \quad (18.8)$$

This integral is only convergent if  $\epsilon < 0$ . Therefore the  $\frac{1}{\epsilon}$  terms will correspond to I.R. divergences, which we will indicate by writing  $\epsilon_{IR}$  and  $\mu_{IR}$  instead of  $\epsilon$  and  $\mu$  in the result\*. We will only need  $\frac{\partial \hat{B}_0}{\partial p^2}$  for  $p^2 = m^2$ , which simplifies the calculation:

$$\begin{aligned} \left. \frac{\partial \hat{B}_0}{\partial p^2} \right|_{p^2=m^2} &= - \frac{i\tilde{\mu}^{2\epsilon}}{(4\pi)^{2-\epsilon}} \Gamma(\epsilon) \epsilon \frac{1}{(m^2)^{1+\epsilon}} \underbrace{\int_0^1 dx (x^2)^{-1-\epsilon} (x^2 - x)}_{\frac{1}{1-2\epsilon} + \frac{1}{2\epsilon}} \\ &= - \frac{i}{(4\pi)^2 m^2} \left[ \frac{1}{2} \ln\left(\frac{\mu_{IR}^2}{m^2}\right) + \frac{1}{2\epsilon_{IR}} + 1 \right] + O(\epsilon). \end{aligned} \quad (18.9)$$

---

\*For U.V. divergences we will always write  $\epsilon$  and  $\mu$

We need one other special case of  $B_0$ :

$$\tilde{B}_0(q^2, m^2) \equiv \int \tilde{d}^d k \frac{\tilde{\mu}^{2\epsilon}}{[k^2 - m^2]_+ [(k+q)^2 - m^2]_+}, \quad (18.10)$$

where  $q^2 > 0$ . We introduce Feynman parameters:

$$\tilde{B}_0(q^2, m^2) = \int_0^1 dx \int \tilde{d}^d k \frac{\tilde{\mu}^{2\epsilon}}{[(k+qx)^2 + q^2(x-x^2) - m^2]_+^2}. \quad (18.11)$$

We substitute  $k+qx \rightarrow k$  and use (18.2):

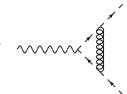
$$\tilde{B}_0(q^2, m^2) = \frac{i\tilde{\mu}^{2\epsilon}}{(4\pi)^{2-\epsilon}} \Gamma(\epsilon) \int_0^1 dx (m^2 + q^2(x^2 - x) - i\epsilon)^{-\epsilon} \quad (18.12)$$

As in (18.6) we can expand the remaining integrand in  $\epsilon$  before doing the integration and we have to expand up to  $O(\epsilon)$  as  $\Gamma(\epsilon)$  involves a  $\frac{1}{\epsilon}$  divergence:

$$\begin{aligned} \tilde{B}_0(q^2, m^2) &= \frac{i\tilde{\mu}^{2\epsilon}}{(4\pi)^{2-\epsilon}} \Gamma(\epsilon) \int_0^1 dx [1 - \epsilon \ln(m^2 + q^2(x^2 - x) - i\epsilon)] + O(\epsilon) \\ &= \frac{i}{(4\pi)^2} \left[ \frac{1}{\epsilon} + \ln\left(\frac{\mu^2}{q^2} + i\epsilon\right) + 2(1 + \ln(2)) - (1 - \beta) \ln(1 - \beta + i\epsilon) \right. \\ &\quad \left. - (1 + \beta) \ln(1 + \beta) + i\pi\beta \operatorname{sgn}(q^2) \right] + O(\epsilon), \end{aligned} \quad (18.13)$$

where  $\beta = \sqrt{1 - \frac{4m^2}{q^2}}$ . This result is valid for  $q^2 < 0$  and  $q^2 > 0$ . The limit of this expression for  $q^2 \rightarrow 0$  gives the correct result for  $\tilde{B}_0(0, m^2)$ . However, we only need  $\tilde{B}_0(q^2, m^2)$  for  $q^2 \geq 4m^2$ .

### 18.4. 3-point integral

When computing  we also need a special case of the scalar 3-point integral, which we will call  $\tilde{C}_0$ . We will assume that  $p_1^2 = p_2^2 = m^2$ :

$$\tilde{C}_0(q^2 = (p_1 + p_2)^2, m^2) \equiv \int \tilde{d}^d k \frac{\tilde{\mu}^{2\epsilon}}{k_+^2 [(k+p_1)^2 - m^2]_+ [(k-p_2)^2 - m^2]_+}. \quad (18.14)$$

Introducing Feynman parameters and using (18.2) we obtain:

$$\tilde{C}_0(q^2, m^2) = \frac{-i\tilde{\mu}^{2\epsilon}}{(4\pi)^{2-\epsilon}} \Gamma(1 + \epsilon) \int_0^1 dx \int_0^{1-x} dy [(xp_1 - yp_2)^2 - i\epsilon]^{-1-\epsilon}. \quad (18.15)$$

Next we do a variable transformation

$$\begin{aligned} x &= uv, & y &= u(1-v), \\ \int_0^1 dx \int_0^{1-x} dy &= \int_0^1 du \int_0^1 dv u, \end{aligned} \quad (18.16)$$

such that we can factor out one of the integration variables:

$$\begin{aligned}\tilde{C}_0(q^2, m^2) &= \frac{-i\tilde{\mu}^{2\epsilon}}{(4\pi)^{2-\epsilon}} \Gamma(1+\epsilon) \int_0^1 du u^{-1-2\epsilon} \int_0^1 dv [(vp_1 - (1-v)p_2)^2 - i\epsilon]^{-1-\epsilon} \\ &= \frac{i\tilde{\mu}^{2\epsilon}}{(4\pi)^{2-\epsilon}} \frac{\Gamma(1+\epsilon)}{2\epsilon} \int_0^1 dv [m^2 - v(1-v)q^2 - i\epsilon]^{-1-\epsilon}.\end{aligned}\quad (18.17)$$

The remaining integral can be expressed with the dilogarithm function  $Li_2$ :

$$\begin{aligned}\tilde{C}_0(q^2, m^2) &= \frac{i\tilde{\mu}^{2\epsilon}}{(4\pi)^{2-\epsilon}} \frac{\Gamma(1+\epsilon)}{(q^2)^{1+\epsilon}} \frac{1}{(y_1 - y_2)} \left[ \frac{\ln(y_2) - \ln(y_1) + i\pi}{\epsilon} + \frac{\ln(y_1 y_2)^2}{2} \right. \\ &\quad \left. - 2\ln(y_2)^2 + [\ln(y_2) - \ln(y_1 - y_2)]^2 + 2Li_2\left(\frac{y_2}{y_2 - y_1}\right) - \frac{2\pi^2}{3} \right. \\ &\quad \left. - 2i\pi \ln(y_1 - y_2) \right],\end{aligned}\quad (18.18)$$

where

$$y_1 = \frac{1+\beta}{2} + i\epsilon, \quad y_2 = \frac{1-\beta}{2} - i\epsilon, \quad \beta = \sqrt{1 - \frac{4m^2}{q^2}}.\quad (18.19)$$

This result is valid for  $q^2 < 0$  and  $q^2 > 0$ . The limit of this expression for  $q^2 \rightarrow 0$  gives the correct result for  $\tilde{C}_0(0, m^2)$ . However, we only need  $\tilde{C}_0(q^2, m^2)$  for  $q^2 \geq 4m^2$ .

## 19. Tensor-Reduction

### 19.1. Introduction

We will apply the method of tensor reduction to express integrals of the form

$$I^{\mu\nu\dots} = \int \bar{d}^d k \frac{\tilde{\mu}^{2\epsilon} k^\mu k^\nu \dots}{[(k+p_1)^2 - m_1^2]_+ [(k+p_2)^2 - m_2^2]_+ \dots} \quad (19.1)$$

as a sum of scalar integrals times some tensor structures. For doing this, we will always start with an Ansatz, where we use that  $I^{\mu\nu\dots}$  can only be a linear combination of those tensor structures that can be built with  $g^{\mu\nu}$  and the vectors  $p_1, p_2 \dots$  appearing inside the integral. A simple example would be:

$$\begin{aligned} \hat{B}_1^\mu(p, m^2) &\equiv \int \bar{d}^d k \frac{\tilde{\mu}^{2\epsilon} k^\mu}{k_+^2 [(k+p)^2 - m^2]_+} \\ &= \hat{B}_1 p^\mu. \end{aligned} \quad (19.2)$$

In this case the Ansatz is very simple. One can now obtain  $\hat{B}_1$  by contracting  $\hat{B}_1^\mu$  with  $p_\mu$ :

$$\hat{B}_1 p^2 = \hat{B}_1^\mu p_\mu = \int \bar{d}^d k \frac{\tilde{\mu}^{2\epsilon} (k \cdot p)}{k_+^2 [(k+p)^2 - m^2]_+}. \quad (19.3)$$

An essential idea of the tensor reduction method is that one can always get rid of terms in the numerator by expressing those terms as a sum of factors in the denominator plus some terms that do not depend on the integration variable and can thus be factored out of the integral. In this case we write  $k \cdot p$  as  $\frac{1}{2}[(k+p)^2 - m^2] - \frac{k^2}{2} + \frac{m^2 - p^2}{2}$  and thus get

$$\hat{B}_1 = \frac{1}{p^2} \left[ \underbrace{\frac{1}{2} \int \bar{d}^d k \frac{\tilde{\mu}^{2\epsilon}}{k_+^2}}_0 - \frac{1}{2} \int \bar{d}^d k \frac{\tilde{\mu}^{2\epsilon}}{[(k+p)^2 - m^2]_+} + \frac{m^2 - p^2}{2} \int \bar{d}^d k \frac{\tilde{\mu}^{2\epsilon}}{k_+^2 [(k+p)^2 - m^2]_+} \right] \quad (19.4)$$

and finally

$$\hat{B}_1(p, m^2)^\mu = \frac{1}{2p^2} \left[ -A_0(m^2) + (m^2 - p^2) \hat{B}_0(p^2, m^2) \right] p^\mu. \quad (19.5)$$

### 19.2. 2-point integral

$$B_1^\mu((p_1, m_1^2), (p_2, m_2^2)) \equiv \int \bar{d}^d k \frac{\tilde{\mu}^{2\epsilon} k^\mu}{[(k+p_1)^2 - m_1^2]_+ [(k+p_2)^2 - m_2^2]_+} \quad (19.6)$$

The tensor-integral  $\hat{B}_1^\mu$  that we dealt with before is a special case of this more general form. We encounter another special case:

$$\tilde{B}_1^\mu(p_1, p_2, m) \equiv \int \bar{d}^d k \frac{\tilde{\mu}^{2\epsilon} k^\mu}{[(k+p_1)^2 - m^2]_+ [(k-p_2)^2 - m^2]_+}, \quad (19.7)$$

which can be reduced to:

$$\tilde{B}_1^\mu(p_1, p_2, m) = -\frac{1}{2} \tilde{B}_0(q^2, m^2) (p_1 - p_2)^\mu, \quad (19.8)$$

where  $q = p_1 + p_2$ .

### 19.3. 3-point integral

$$C_1^\mu((p_1, m_1^2), (p_2, m_2^2), (p_3, m_3^2)) \equiv \int d^d k \frac{\tilde{\mu}^{2\epsilon} k^\mu}{[(k+p_1)^2 - m_1^2]_+ [(k+p_2)^2 - m_2^2]_+ [(k+p_3)^2 - m_3^2]_+} \quad (19.9)$$

Again we do not have to evaluate this integral in its general form but only need the following special case:

$$\tilde{C}_1^\mu(p_1, p_2, m) \equiv \int d^d k \frac{\tilde{\mu}^{2\epsilon} k^\mu}{k_+^2 [(k+p_1)^2 - m^2]_+ [(k-p_2)^2 - m^2]_+}. \quad (19.10)$$

For  $p_1^2 = p_2^2 = m^2$  we can reduce  $\tilde{C}_1^\mu(p_1, p_2, m)$  to:

$$\tilde{C}_1^\mu(p_1, p_2, m) = \frac{1}{4m^2 - q^2} \left[ \hat{B}_0(m^2, m^2) - \tilde{B}_0(q^2, m^2) \right] (p_1 - p_2)^\mu, \quad (19.11)$$

where  $q = p_1 + p_2$ .



## 20. Phase space integrals

In this section we will calculate several integrals of the form

$$\int f(k_1, \dots, k_n) d\text{LIPS}_n(q), \quad (20.1)$$

where the invariant, n-particle phase space measure in  $d = 4 - 2\epsilon$  dimensions is defined as:

$$\begin{aligned} d\text{LIPS}_n(q) &\equiv (2\pi)^d \tilde{\mu}^{-2\epsilon} \delta^d(q - \sum_{j=1}^n k_j) \prod_{j=1}^n d\tilde{k}_j, \\ \tilde{d}k &\equiv \tilde{\mu}^{2\epsilon} \frac{d^d k}{(2\pi)^d} \theta(k^0) (2\pi) \delta(k^2 - m^2) = \tilde{\mu}^{2\epsilon} \frac{d^{d-1} k}{(2\pi)^{d-1} 2k^0}. \end{aligned} \quad (20.2)$$

In the last expression  $k^0 = \sqrt{\mathbf{k}^2 + m^2}$  is a function of  $\mathbf{k}$ . Sometimes one only needs the size of the phase space. We define  $\text{PS}_n(q^2, \epsilon)$  as the size of the n-particle phase space:

$$\text{PS}_n(q^2, \epsilon) \equiv \int d\text{LIPS}_n(q). \quad (20.3)$$

### 20.1. 2 particle phase space integrals

$\int d\text{LIPS}_2(q)$

$$\begin{aligned} \text{PS}_2(q^2, \epsilon) &= \int d\text{LIPS}_2(q) \\ &= \int \tilde{\mu}^{-2\epsilon} \delta^d(q - p_1 - p_2) \tilde{\mu}^{2\epsilon} \frac{d^d p_1}{(2\pi)^{d-1}} \theta(p_1^0) \delta(p_1^2 - m^2) \tilde{\mu}^{2\epsilon} \frac{d^d p_2}{(2\pi)^{d-1}} \theta(p_2^0) \delta(p_2^2 - m^2) \\ &= \tilde{\mu}^{2\epsilon} (2\pi)^{-d+2} \int \frac{d^{d-1} p_2}{2p_2^0} \frac{\delta(q^0 - p_1^0 - p_2^0)}{2p_1^0}. \end{aligned} \quad (20.4)$$

In the CMS frame we have  $q^0 = \sqrt{q^2}$  and  $p_1^0 = p_2^0 = \sqrt{\mathbf{p}_2^2 - m^2}$ . We get:

$$\begin{aligned} \text{PS}_2(q^2, \epsilon) &= \tilde{\mu}^{2\epsilon} \frac{(2\pi)^{-d+2}}{4} \int \frac{\underbrace{d^{d-1} p_2}_{|\mathbf{p}_2|^{d-2} d|\mathbf{p}_2| d\Omega_{d-1}}}{(p_2^0)^2} \frac{\delta(\sqrt{q^2} - 2p_2^0)}{(p_2^0)^2} \\ &= \tilde{\mu}^{2\epsilon} \frac{(2\pi)^{-d+2}}{4} \Omega_{d-1} \int dp_2^0 \delta\left(\frac{\sqrt{q^2}}{2} - p_2^0\right) \frac{|\mathbf{p}_2|^{d-3}}{2p_2^0} \\ &= \tilde{\mu}^{2\epsilon} \frac{(2\pi)^{-d+2} \Omega_{d-1}}{4\sqrt{q^2}} \left(\frac{q^2}{4} - m^2\right)^{\frac{d-3}{2}}, \end{aligned} \quad (20.5)$$

Expanding this result up to  $O(\epsilon)$  we obtain:

$$\text{PS}_2(q^2, \epsilon) = \frac{\beta}{8\pi} \left[ 1 + 2\epsilon + \epsilon \log\left(\frac{\mu^2}{q^2 \beta^2}\right) \right] + O(\epsilon^2), \quad (20.6)$$

where  $\beta = \sqrt{1 - \frac{4m^2}{q^2}}$ .

## 20.2. 3 particle phase space integrals

In section 4, the 3 particle phase space integral (4.12) has to be computed in  $d$  dimensions\*. Two of the particles have the same mass and the third particle is massless. We will call the momenta of the massive particles  $p_1, p_2$ , the one of the massless particle  $k$  and the total momentum  $q$ .

We introduced the following three invariants:

$$x \equiv \frac{2(p_1 \cdot q)}{q^2}, \quad y \equiv \frac{2(p_2 \cdot q)}{q^2}, \quad z \equiv \frac{2(k \cdot q)}{q^2}. \quad (20.7)$$

$x, y$  and  $z$  are two times the energy of the respective particles divided by total energy in the CMS. One has the identity:

$$x + y + z = 2. \quad (20.8)$$

The function that is integrated over this phase space in (4.12) can be expressed by the two invariants  $y$  and  $z$ . The phase space integral has the following form:

$$\begin{aligned} I_3 &= \int f(y, z) d\text{LIPS}_3(q) \\ &= \int f(y, z) \tilde{\mu}^{-2\epsilon} \delta^d(q - p_1 - p_2 - k) \\ &\quad \tilde{\mu}^{2\epsilon} \frac{d^d p_1}{(2\pi)^{d-1}} \theta(p_1^0) \delta(p_1^2 - m^2) \tilde{\mu}^{2\epsilon} \frac{d^d p_2}{(2\pi)^{d-1}} \theta(p_2^0) \delta(p_2^2 - m^2) \tilde{\mu}^{2\epsilon} \frac{d^d k}{(2\pi)^{d-1}} \theta(k^0) \delta(k^2). \end{aligned}$$

We will first rewrite this  $d$ -dimensional phase space integration to an integration over  $y$  and  $z$ :

$$\begin{aligned} I_3 &= \int dy dz f(y, z) (2\pi)^{-2d+3} \tilde{\mu}^{4\epsilon} \\ &\quad \underbrace{\int \frac{d^{d-1} p_1}{2p_1^0} \frac{d^{d-1} p_2}{2p_2^0} \frac{d^{d-1} k}{2k^0} \delta^d(q - p_1 - p_2 - k) \delta\left(y - \frac{2(p_2 \cdot q)}{q^2}\right) \delta\left(z - \frac{2(k \cdot q)}{q^2}\right)}_{\equiv h(y, z)}. \end{aligned}$$

We will compute the invariant  $h(y, z)$  in the CMS. Then  $\delta^{d-1}(q - p_1 - p_2 - k)$  fixes  $\mathbf{p}_1$  to  $-\mathbf{p}_2 - \mathbf{k}$ . After integrating  $d^{d-1} p_1$  there are three  $\delta$  functions left, that we can rewrite as follows:

$$\begin{aligned} \theta(|\mathbf{k}|) \delta\left(z - \frac{2(k \cdot q)}{q^2}\right) &= \theta(z) \frac{\sqrt{q^2}}{2} \delta\left(|\mathbf{k}| - \frac{z\sqrt{q^2}}{2}\right), \\ \theta(|\mathbf{p}_2|) \delta\left(y - \frac{2(p_2 \cdot q)}{q^2}\right) &= \theta(y - r) \frac{p_2^0 \sqrt{q^2}}{2|\mathbf{p}_2|} \delta\left(|\mathbf{p}_2| - \frac{\sqrt{q^2}}{2} \sqrt{y^2 - r^2}\right), \\ \theta(1 - |\cos(\theta)|) \delta(q^0 - p_1^0 - p_2^0 - k^0) &= \theta(1 - |\cos(\hat{\theta})|) \frac{p_1^0}{|\mathbf{k}||\mathbf{p}_2|} \delta\left(\cos(\theta) - \cos(\hat{\theta})\right), \\ \cos(\hat{\theta}) &\equiv \frac{2 - 2z - 2y + yz}{z\sqrt{y^2 - \frac{4m^2}{q^2}}}. \end{aligned} \quad (20.9)$$

---

\*doing the phase space with  $\epsilon \neq 0$  integrals regularizes the I.R. divergences

Where  $r \equiv \frac{2m}{\sqrt{q^2}}$ .  $\theta$  is the angle between  $\mathbf{p}_2$  and  $\mathbf{k}$ . Using (18.1) we rewrite the integration measure as follows:

$$\begin{aligned} d^{d-1}k &= |\mathbf{k}|^{d-2} d|\mathbf{k}| d\Omega_{d-1}, \\ d^{d-1}p_2 &= |\mathbf{p}_2|^{d-2} [1 - \cos(\theta)^2]^{\frac{d-4}{2}} d|\mathbf{p}_2| d\cos(\theta) d\Omega_{d-2}. \end{aligned} \quad (20.10)$$

Now the integration can be carried out easily and results in:

$$\begin{aligned} h(y, z) &= \Omega_{d-2} \Omega_{d-1} \frac{q^2 [1 - \cos(\theta)^2]^{\frac{d-4}{2}} |\mathbf{k}|^{d-4} |\mathbf{p}_2|^{d-4}}{32} \\ &\quad \theta(z) \theta(y - r) \theta(1 - |\cos(\theta)|). \end{aligned} \quad (20.11)$$

$|\mathbf{k}|$ ,  $|\mathbf{p}_2|$  and  $\cos(\theta)$  are understood as the values fixed by the  $\delta$  functions. The  $\theta$  functions restrict the domain of integration for  $y$  and  $z$ . After working out these boundaries and inserting  $h(y, z)$  in (20.9), we obtain:

$$\begin{aligned} I_3 &= \underbrace{\tilde{\mu}^{4\epsilon} \frac{\Omega_{d-1} \Omega_{d-2}}{(2\pi)^{2d-3} 32} (q^2)^{1-\epsilon} m^{-2\epsilon} 4^\epsilon}_{\equiv F_3} \int_r^1 dy \int_{z_-}^{z_+} dz f(y, z) \left[ \frac{4}{r^2} (1-x)(1-y)(1-z) - z^2 \right]^{-\epsilon}, \\ z_{\pm} &\equiv \frac{2(1-y)}{2-y \mp \sqrt{y^2 - r^2}}. \end{aligned} \quad (20.12)$$

Using this result we will do several phase space integrals that we encounter in section 4.

$$\int \frac{1}{(1-y)^2} \mathbf{dLIPS}_3(q)$$

$$\begin{aligned} I &\equiv \int \frac{1}{(1-y)^2} \mathbf{dLIPS}_3(q) \\ &= F_3 \int_r^1 dy \int_{z_-}^{z_+} dz \frac{1}{(1-y)^2} \left[ \frac{4}{r^2} (1-x)(1-y)(1-z) - z^2 \right]^{-\epsilon} \end{aligned} \quad (20.13)$$

First, we do the  $z$  integration and obtain:

$$I = F_3 \frac{\Gamma(2-\epsilon) \sqrt{\pi} r^{4\epsilon}}{\Gamma\left(\frac{3}{2}-\epsilon\right) (1-\epsilon) 2^{1+2\epsilon} (1-r^2)^\epsilon} \int_r^1 dy \frac{1}{(1-y)^{1+2\epsilon}} \frac{\sqrt{y^2 - r^2}}{1-y + \frac{r^2}{4}} + O(\epsilon). \quad (20.14)$$

The remaining integral is of the form

$$I = \int_r^1 dy \frac{f(y, \epsilon)}{(1-y)^{1+2\epsilon}}. \quad (20.15)$$

$f(y, \epsilon)$  is finite for the whole integration domain, but due to  $\frac{1}{(1-y)^{1+2\epsilon}}$  the integrand is divergent for  $y \rightarrow 1$  if  $\epsilon > -\frac{1}{2}$ . The integral is finite for  $\epsilon < 0$ . One only needs regularization for  $y \rightarrow 1$  and can simplify the calculation by setting  $\epsilon = 0$  for the rest of the integration domain. For doing this one can split the integral as follows:

$$I = \int_r^1 dy \frac{f(y, \epsilon) - f(1, \epsilon)}{(1-y)^{1+2\epsilon}} + \int_r^1 \frac{f(1, \epsilon)}{(1-y)^{1+2\epsilon}}. \quad (20.16)$$

The second integral can be done easily for a general  $\epsilon$  and the first is now finite for  $\epsilon = 0$ . Therefore, we only need to compute:

$$I = \int_r^1 dy \frac{f(y, 0) - f(1, 0)}{1 - y} + \int_r^1 \frac{f(1, \epsilon)}{(1 - y)^{1+2\epsilon}} + O(\epsilon). \quad (20.17)$$

This is significantly simpler than the full computation for a general  $\epsilon$ . Finally we obtain:

$$\int \frac{1}{(1 - y)^2} d\text{LIPS}_3(q) = F_3 \left[ -\frac{1}{\epsilon_{IR}} \frac{2\beta}{1 - \beta^2} + \frac{-4\beta + 12\beta \log(1 - w) + (4 - 6\beta + 2\beta^2) \log(w)}{1 - \beta^2} \right], \quad (20.18)$$

where  $\beta = \sqrt{1 - \frac{4m}{q^2}}$  and  $w = \frac{1 - \beta}{1 + \beta}$ .

$$\int \frac{1}{(1 - x)(1 - y)} d\text{LIPS}_3(q)$$

$$\begin{aligned} I &\equiv \int \frac{1}{(1 - x)(1 - y)} d\text{LIPS}_3(q) \\ &= F_3 \int_r^1 dy \int_{z_-}^{z_+} dz \frac{1}{(-1 + y + z)(1 - y)} \left[ \frac{4}{r^2} (1 - x)(1 - y)(1 - z) - z^2 \right]^{-\epsilon} \end{aligned} \quad (20.19)$$

The expression that one obtains after doing the  $z$  integration looks more complicated than (20.14), but it is again of the form (20.15). Rewriting the expression as in (20.17) simplifies the calculation significantly:

$$\begin{aligned} \int_r^1 dy \frac{f(y, 0) - f(1, 0)}{1 - y} &= F_3 \int_r^1 dy \frac{1}{1 - y} [2 \log(1 - \beta) - 2 \log(1 + \beta) \\ &\quad - \log(2 - y - \sqrt{-1 + y^2 + \beta^2}) - \log(y - \sqrt{-1 + y^2 + \beta^2}) \\ &\quad + \log(2 - y + \sqrt{-1 + y^2 + \beta^2}) + \log(y + \sqrt{-1 + y^2 + \beta^2})] \\ &= F_3 \left[ -\frac{\pi^2}{2} - \frac{\log(w)^2}{2} + 4 \log(1 - \sqrt{w}) + 2 \log(w) \log(1 + w) \right. \\ &\quad \left. + 4Li_2(w) + 2Li_2(-w) \right] \end{aligned} \quad (20.20)$$

and

$$\begin{aligned} \int_r^1 \frac{f(1, \epsilon)}{(1 - y)^{1+2\epsilon}} &= F_3 \left[ \frac{\log(w)}{\epsilon} - \frac{\pi^2}{6} + \log(w)^2 - 4 \log(1 - \sqrt{w}) \log(w) \right. \\ &\quad \left. + 2 \log(w) \log(1 + w) + 2Li_2(w) + 2Li_2(-w) \right] + O(\epsilon) \end{aligned} \quad (20.21)$$

In the final result the  $\log(1 - \sqrt{w}) \log(w)$  terms cancel:

$$\begin{aligned} \int \frac{1}{(1 - x)(1 - y)} d\text{LIPS}_3(q) &= F_3 \left[ \frac{\log(w)}{\epsilon_{IR}} - \frac{2\pi^2}{3} + \log(w)^2 + 4 \log(w) \log(1 + w) \right. \\ &\quad \left. + 6Li_2(w) + 4Li_2(-w) \right]. \end{aligned} \quad (20.22)$$

$$\int \frac{1}{(1-y)} \mathbf{dLIPS}_3(q)$$

The remaining two integrals that we encounter in section 4 are much easier as they contain no divergences and can thus be carried out in  $d = 4$  dimensions.

$$\begin{aligned} \int \frac{1}{1-y} \mathbf{dLIPS}_3(q) &= F_3 \int_r^1 dy \int_{z_-}^{z_+} dz \frac{1}{1-y} \\ &= F_3 \left[ -\beta - \frac{\log(w)}{2} - \frac{\beta^2}{2} \log(w) \right]. \end{aligned} \quad (20.23)$$

$$\int \mathbf{dLIPS}_3(q)$$

The last integral is simply the phase space volume:

$$\begin{aligned} \int \mathbf{dLIPS}_3(q) &= F_3 \int_r^1 dy \int_{z_-}^{z_+} dz \\ &= F_3 \left[ \frac{3\beta - \beta^3}{4} + \frac{3 \log(w)}{8} - \frac{2\beta^2 + \beta^4}{8} \log(w) \right]. \end{aligned} \quad (20.24)$$



# Bibliography

- [1] Combination of higgs boson searches with up to 4.9 fb<sup>-1</sup> of pp collisions data taken at a center-of-mass energy of 7 tev with the atlas experiment at the lhc. Technical Report ATLAS-CONF-2011-163, CERN, Geneva, Dec 2011.
- [2] Combination of sm higgs searches. Technical Report CMS-PAS-HIG-11-032, CERN, Geneva, Dec 2011.
- [3] Gerald Aarons et al. International Linear Collider Reference Design Report Volume 2: PHYSICS AT THE ILC. 2007. This is one section of the ILC Design Report.
- [4] M. Abramowitz and I.A. Stegun. Handbook of mathematical functions with formulas, graphs, and mathematical tables. Number v. 55, no. 1972 in Applied mathematics series. U.S. Govt. Print. Off., 1964.
- [5] B.C. Allanach, M. Battaglia, G.A. Blair, Marcela S. Carena, A. De Roeck, et al. The Snowmass points and slopes: Benchmarks for SUSY searches. Eur.Phys.J., C25:113–123, 2002.
- [6] Johan Alwall, Michel Herquet, Fabio Maltoni, Olivier Mattelaer, and Tim Stelzer. MadGraph 5 : Going Beyond. JHEP, 06:128, 2011.
- [7] Christian W. Bauer, Sean Fleming, Dan Pirjol, and Iain W. Stewart. An Effective field theory for collinear and soft gluons: Heavy to light decays. Phys.Rev., D63:114020, 2001.
- [8] W. Beenakker, R. Höpker, and P. M. Zerwas. Gluon radiation off scalar stop particles. Physics Letters B, 349(4):463 – 468, 1995.
- [9] M. Beneke, B. Jantzen, and P. Ruiz-Femenia. Electroweak non-resonant NLO corrections to  $e^+e^- \rightarrow W^+W^-b\bar{b}$  in the  $t\bar{t}$  resonance region. Nucl.Phys., B840:186–213, 2010.
- [10] M. Beneke and V.A. Smirnov. Asymptotic expansion of feynman integrals near threshold. Nuclear Physics B, 522(1-2):321 – 344, 1998.
- [11] Geoffrey T. Bodwin, Eric Braaten, and G.Peter Lepage. Rigorous QCD analysis of inclusive annihilation and production of heavy quarkonium. Phys.Rev., D51:1125–1171, 1995.
- [12] W.E. Caswell and G.P. Lepage. Effective Lagrangians for Bound State Problems in QED, QCD, and Other Field Theories. Phys.Lett., B167:437, 1986.
- [13] K.G. Chetyrkin. Combinatorics of  $R$ ,  $R^{*(-1)}$ , and  $R^*$  operations and asymptotic expansions of Feynman integrals in the limit of large momenta and masses. 1991.
- [14] K.G. Chetyrkin and V.A. Smirnov.  $R^*$ -operation corrected. Physics Letters B, 144(5-6):419 – 424, 1984.

## Bibliography

- [15] S. Dimopoulos and G.F. Giudice. Naturalness constraints in supersymmetric theories with nonuniversal soft terms. Phys.Lett., B357:573–578, 1995.
- [16] Savas Dimopoulos and Howard Georgi. Softly Broken Supersymmetry and SU(5). Nucl.Phys., B193:150, 1981.
- [17] A. Djouadi, W. Hollik, and C. Junger. QCD corrections to scalar quark decays. Phys.Rev., D55:6975–6985, 1997.
- [18] Manuel Drees and Gilles Gerbier. Mini-Review of Dark Matter: 2012. 2012.
- [19] John R. Ellis and Serge Rudaz. Search for Supersymmetry in Toponium Decays. Phys.Lett., B128:248, 1983.
- [20] Howard Georgi. An Effective Field Theory for heavy quarks at low energies. Phys.Lett., B240:447–450, 1990.
- [21] I.S. Gradshteyn, I.M. Ryzhik, S. Technica, and A. Jeffrey. Table of integrals, series, and products: V. Geronimus [and] M. Yu : Tseytlin. Academic Press. A subsidiary of Harcourt Brace Jovanovich, 1965.
- [22] D.J. Griffiths. Introduction to Elementary Particles. Physics Textbook. Wiley-VCH, 2008.
- [23] Ken-ichi Hikasa and Makoto Kobayashi. Light Scalar Top at  $e^+ e^-$  Colliders. Phys.Rev., D36:724, 1987.
- [24] A.H. Hoang, A.V. Manohar, Iain W. Stewart, and T. Teubner. The Threshold  $t$  anti- $t$  cross-section at NNLL order. Phys.Rev., D65:014014, 2002.
- [25] Andre Hoang. The top pair threshold: Status and new developments. 2006.
- [26] Andre H. Hoang. Heavy quarkonium dynamics. 2002. To be published in 'At the Frontier of Particle Physics / Handbook of QCD, Volume 4', edited by M. Shifman (World Scientific, Singapore).
- [27] Andre H. Hoang. Top pair production at threshold and effective theories. Acta Phys.Polon., B34:4491–4509, 2003.
- [28] Andre H. Hoang, Christoph J. Reisser, and Pedro Ruiz-Femenia. Phase Space Matching and Finite Lifetime Effects for Top-Pair Production Close to Threshold. Phys.Rev., D82:014005, 2010.
- [29] Andre H. Hoang and Pedro Ruiz-Femenia. Renormalization group analysis in NRQCD for colored scalars. Phys.Rev., D73:014015, 2006.
- [30] Grant Larsen, Yasunori Nomura, and Hannes L.L. Roberts. Supersymmetry with Light Stops. 2012.
- [31] T.D. Lee and M. Nauenberg. Degenerate Systems and Mass Singularities. Phys.Rev., 133:B1549–B1562, 1964.



- [32] H. Lehmann, K. Symanzik, and W. Zimmermann. On the formulation of quantized field theories. Nuovo Cim., 1:205–225, 1955.
- [33] H. Leutwyler. On the foundations of chiral perturbation theory. Annals Phys., 235:165–203, 1994.
- [34] Michael E. Luke, Aneesh V. Manohar, and Ira Z. Rothstein. Renormalization group scaling in nonrelativistic QCD. Phys.Rev., D61:074025, 2000.
- [35] Aneesh V. Manohar and Pedro Ruiz-Femenia. The Orthopositronium decay spectrum using NRQED. Phys.Rev., D69:053003, 2004.
- [36] Stephen P Martin. A supersymmetry primer. Nature, (December):1–128, 2008.
- [37] Manel Martinez and Ramon Miquel. Multiparameter fits to the  $t$  anti- $t$  threshold observables at a future  $e^+e^-$  linear collider. Eur.Phys.J., C27:49–55, 2003. 21 pages, 7 figures. v2: Minor changes, mostly to style of figures Journal-ref: Eur. Phys. J. C27 (2003) 49.
- [38] K Nakamura and Particle Data Group. Review of particle physics. Journal of Physics G: Nuclear and Particle Physics, 37(7A):075021, 2010.
- [39] Keith A. Olive and Serge Rudaz. Light stops in the MSSM: Implications for photino dark matter and top quark decay. Phys.Lett., B340:74–80, 1994.
- [40] M.E. Peskin and D.V. Schroeder. Introduction to quantum field theory. Advanced Book Program. Addison-Wesley Pub. Co., 1995.
- [41] A. Pineda and J. Soto. Effective field theory for ultrasoft momenta in NRQCD and NRQED. Nucl. Phys. Proc. Suppl., 64:428–432, 1998.
- [42] Christoph J. Reisser. Effects of the top quark decay in  $e^+e^- \rightarrow t\bar{t}$  near threshold, 2005.
- [43] Christoph J. Reisser. Finite Lifetime Effects in Top Quark Pair Production at Threshold. PhD thesis, Technical University Munich, 2008.
- [44] Janusz Rosiek. Complete set of Feynman rules for the MSSM: Erratum. 1995.
- [45] V.A. Smirnov. Evaluating Feynman Integrals. Number no. 211 in Springer Tracts in Modern Physics. Springer, 2004.
- [46] M.A. Srednicki. Quantum field theory. Cambridge University Press, 2007.
- [47] M. Stahlhofen. Ultrasoft renormalization of the potentials in vNRQCD. PhD thesis, Technical University Munich, 2009.
- [48] Gerard 't Hooft and M.J.G. Veltman. Regularization and Renormalization of Gauge Fields. Nucl.Phys., B44:189–213, 1972.
- [49] Gerard 't Hooft and M.J.G. Veltman. Regularization and Renormalization of Gauge Fields. Nucl.Phys., B44:189–213, 1972.
- [50] M. Veltman. Diagrammatica: the path to Feynman rules. Cambridge lecture notes in physics. Cambridge University Press, 1994.

*Bibliography*

- [51] J. C. Ward. An identity in quantum electrodynamics. Phys. Rev., 78:182–182, Apr 1950.

## Abstract

We study the cross section for stop-antistop pair production in the electron-positron collision close to threshold for unstable squarks. Scales appearing in this process are the mass of the stop  $m$ , their 3-momentum  $\sim mv$  and their kinetic energy  $\sim mv^2$ , where  $v$  is the relative velocity of the squarks in the center of mass frame. Close to production threshold ( $v \ll 1$ ) we need to resum terms  $\sim (\alpha_s/v)^n$  as well as large logarithms of ratios of the physical scales in quantum corrections to the cross section. To achieve this we employ the scalar version of the effective field theory framework vNRQCD. The finite width  $\Gamma_{\tilde{t}_1}$ , which we count as  $O(mv^2)$ , is an additional scale in the problem. Stop instability effects generate divergences in the phase space integrals and to deal with these in the effective theory kinematic cuts on the final states are introduced. Phase space divergences already enter at leading order and also background diagrams are substantially more important than for top-antitop pair production.

## Zusammenfassung

Wir studieren die Stop-Antistop Paarproduktion in Elektron-Positron Kollisionen, wenn die invariante Masse des Eingangszustandes in der Nähe der Schwellenenergie liegt. Mit  $v$  bezeichnen wir die Relativgeschwindigkeit der Squarks im Schwerpunktsystem. Die Masse der Stop Teilchen  $m$ , ihr räumlicher Impuls  $\mathbf{p} \sim mv$  und ihre kinetische Energie  $\sim mv^2$  sind Skalen welche in diesem Problem auftreten. Bei der Berechnung des Wirkungsquerschnittes in der Nähe der Produktionsschwelle ( $v \ll 1$ ) müssen Terme der Form  $\sim (\alpha_s/v)^n$  sowie große Logarithmen von Quotienten der drei oben erwähnten Skalen resummiert werden. Um das zu erreichen wenden wir die *Effektive Quantenfeldtheorie* vNRQCD an. Die Zerfallsbreite der Stops  $\Gamma_{\tilde{t}_1}$  stellt eine zusätzliche Skala dar, welche wir als  $O(mv^2)$  zählen. Aufgrund der Instabilität des Stops kommt es in der effektiven Theorie zu Phasenraumdivergenzen, welche durch das Einführen von Phasenraumcuts auf die Zerfallsprodukte der Stops vermieden werden können. Ähnliche Effekte treten auch bei der Top-Antitop Paarproduktion auf. Bei der Stop-Antistop Paarproduktion treten Phasenraumdivergenzen allerdings bereits auf führender Ordnung auf. Auch der Beitrag von Hintergrunddiagrammen ist relativ zur führenden Ordnung gesehen größer als im Falle der Top-Antitop Paarproduktion.

# Curriculum Vitae

## Personal Information

Name	<b>Peter Poier</b>
E-Mail	peter.poier@univie.ac.at
Date of birth	30.3.1987
Nationality	Austria

## Education

1993-1997	Primary school
1997-2005	Secondary school
2005	Matura (high school leaving exam) at Stiftsgymnasium Admont, with honor
2006-2012	Study of physics at University of Vienna
September 2007, 2008	Summer student at the Institute for Quantum Optics and Quantum Information (IQOQI), Vienna
2008	Academic stage 1 completed, with honor
July-September 2010	Summer Student at CERN, Geneva
2010	Academic stage 2 completed, with honor
November 2010	Start of work for diploma thesis in theoretical particle physics with André Hoang
2012	First part of academic stage 3 completed, with honor

## Experience Abroad

Winter term 2009	Semester abroad at the University College Dublin
------------------	--

## Teaching Experience

2008-2012	Tutor for <i>Unterstützung zu L1/L2 mit Schwerpunkt Schulbezug</i> (supplementary courses to lectures teaching classical mechanics and quantum mechanics to teachers), University of Vienna
Winter term 2010	Tutor for <i>Übungen zur Einführung in die physikalischen Rechenmethoden I+II</i> (basic math exercises for first-term physics students), University of Vienna
Summer term 2012	Tutor for <i>Theoretische Physik II: Quantenmechanik I - Übungen</i> (exercise class for an introductory lecture on quantum mechanics), University of Vienna

## Work Experience

July-October 2008	Technische Akustik SV GmbH (development of the software for a system to measure the effectiveness of sound barriers)
March-May 2012	Catalysts GmbH (company developing individual software solutions for industrial and scientific applications)

## Language Skills

German	Mother tongue
English	Fluent
French	Basic knowledge

## Miscellaneous

August 2005	Winner of a bronze medal at the <i>17th International Olympiad in Informatics</i> in Nowy Sacz, Poland
2005-2006	Alternative civilian service at the Lebenshilfe in Liezen